5-1-2020

RESERVOIR SCALE IMPLICATION OF MICROBIAL COAL-TO-METHANE CONVERSION

Rohit Pandey
Southern Illinois University Carbondale, rohit.mining1990@gmail.com

RESERVOIR SCALE IMPLICATION OF MICROBIAL COAL-TO-METHANE CONVERSION

by

Rohit Pandey

B.S., Bengal Engineering and Science University, 2013
M.S., Southern Illinois University, 2015

A Dissertation
Submitted in Partial Fulfillment of the Requirements for the
Doctor of Philosophy Degree

College of Engineering
in the Graduate School
Southern Illinois University Carbondale
May 2020

DISSERTATION APPROVAL

RESERVOIR SCALE IMPLICATION OF MICROBIAL COAL-TO-METHANE CONVERSION

by

Rohit Pandey

A Dissertation Submitted in Partial

Fulfillment of the Requirements

for the Degree of

Doctor of Philosophy

in the field of Engineering Science

Approved by:

Satya Harpalani, Chair

Yanna Liang

Steven Esling

Bruce DeVantier

Shimin Liu

Graduate School
Southern Illinois University Carbondale
November 6, 2019

AN ABSTRACT OF THE DISSERTATION OF

Rohit Pandey, for the Doctor of Philosophy degree in Engineering Science, presented on November 6, 2019, at Southern Illinois University Carbondale.

TITLE: RESERVOIR SCALE IMPLICATION OF MICROBIAL COAL-TO-METHANE CONVERSION

MAJOR PROFESSOR: Dr. Satya Harpalani

Increased world-wide interest in reducing the carbon-footprint of human activities has driven the coal-fueled energy industry to transition to a natural gas fueled future. Coupled with the continually increasing energy demand, the interest in alternate sources of natural gas has gained momentum. Microbially enhanced coalbed methane (MECBM), which aims at microbially converting *in situ* coal to methane provides one such alternate source of natural gas. Feasibility of MECBM as a viable technology is two-pronged, focusing on associated microbiology, and flow-governing reservoir response. The general advance of research in this area has thus far been from a microbial perspective, where coal-to-methane bioconversion has been successfully reported for several coal types worldwide. However, insights into reservoir properties governing flow and transport of fluids in a MECBM reservoir is missing. Given that coal is both the source and reservoir rock of the produced biogenic methane, a sound knowledge of the effect of bioconversion on flow governing properties of coal is decisive from a production perspective. Evaluating the flow governing reservoir response of a MECBM reservoir is the focus of the work presented in this dissertation.

In order to investigate the effect of bioconversion on the Darcian flow regime existing in the natural fractures in coal, two experimental studies were undertaken. First, variation in coal's flow governing micro- and macro- porosity was investigated using high-resolution scanning electron microscopy. The observed changes were quantified and the expected change in

permeability of coal post-bioconversion was estimated. In the second set of experiments, the sorption-induced-strain response of coal pre- and post-bioconversion was studies. Finally, the experimental data was used to model and predict the geomechanical-coupled flow behavior of a MECBM reservoir during bioconversion and production of the produced biogenic methane.

Experimental results from the imaging study revealed that bioconversion results in swelling of the coal matrix. This reduces the cleat (macroporous fracture) aperture post-bioconversion, reducing the permeability of the coal significantly. This validated the recently reported results, where measured permeability of coal packs and coal cores dropped by ~70% post-bioconversion. Bioconversion, however, resulted in increase in the cleat width of fractures greater than 5 microns wide, which constituted <5% of the fractures imaged. This is indicative of the possibility of enhanced reservoir performance in artificially fractured coal formations or, ones with wide-aperture fractures, like depleted coalbed methane (CBM) reservoirs and abandoned mines. Investigation into the sorption-induced-strain response of coal revealed suppression of the strain response post-bioconversion. Results from helium and methane flooding revealed that bioconversion softens the coal matrix, reducing the Langmuir pressure and strain constants post-bioconversion. The modeling exercise revealed that the depletion induced the permeability increase commonly associated with producing CBM will be suppressed post-bioconversion. Detailed analysis of the behavioral variation in multiple reservoir parameters was used to define the ideal condition, beyond which the reservoir flow during biogenic methane production improved. Additionally, a rating system is proposed, which can be used to rank coal deposits to rate their suitability for bioconversion from a flow perspective.

ACKNOWLEDGMENTS

The path towards this dissertation has been exciting, challenging and extremely rewarding in all aspects of my life: professional and personal. While I am the sole author of this work, its completion was made possible by the integral support of numerous individuals. In what follows, I acknowledge their role and thank them for the constant guidance and encouragement.

I would first like to thank my advisor, Dr. Harpalani, for his dedicated support towards my academic and professional career. Continuous progress is a function of a seemingly complex decision-making process, along with a dedicated effort to make it to come to fruition. Dr. Harpalani relentlessly provided a directional wind to me, brainstorming through my decision-making process while continually calibrating the subsequent effort. This is not constrained to only my scientific and professional pursuits, rather has translated to shaping me as an individual. A significant part of my doctoral training has been inspired from his commitment to perfection, where any work was only criticized with a motivation to do/achieve better.

I am very thankful to my committee member, Dr. Yanna Liang, for her invaluable pointers to my experimental design work and encouragement throughout the course of my research endeavors. I am also thankful to Dr. Shimin Liu for his input, which inevitably helped me decode numerous underlying scientific phenomena from my experimental results. I am thankful to Dr. Steven Esling, whose two courses in Hydrogeology strengthened my basic understanding of characterizing flow behavior and equipped me with confidence of working with excel macros while processing large volumes of data. I am also thankful to Dr. Bruce DeVantier for his inputs, which helped me draw parallels from soil flow and compaction studies to reservoir characterization.

I am grateful for receiving research support during my Ph.D. from grants sponsored by the Department of Energy (DOE), Alpha Foundation, Illinois Clean Coal Institute (ICCI), British Petroleum and SIU Graduate School. I am also thankful to all the students in the Department of Mining Engineering, who have made my teaching experience extremely enjoyable and something that I looked forward to everyday.

I am extremely thankful for the help from Greg Moroz and Tim Attig for their assistance in setting up my experimental studies and bringing paper ideas to life. My thanks go out to Diana Lyall and Jennifer Langin for their assistance with the seemingly never-ending paperwork and administrative processes.

My thanks go out to all my colleagues over the years, especially Suman Saurabh, Dr. Ruimin Feng and Dr. Ji Zhang, where we navigated the highs and the lows of graduate school together, having a lot of fun in the process.

My academic and personal growth would have definitely been stunted, if not for the role that my friends have played over these years. Over these years, I have been fortunate to have met so many amazing people from all corners of the world. I thank them for bearing with my irritably persistent idiosyncrasies, and to have journeyed through my culinary failures and successes.

Finally, my most sincere gratitude to my parents, my sister, and everyone in my extended family. I owe my journey to my parents' indomitable spirit to strive to do better through hard work, and to their constant love and support.

DEDICATION

Dedicated to Bob and Mami, whose love transcends all boundaries.

PREFACE

This dissertation is submitted for the degree of Doctor of Philosophy in Engineering Science at the Southern Illinois University Carbondale. The research described herein was carried out under the supervision of Dr. Satya Harpalani in the College of Engineering, Southern Illinois University Carbondale, between August 2015 and November 2019.

This study is original, except where references are made to previous work. Neither this, nor any substantially similar dissertation has been or is being submitted for any other degree, diploma or other qualification at any other university.

The main body of the dissertation consists of Chapters 2, 3 and 4, which correspond with the three published peer-reviewed journal papers respectively. In order of chapter appearance, these papers are:

- Pandey , R., & Harpalani, S. (2018). Imaging and fractal-based approach to understand reservoir-scale changes in bioconverted coal. *Fuel, 230, 282-297.*
- Pandey , R., & Harpalani, S. (2019). Impact of bioconversion on matrix strain response of coal reservoirs: Part 1- Experimental insights. *Fuel, 239, 1363-1375.*
- Pandey , R., & Harpalani, S. (2019). Impact of bioconversion on matrix strain response of coal reservoirs: Part 2- Reservoir insights. *Fuel, 239, 1376-1387.*

My co-authorship in the above listed papers implies my principle role in conducting experiments, data analysis and interpretation.

Rohit Pandey

November 2019

TABLE OF CONTENTS

LIST OF TABLES

TABLE PAGE

LIST OF FIGURES

FIGURE PAGE

CHAPTER 1

INTRODUCTION

1.1 Introductory Statement

Worldwide efforts to curb CO_2 emissions and maintain a sustainable carbon footprint has made the use of natural gas (methane and higher hydrocarbons) for generation of electricity an inevitable transition from coal-to-renewably fueled future. This has resulted in increased interest in the quest for unconventional sources of natural gas. Methane stored in coal seams provide one such source. The origin of coalbed methane can be distinctly related to two processes: thermogenic and biogenic. Thermogenic methane is formed gradually over the process of coalification, when the coal attains a rank of approximately 0.5 – 0.6% vitrinite reflectance (high volatile, bituminous). At this point, due to continued application of heat and overlying pressure, thermogenic gases like CO_2, H_2O, CH_4, C_2H_6, H_2S and other higher hydrocarbon gases are devolatilized (Faiz and Hendry 2006; Moore 2012a). Biogenic methane, as the name suggests originates due to the effect of microbial action on coal. Primary biogenic methane is formed during the initial stages of peat formation at shallow depths. Due to high porosity and lower burial rates, primary biogenic methane is volatized over time or dissolved in water and expelled during compaction (Rice, Dudley D., U. S. Geological S 2002). Late-stage or secondary biogenic methane is formed post-compaction in all ranks of coal due to combination of active groundwater flow recharging the underground systems with suitable microbes, along with uplift of the basin helping in meteoric recharge (Faiz and Hendry 2006; Rice, Dudley D., U. S. Geological S 2002).

Taking cue from the widespread application of microbes in the oil industry as a means to increase overall recovery, and the impact that naturally occurring microbes have in producing

methane in coal, Scott introduced the concept of microbially enhanced coalbed methane (MECBM) (Scott 1999a). It aimed at replicating the natural process of secondary biogenic gasification by treating coal with methanogens along with suitable nutrient amendments and trace elements. Studies conducted by Strapoc´ and Opara (Opara et al. 2012; Strapoć et al. 2007) further provided substantial evidence of the potential of generating methane by treating coal fines with microbial inoculations. Research in the area of MECBM and bioconversion has accelerated in the last few years for several reasons. First, natural gas is considered a cleaner and, therefore, preferred source of energy. Second, this technology is applicable to unmineable coals and abandoned coal mines with large amounts of coal left behind. Third, the technology is applicable to coal waste in the form of fines or poor-quality material. Fourth, several regions with significant coalbed methane (CBM) activity are maturing, thus providing a large number of wells along with other supporting infrastructure required for injection of microbes/nutrients as well as gas recovery and utilization. Finally, the technology is applicable to CBM wells that are abandoned due to poor production rates and recovery, such as, the Illinois basin.

Techno-economic feasibility of in situ coal bioconversion depends on two major aspects, focusing on microbial processes and reservoir flow behavior. The general advance of research has been towards characterizing and improving the microbial solutions, primarily aimed to economically increase the amount of methane produced. The results of these studies clearly showed that that the process of bioconversion, in general, is a relatively slow process. Significant production of methane has been observed over a period of thirty to sixty days, or even higher in some instances (Opara et al. 2012; Strąpoć et al. 2008; J. Zhang, Liang, Pandey, et al. 2015; J. Zhang, Liang, Yau, et al. 2015; Ji Zhang et al. 2016; Ji Zhang and Liang 2017). However, these studies were conducted on powdered coal, providing additional surface areas for the microbes to

act on. Production rates for *in situ* deposits are expected to be even lower given the limited ability of coal to allow fluid transport. Under such time dependent production characteristics, it is important to identify the reservoir properties affecting flow and documenting the changes in these properties. Insights into the effect of bioconversion on the reservoir structure, and its subsequent effect on flow-coupled-geomechanical behavior is lacking at this time. Given that the bioconverted coal will serve both as the source and reservoir rock for the produced methane, knowledge of expected gas flow rates and reservoir response during bioconversion as wee as during treatment is crucial from an operator's perspective, which is the focus area of this dissertation.

1.2 Problem Statement

Understanding reservoir response of coal as a reservoir rock requires characterization of storage and transport behavior that dictates fluid flow. These mechanisms in coal are different compared to conventional natural gas reservoirs. Flow in a CBM reservoir is governed by the physical structure of coal, typically characterized as a dual-porosity rock, where micro- and macro- porosities affect flow of fluids. Micropores occur as a part of the coal matrix, and serve as a storehouse for over 95% of the gas in adsorbed form (Gray 1987). The macropore system consists of a network of closely placed natural fractures surrounding the coal matrix blocks, known as the cleat system. In course of CBM production, pumping out water, which saturates the coal, reduces the pore pressure. This results in desorption of methane from the microporous matrix surface, contributing to the first stage of fluid flow in coal. Once desorbed, methane diffuses across the complex pore geometry of coal in accordance with Fick's second law of diffusion. Methane then reaches the fracture network, that is, the cleat system, where the transport mechanism becomes Darcian, controlled by the permeability, and is dependent on cleat

parameters, such as, aperture, continuity and spacing. The effect on bioconversion on the sorption-diffusion properties of coal was recently reported (Pandey et al. 2016; Pandey 2015a). It was revealed that post-bioconversion, the sorption capacity of coal increased, as did the associated diffusive flow-rates in the microscopic scale. This is indicative of altered pore structure of coal, where increased micro-porosity is directly associated with increased sorptive and diffusive behavior. However, the effect of bioconversion on Darcian flow in the cleats has not been reported and will be the first focus area of the work presented in this dissertation.

Another distinctive feature of CBM reservoirs, setting it apart from traditional gas reservoirs, is the competing mechanisms of poro-mechanical cleat compression and desorption-induced matrix shrinkage governing the Darcian flow. Removal of water to initiate gas production results in reduction in pore pressure and, hence, increase in effective stress. The existing pressure that keeps the cleat apertures open, starts to decrease, thereby closing the cleats and decreasing the flowrates. On the other hand, as methane desorbs from the micro-porous coal surface, it results in shrinkage of the coal matrix which, in turn, results in widening of the cleat/fracture apertures in coal, thereby boosting flowrates. The shrinkage behavior competes with the changes in effective horizontal stress, dictating the flow patterns and permeability variation with depletion in CBM reservoirs. It is critical to have a detailed understanding of the flow and dynamic strain response of CBM reservoirs, and the impact of bioconversion on it, in order to model and predict techno-economic feasibility of a prospective MECBM reservoir. This will be the second area of focus of the work presented here.

1.3 Objectives of the Research

On the premise of improving the current understanding of the response of a reservoir to coal bioconversion, the overall aim of this dissertation is to investigate the following:

- Changes in flow-governing physical structure of coal (micro- and macro-pores) due to bioconversion.
- Validate previously reported variation in sorption and diffusion behavior in bioconverted coal.
- Determine changes in sorption-induced strain response in coal samples, post-bioconversion.
- Provide reservoir-scale insights into the expected flow-coupled-geomechanical response of a reservoir while undergoing bioconversion, and during production of the biogenic methane.
- Derive a theoretical framework identifying suitable conditions for coal bioconversion from a reservoir perspective and provide a parametric site-selection criterion.

1.4 Research Methodology

The work presented in this dissertation includes experimental investigation and reservoir scale analysis. These are summarized below:

- Experimental Investigation: This included laboratory experiments to determine the changes in macro- and micro- porous structure of Illinois coal using the scanning electron microscopy (SEM) techniques. Additionally, change in the sorption-induced-strain response of coal due to microbial treatment was investigated using dynamic strain measurement with helium and methane flooding.
- Reservoir Scale Interpretation: Experimental results were analyzed, providing insights into the reservoir-scale implication of coal bioconversion. The role of bioconversion on parameters governing flow-coupled-geomechanical behavior of a depleting biogenically recharged CBM reservoir is discussed. The measured and modeled variation in these parameters was then used to assess the effect of microbial treatment on a bioconverted CBM reservoir.

In order to accomplish the above tasks, the thrust of the dissertation is presented as three primary chapters. The major area of focus for each of the chapters is as follows:

Chapter 2 - Imaging Investigation: High resolution images of coal chunks were obtained using scanning electron microscopy before and after bioconversion to reveal changes in the physical structure of coal. Given that the physical (dual porosity) structure of coal dictates fluid flow and transport, changes in both micro- and macro-porosity were captured. Nanometer scale resolution images were used to understand the previously measured increase in sorption-diffusion behavior post-bioconversion. Additionally, micro- and millimeter scale resolution images provided insights into the previously undocumented changes in the macro-porous fracture network of coal.

Chapter 3 - Experimental Work: Solid coal matrix shrinks during methane production due to the desorption-induced-shrinkage behavior. Similarly, the matrix swells upon adsorption of methane. Ad/de-sorption-induced-swelling/shrinkage affects the cleat apertures, which dictate the Darcian flow in a CBM reservoir. Since bioconversion would result in storage of the produced biogenic methane in coal, which will subsequently be extracted during production, knowledge of sorption-induced-strain response of the reservoir is critical from a production perspective. This chapter focuses on the design and results of the experimental efforts undertaken to investigate the effect of bioconversion on coal's volumetric response. The obtained data was analyzed to understand the expected flow behavior during production form biogenically recharged depleted CBM reservoirs.

Chapter 4 - Reservoir Insights: The experimental data, as reported in chapter 3, was used to evaluate the reservoir-scale implications of coal bioconversion. Detailed analysis revealed the dependence of reservoir parameters, such as, Langmuir-type strain constants, rebound and recovery pressures on the volume of biogenic gas being produced. Additional insights into the

variation of solid-matrix and shrinkage-swelling compressibility was also evaluated. Finally, a theoretical analysis of the observed changes in reservoir-response post-bioconversion was used to rate the suitability of a reservoir to bioconversion.

Chapter 5 – Summary: The last chapter of the dissertation summarizes the major conclusions of the three preceding chapters, where the effect of bioconversion on the geomechanical and flow governing micro- and macro-porous properties are elucidated.

CHAPTER 2

IMAGING INVESTIGATION

This chapter presents an exact copy (except for format change) of the journal paper entitled “Imaging and fractal-based approach to understand reservoir-scale changes in bioconverted coal” published in *Fuel*, 2018. DOI: doi.org/10.1016/j.fuel.2018.04.171.

Authors:

Rohit Pandey, Satya Harpalani

Abstract

Microbially enhanced coalbed methane (MECBM) aims to replicate the natural process of microbial methane generation in coal under *in situ* conditions. Considerable work has been reported over the years to optimize the associated microbial geo-chemistry. However, there is very little insight with regards to changes in the physical structure of the coal due to bioconversion, and its impact on fluid flow properties. This paper presents the result of an image and fractal based approach used to evaluate the changes in physical properties of coal. Samples of coal treated over 30, 60 and 120 days respectively were imaged before and after bioconversion. The results revealed that coal bioconversion resulted in swelling of the coal matrix. Cleats narrower than 5 microns reduced in its width post-bioconversion. A 77% drop in permeability of coal is expected from the obtained results. Bioconversion also resulted in separation of thin layers of coal flakes from the coal surface, serving as a potential source of fines. Fractal analysis of the images revealed a smoother surface post-bioconversion, which is in agreement with previously reported studies, and corroborated the sorption-trends observed due to

bioconversion in previous studies. Bioconversion also resulted in formation of new pores/fractures. Shorter treatment duration resulted in nanometer-scale discontinuous pores, which do not contribute to Darcian flow. Longer treatment periods resulted in sub-micron wide continuous pores. Also, few larger fractures (>5 microns wide) saw an increase in its aperture post-treatment. This opens up new avenues, such as, utilizing artificially induced fracturing techniques to enhance biogenic methane production in future.

Keywords: Coal bioconversion, SEM imaging, fractal analysis, reservoir flow properties.

1. Introduction and Background

Burning natural gas (methane and higher hydrocarbons) to produce electricity results in half the CO_2 emissions compared to coal-fired power plants (Tollefson 2012). With the scientific community aiming to fuel the earth's energy needs leaving minimum carbon footprint, the use of natural gas is considered an inevitable transition from a coal-to-renewably fueled future. Emissions from burning natural gas also result in lower sulfur, mercury and particulate matter compared to burning coal (Agyarko and Mansoori 2013). Furthermore, recent developments in high-temperature and more efficient natural gas combustion turbines add to the lure of natural gas. While naturally occurring conventional gas deposits are easy to exploit, there needs to be an increase in the resource base to provide a sustainable solution to the world's energy demand. This has resulted in a surge in worldwide interest in unconventional sources of natural gas.

Methane stored in coal seams provides one such avenue to cater to the world's energy need. Since the eighties, methane from coal has been commercially extracted worldwide. Several coal basins, such as, San Juan and Powder River in the United States, have seen tremendous success (Moore 2012a). Given that coalbed methane (CBM) wells economically produce methane for more than twenty years, there exists at present, a number of depleted reservoirs

worldwide. Post gas depletion, the coal *in situ* remains, which could potentially serve as an untapped source of energy.

Significant amount of methane extracted from coal has microbial (biogenic) origin (Flores et al. 2008; Midgley et al. 2010; Penner, Foght, and Budwill 2010; Strąpoć et al. 2008). Hydrocarbon production, primarily methane, is a result of microbial breakdown of the organic fraction in coal (Ahmed and Smith 2001). Taking cue from the widespread application of microbes in the oil industry as a means to increase the overall recovery, Scott (Scott 1999b) introduced the concept of microbially enhanced coalbed methane (MECBM). MECBM is aimed at replicating the natural process of biogenic methane generation in coal by treating it with suitable microbial consortia and nutrient amendments. Following this, several research studies have provided evidence of the potential of generating methane by treating coal fines with microbial inoculations (Jones et al. 2010; Opara et al. 2012; Strąpoć et al. 2008; Suman and Harpalani 2018; J. Zhang, Liang, Pandey, et al. 2015).

Research in the area of MECBM has accelerated in the past decade due to a number of reasons. First, natural gas is a cleaner source of energy. Second, the technology has potential application to unmineable coals and abandoned coal mining operations. Third, vast amounts of coal fines, unusable when combusting coal for electricity production, are stored in slurry ponds worldwide, where microbial gasification provides a suitable solution to utilize this waste. Finally, several areas in mature coalbed methane producing coal basins, like San Juan, are depleted, or nearing depletion, providing the infrastructure required for injection of nutrients and subsequent production of biogenic methane.

Understanding and improving the microbial process to enhance methane production from coal requires extensive research. Over the years, the primary focus of research in MECBM has

been from a microbial perspective. It has been recognized that the process of bioconversion is a relatively slow process, with significant methane production under laboratory conditions requiring more than thirty days in most reported studies (J. Zhang, Liang, Pandey, et al. 2015; Ji Zhang and Liang 2017). Given that these studies were conducted on powdered coal, providing additional surface areas for microbes, production rates from *in situ* deposits is expected to be significantly lower and slower. Under such time-dependent production characteristics, it is important to identify the reservoir properties affecting flow and document the changes in these properties. Understanding associated reservoir flow characteristics would enable determining the techno-economic feasibility/pre-feasibility studies of the process.

Coal is characterized as a dual-porosity rock, where micro- and macro- porosity affect flow of fluids through coal. Micropores occur as a part of the coal matrix and serve as a storehouse for over 95% of the gas in adsorbed form (Gray 1987). The macropore system consists of a network of closely placed natural fractures surrounding matrix blocks, known as the cleat system. The dual porosity structure of coal dictates the gas flow and transport of fluids in the reservoir. In course of CBM production, pumping out water, which saturates the coal, reduces the pore pressure. This reduction results in desorption of methane from the microporous matrix surface, contributing to the first stage of fluid flow in coal. Once desorbed, molecules of methane diffuse across the complex pore geometry of coal in accordance with Fick's second law of diffusion. Methane then reaches the fracture network, that is, the cleat system, where the transport mechanism becomes Darcian, controlled by the permeability, and is dependent on cleat parameters, like the aperture, continuity and spacing. Experimental work conducted on powdered coal to characterize changes in sorption properties as a result of bioconversion was first reported by Pandey et al in 2016 (R. Pandey et al. 2016), and more recently by Zhang et al (R. Zhang et

al. 2017). It was reported that increase in micro-porous surface area post-conversion results in increased sorption capacity of coal. Bioconversion also resulted in increased diffusion rates for methane and carbon dioxide (R. Pandey et al. 2016). Such variations translate to increased microporous surface area available for sorption and altered pore geometry, resulting in increased flow rates (diffusive) at the microscopic scale. The effect of bioconversion on the third transport phenomenon, Darcian flow in cleats, is yet to be reported. It is well accepted that production from coalbed methane reservoirs is a function of the permeability of coal to methane and water. There exist a number of CBM reserves worldwide with significant gas content but are unattractive due to low permeability for commercial extraction of methane. An improved understanding of the Darcian flow and the effect of bioconversion on it is, therefore, critical in order to move forward with commercial application of the technology. This paper aims to elucidate the dynamics of permeability as a result of bioconversion.

Work presented in this paper was conducted on one-inch sized chunks of coal, providing smaller surface areas for the microbes to act on, and a better representation of *in situ* conditions. The coal samples were imaged before and after bioconversion using a scanning electron microscope (SEM). Treatment of coal chunks helped in retaining its overall physical structure, representing cleats and fractures associated with the coal type. High resolution imaging enabled studying the macro-/micro- porous geometries associated with the coal, and thereby documenting changes as a result of bioconversion.

Although two dimensional SEM images showing the surface of coal provide a reliable and a simple tool to characterize/study physical macroporous properties of coal, characterizing microporous properties bring unavoidable complexities, especially when working with grayscale images of coal. Use of fractal dimensions has proven to be a reliable approach under such

conditions. The fractal theory, proposed by Mandelbrot (Mandelbrot 1990), was successful in characterizing some irregular, unsmooth, and non-differentiable objects or shapes in nature. Starting from characterizing complexities associated with neurons in animal and plant morphology, to characterizing particle roughness and pore size distribution in soils, fractals have found application in a number of scenarios. Fractal characterization has also been successfully applied in studying the roughness, pore size distribution and adsorption behavior characterization of porous media, such as, coal and shale.

Fractals, characterized by their dimension (D), is a study of geometry. Researchers have characterized fractal dimension of coal by utilizing various methods, including mercury intrusion porosimetry, transmission electron microscopy (TEM), SEM, nuclear magnetic resonance (NMR), small X-ray scattering (SAXS) and gas adsorption techniques (Sun et al. 2015; Yang, Ning, and Liu 2014). In this study, we make use of the SEM images obtained to evaluate the fractal dimension of coal. The box-counting dimension, similar to the work reported by Liu and Nie (X. Liu and Nie 2016) in 2016 was used in this study and discussed in more detail in section 3.3.2.

The overarching goal of MECBM as a technology is to produce biogenic methane from *in situ* coal. The major goals of the work presented in this paper is to report changes in coal's flow governing dual-porosity structure, as observed from the SEM images, obtained before and after bioconversion. The findings aid in providing a deeper understanding of the effect of bioconversion to all the transport processes associated with flow in a coalbed methane reservoir.

2. Experimental setup and procedure

SEM imaging was used to study changes in the coal fabric due to bioconversion. Images were analyzed using the open source software ImageJ (Rasband 1997).

2.1 Sample procurement and preparation

Coal for this study was obtained from the Illinois #6 seam in southern Illinois. Large chunks of coal were broken into smaller, manageable sizes.

2.2 Imaging

Six chunks of coal, weighing ~10 g each, were obtained and numbered S1 through S6. Three pairs were formed, picking from the six randomly. The first pair P1 (S1 and S2) was treated for a duration of 30 days, the second pair P2 (S3 and S5) for 60 days, and he pair P3 (S4 and S6) for 120 days.

High resolution SEM imaging requires gold-palladium (Au-Pd) ion sputtering on the surface to be imaged. However, effect of sputter coating coal on the process of bioconversion was a serious concern. Hence, one sample from each pair was imaged with sputter coating and the second without it. Table 1 lists the samples used, specifying the treatment duration and the presence/ absence of sputter coating. The sputtered samples were imaged under the Everhart-Thornley detector (ETD), which is a back-scattered electron detector used in SEMs (Everhart and Thornley 1960). The un-sputtered samples were imaged under the better suited Large Field detector (LFD). The imaging exercise was conducted at the SIU Image Lab, with a FEI Quanta FEG 450 SEM. Sputtering was carried out using the Denton Vacuum-Desk II coater. The SEM imaging and sputter coating setups are shown in figure 1. Samples were coated for 120 seconds each, providing a 400 A^o thick coating. Images were obtained before and after treatment, which captured changes in the visible/measurable properties of coal as a result of bioconversion.

Table 1: Specification of samples treated

Sample Details	**30 Days (P1)**	**60 Days (P2)**	**120 Days (P3)**
Sputtered	Sample 2 (S2)	Sample 3 (S3)	Sample 6 (S6)

Unsputtered Sample 1 (S1) Sample 5 (S5) Sample 4 (S4)

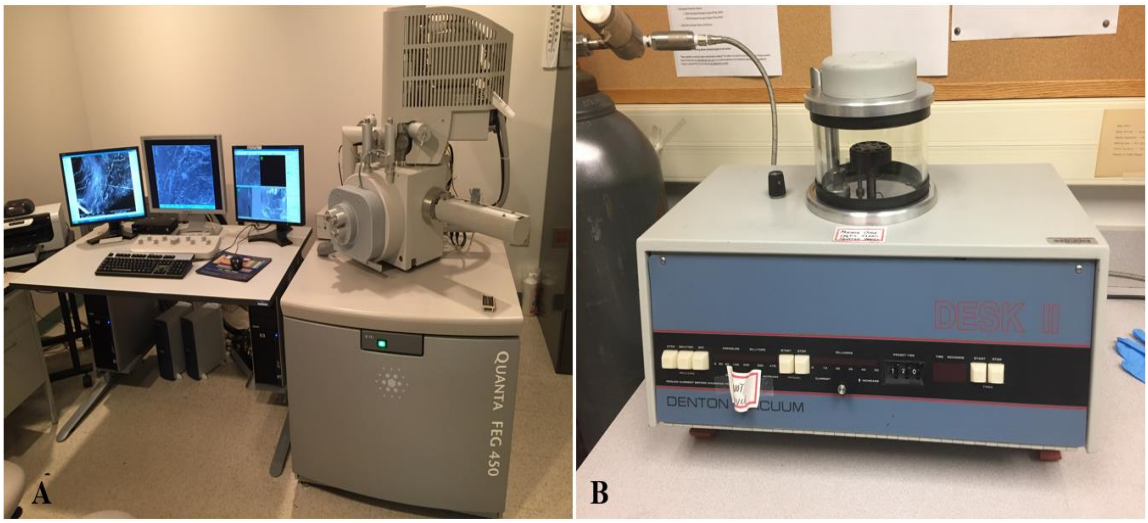

Figure 1: (A) SEM imaging setup used for this study, (B) Denton Vacuum-Desk II sputter coater.

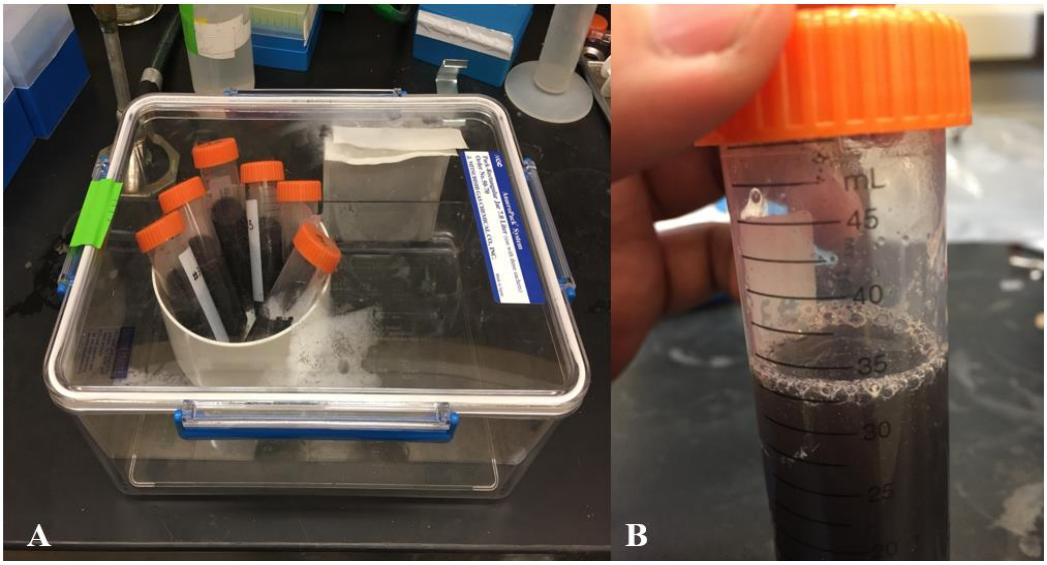

Figure 2: (A) Six vials containing samples for the imaging study, (B) A close up view of a vial during bioconversion

2.3 Treatment

As shown in figure 2, coal samples were treated in 50 ml airtight vials under anaerobic conditions, with nitrogen purged headspace. The vials were stored in a dark, airtight chamber at *in situ* temperature (32^{o}C) for the duration of treatment. Details of the treatment procedure can be found in Zhang et al (Ji Zhang and Liang 2017). Gas content was measured from each vial only when the duration of the treatment was complete. Gas production was not obtained at regular intervals to ensure integrity of the setup for the intended treatment duration. The composition of the gas produced was analyzed using a gas chromatograph.

3. Results and Discussion

3.1 Gas Content

Table 2 presents the amount of gas produced by the samples. The measured values were in moles of methane/gram of coal, converted to standard cubic feet of methane per ton of coal (scft), unit typically used in US operations. As seen from the reported values, each sample belonging to a single pair had similar volumes of methane produced as a result of treatment. This implies that *sputtering coal sample had no impact on the process of bioconversion* and should be the preferred approach in future imaging studies. Gas production for the first pair, treated for 30 days, averaged 258 scft. Gas production increased to 326 scft in 60 days. However, gas production in coal treated for 120 days was 140 scft. Reduction in methane production over longer treatment duration has been reported in the past (Ji Zhang and Liang 2017). Over time, the produced biogenic methane presents itself to be a readily bio-available substrate, instead of the more complex coal molecule. This results in a reduction in the methane content over time. Given that the work presented here aims to study the changes in physical coal properties due to bioconversion, variation in gas production and its implication has not been investigated.

Table 2: Methane production due to coal bioconversion.

Pair	**1 (30 days)**		**2 (60 days)**		**3 (120 days)**	
Sample	**1**	**2**	**3**	**5**	**4**	**6**
CH_4 Production (scft)	260	254	325	327	137	142

3.2 Images

A total of 9 random locations were imaged in the six samples, two each in samples 1, 2 and 3, and one location each for the remaining three samples. For every location, images were first obtained at low magnification (mm scale), and consequently magnified at intermediate steps to a higher magnification (nm scale). A total of 552 images were obtained for the six samples before and after treatment. Although a sizeable number of these images captured duplicate information, close to 200 images were selectively analyzed to ascertain the effect of bioconversion. Given the number of images analyzed, results from one specific sample **(sample 2)** are discussed in detail. Images from this sample encompass majority of the observed changes across all samples. For aspects of coal bioconversion that the sample failed to capture, certain images from other locations are also presented.

3.2.1 Sample 2

Sample 2 belonged to the first pair, that is, treated for 30 days. Images of two different locations were obtained after sputtering.

3.2.1.1 Location 1 (S2_L1):

A total of 18 images were acquired at the first location in sample 2. The maximum resolution providing images at one micron scale was obtained at a magnification of 374,500. Five pairs of images are presented below.

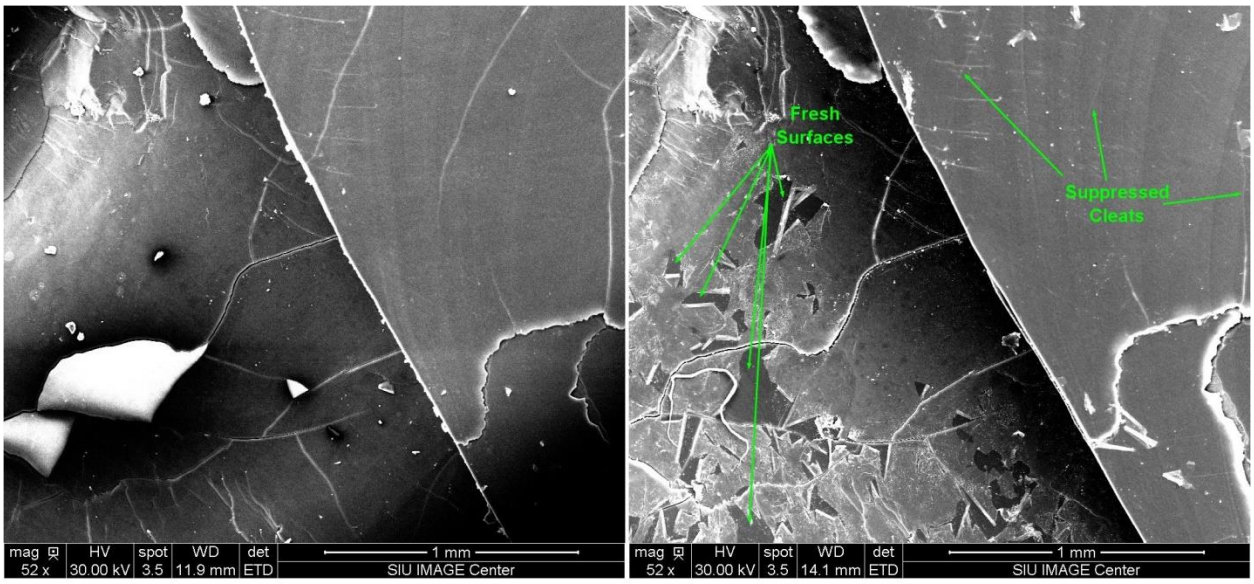

Figure 3: Before and after bioconversion images of S2_L1 at 1 mm resolution.

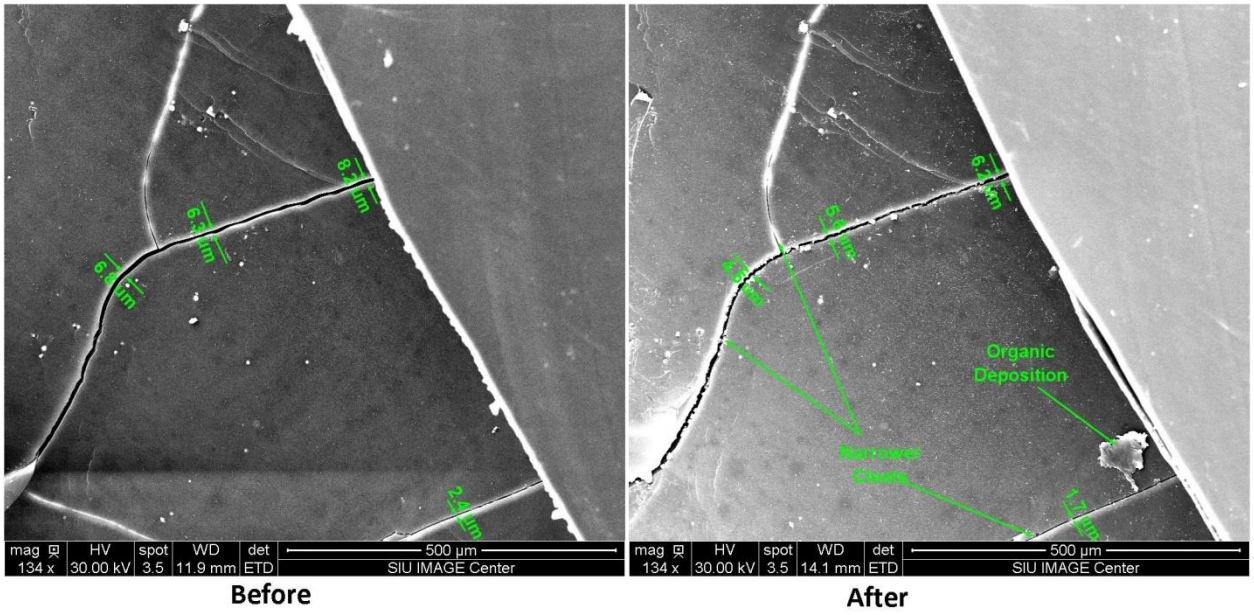

Figure 4: Before and after bioconversion images of S2_L1 at 500 micron resolution.

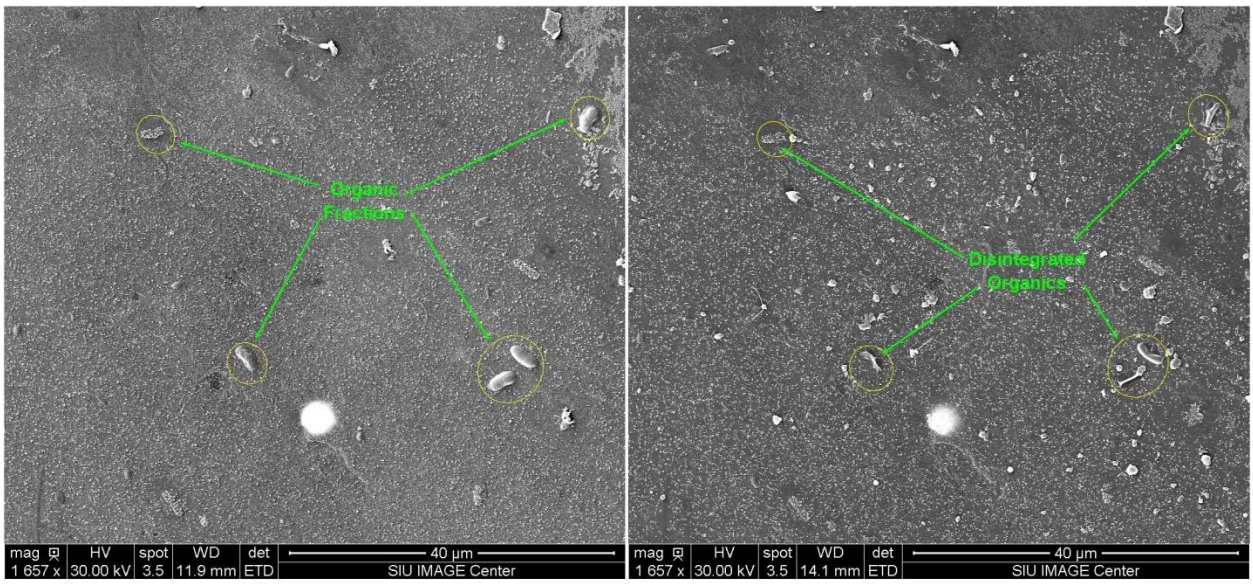

Figure 5: Before and after bioconversion images of S2_L1 at 40 micron resolution.

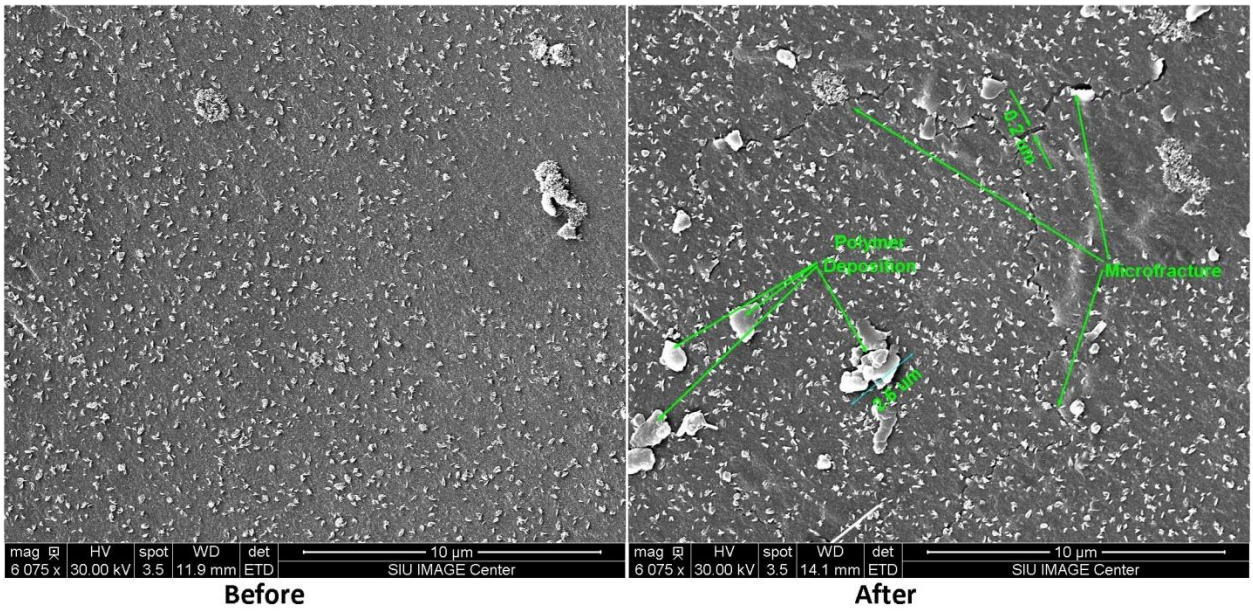

Figure 6: Before and after bioconversion images of S2_L1 at 10 micron resolution.

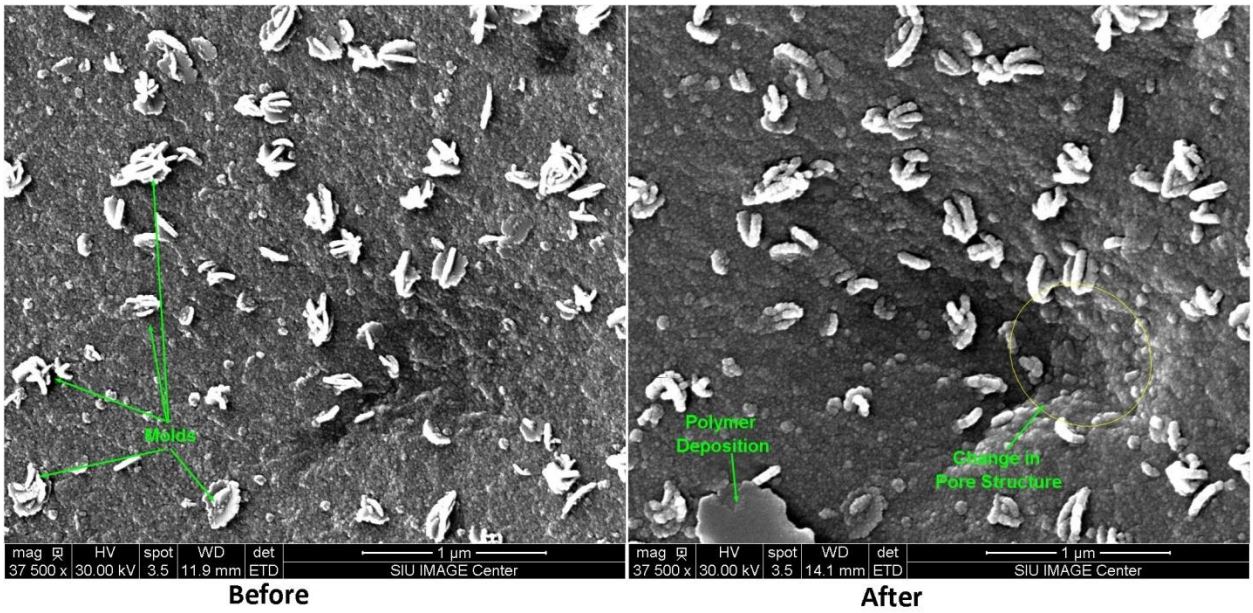

Figure 7: Before and after bioconversion images of S2_L1 at 1 micron resolution.

Following observations are made from the acquired images from S2_L1:

a) Pre-treatment, the image (figure 3) showed a distinct cleat/fracture geometry. However, post-bioconversion, the cleat geometry appeared suppressed and hard to distinguish. A few of these cleats/fractures, as seen in figure 4, reduced in width by ~20%.

b) Figure 3 showed missing flakes of coal from the coal surface post-conversion.

c) Figure 5 highlights the organic fraction preset on the coal surface, which degraded as a result of microbial treatment. This particular location in the sample was infested with mold, as shown in figure 7, which possibly enhanced the degradation of easily available (visible) organics in the sample.

d) Bioconversion of coal results in deposition of polymers on coal surfaces. This has been observed across all samples imaged, and can be seen in figures 6 and 7.

e) Figure 6 shows a visible microfracture, ~200 nm wide, extending across the sample, formed as a result of treatment. Bioconversion of coal results in the formation of such

microfractures/pores in the matrix. Such fractures were observed in all samples imaged in this study.

3.2.1.2 Location 2 (S2_L2):

A total of 23 images were acquired at the second location in sample 2. The highest resolution providing images at a 300 nm scale was obtained at a magnification of 185,881. Four pairs of images are presented below.

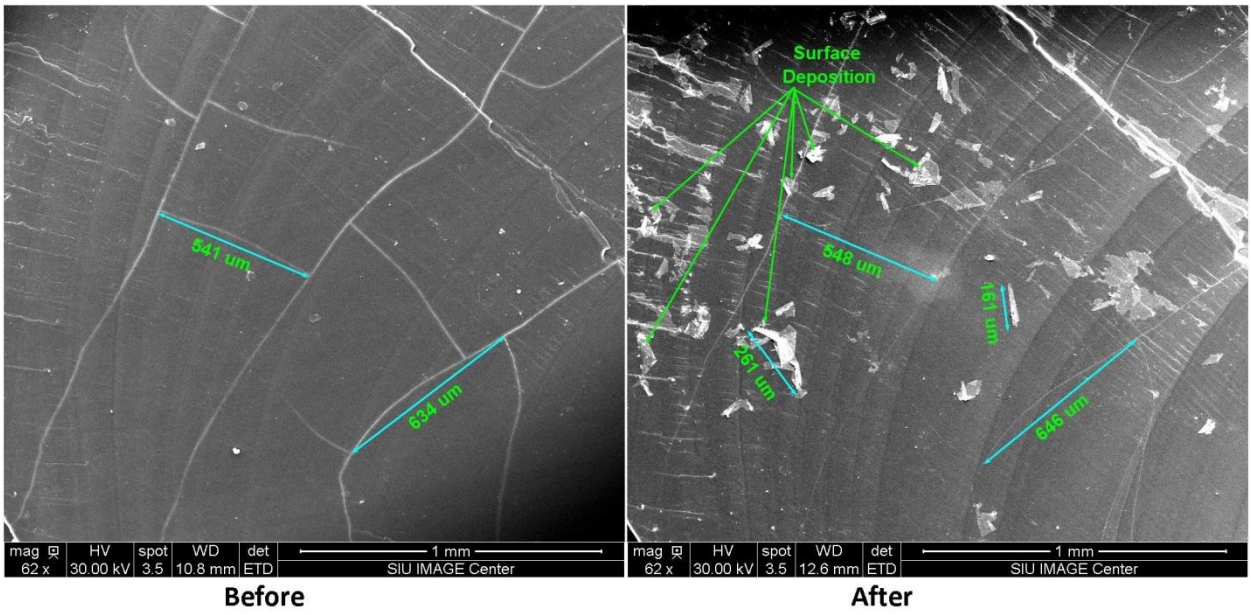

Figure 8: Before and after bioconversion images of S2_L2 at 1 mm resolution.

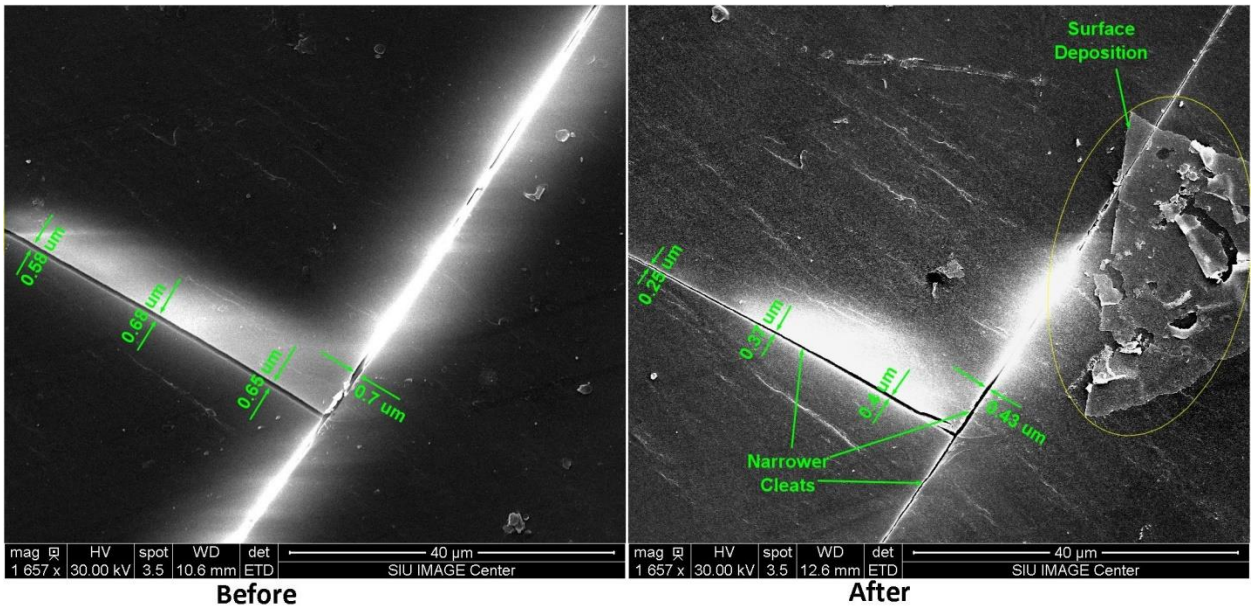

Figure 9: Before and after bioconversion images of S2_L2 at 40 micron resolution.

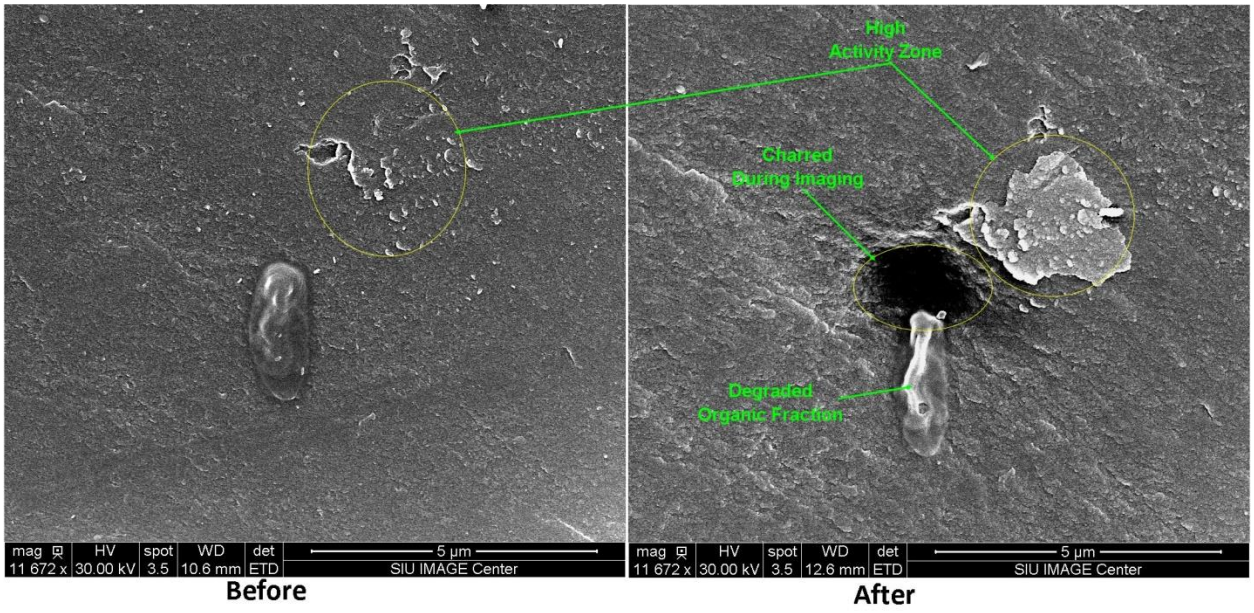

Figure 10: Before and after bioconversion images of S2_L2 at 5 micron resolution.

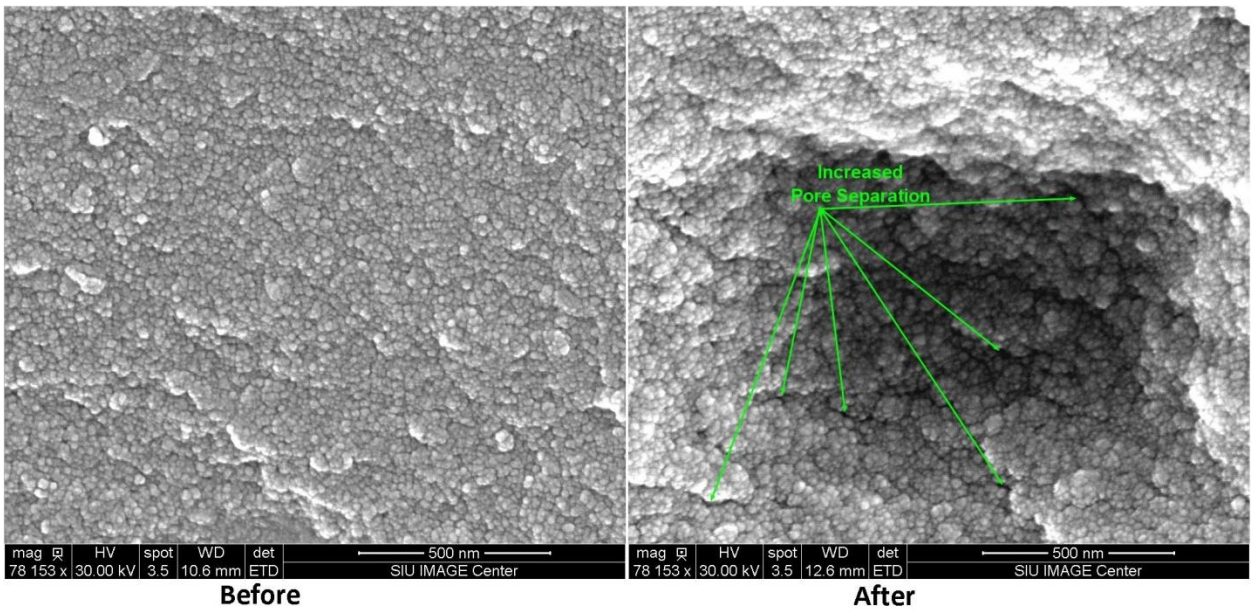

Figure 11: Before and after bioconversion images of S2_L2 at 500 nanometer resolution.

The following observations are made based on the images acquired from S2_L2:

a) This particular location exhibited a distinct face and butt cleat geometry, as seen in figure 8. The cleat spacing before treatment was ~0.5mm.

b) Linear measurements along specific locations on the matrix revealed that there was swelling post-conversion. Two specific locations shown in figure 8 revealed linear swelling of ~1.5%. The measured strain (= change in length/original length) at the two locations were 0.0129 and 0.018 respectively. As illustrated in figure 9, the visible cleat width reduced by ~50% post-treatment.

c) Post-conversion, as seen in figures 8 and 9, the sample had numerous depositions on the surface. Compared to the polymer films and other organic depositions noticed previously, the size of these deposits is larger (>100 microns) and can be characterized by elemental disperse X-ray (EDX) tests, which was beyond the scope of this study.

d) Clusters of bright spots visible on pre-treated coal in figure 10, indicative of the presence of concentrated organic fractions, showed significant changes in its structure post-

treatment. As was apparent in the last set of images, degradation of organics was also observed post-treatment.

e) Looking at images in the nanometer scale (figure 11), new pores form in treated coal post-treatment. Open pores present themselves as dark spots in a lighter colored surrounding. There is an increase in the density of these dark spots in treated coal. The central portion of the image of treated coal was slightly charred during the process of focusing. However the opening up of pores, possibly due to swelling of the matrix during treatment is clearly exhibited.

3.2.2 Other Locations

Presented below are 5 pairs of images across other samples that were imaged in this study. Effects of bioconversion on the physical properties of coal are distinctly visible in these images.

Figures 12 and 13 are obtained from the first location in sample 5 (S5_L1). There are visible changes in the matrix porosity, as seen in figure 12. Matrix swelling resulted in opening up of a 0.2 micron wide circular pore to 0.4 micron post bioconversion. A narrow (<0.1 micron) pore entry widened to 0.14 microns post-bioconversion. Nearby regions of the widened pore in figure 12 show distinct changes in its geometry along the vertical (Z) profile , with rounded edges of pores in the matrix distinctly visible. A magnified image of the same location at 500 nm scale (figure 13) shows formation of a new pore/microfracture after bioconversion. At the widest point, the new pore was 270 nm in width and 690 nm in length. Sub-micron wide fractures running along the length of the image were also developed post-bioconversion in sample 6, as seen in figure 14.

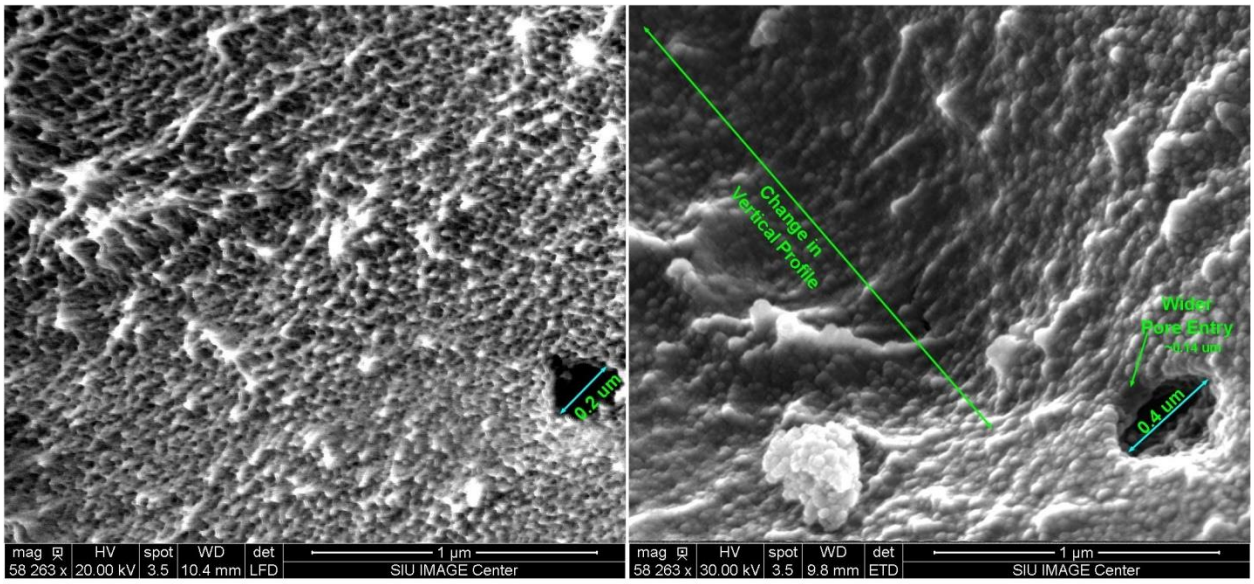

Figure 12: Before and after bioconversion images of S5_L1 at 1 micron resolution.

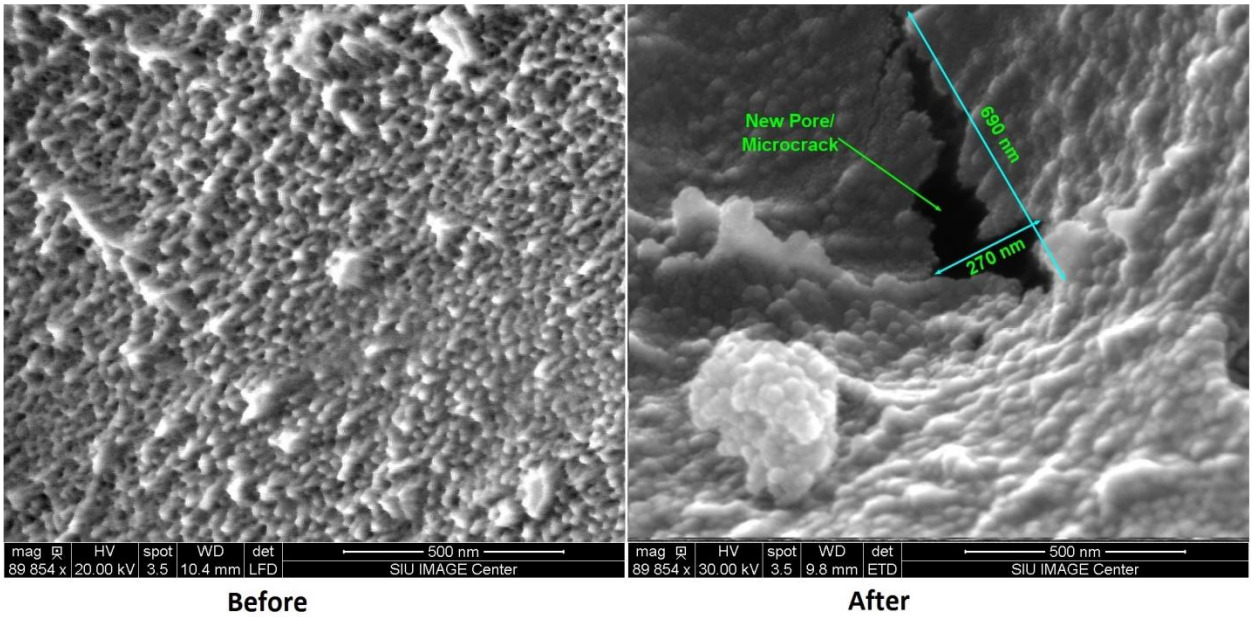

Figure 13: Before and after bioconversion images of S5_L1 at 500 nanometer resolution.

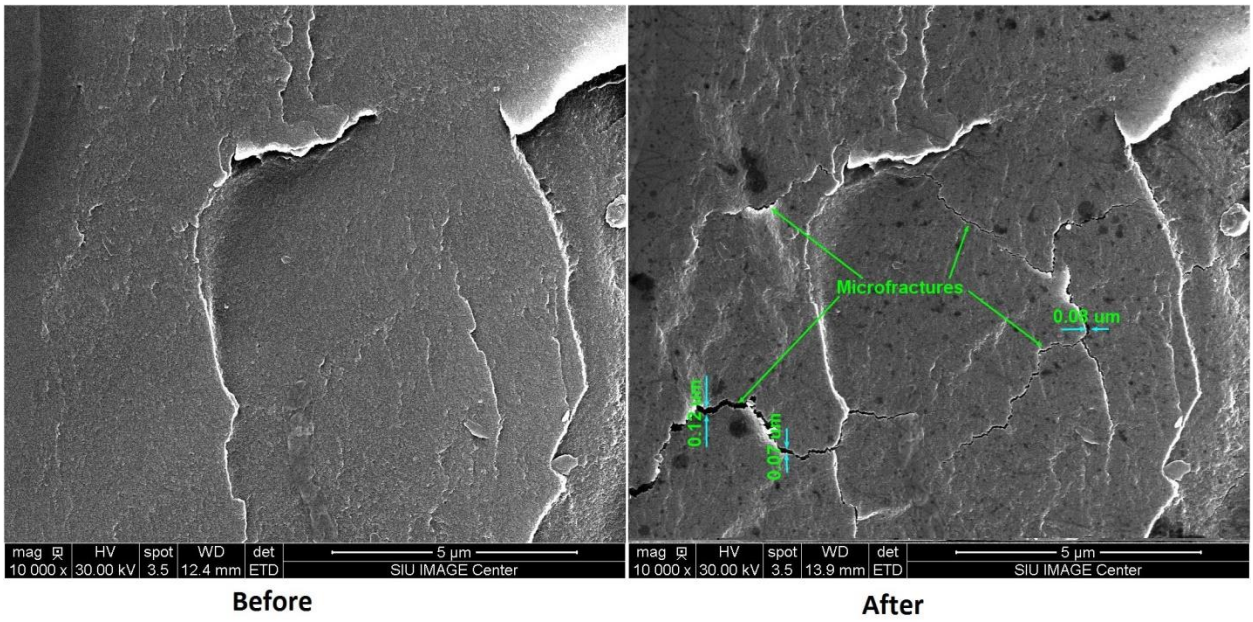

Figure 14: Before and after bioconversion images of S6_L1 at 5 micron resolution.

Figures 15 and 16 are images of sample 3. Figure 15 presents a set of two fractures/cleats forming an inverse T-junction. The fracture imaged along the top half of the sample, as seen in the figure, was 2.6 microns. Post-bioconversion, as seen in other samples, the cleat width reduced by ~30% to 1.8 microns. However, the second fracture, forming the base of the inverse T junction, 6 micron wide before treatment, more than doubled in width to 13 microns post-treatment. Such increase in fracture width was not a single occurrence. Across the nine locations imaged, few cleats/fractures presented with widths greater than 5 microns. Increase in cleat width post-bioconversion was observed in these wider fractures.

Also visible in figure 15 are dark spots as a result of flaking of the coal surface post-treatment. Figure 16 provides a zoomed view of one such spot, where a section of the coal surface is missing. Adjacent to the flaked out spot, cracks are visible along the coal surface, indicative of the coal weakening. These missing coal flakes are a potential source of fines in the reservoir.

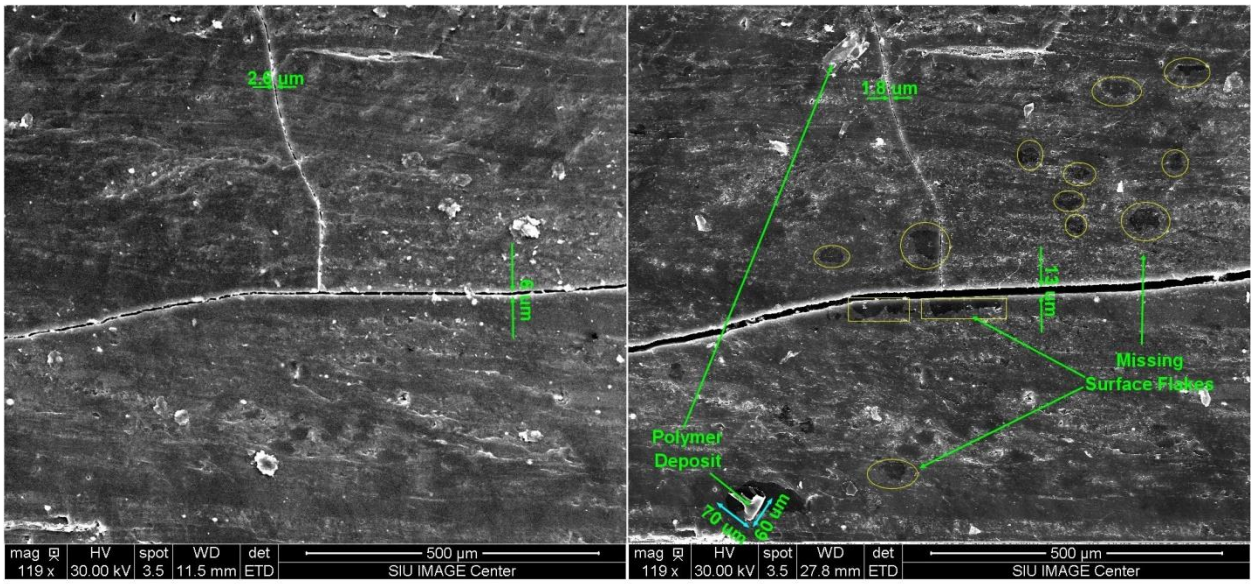

Figure 15: Before and after bioconversion images of S3_L1 at 500 micron resolution.

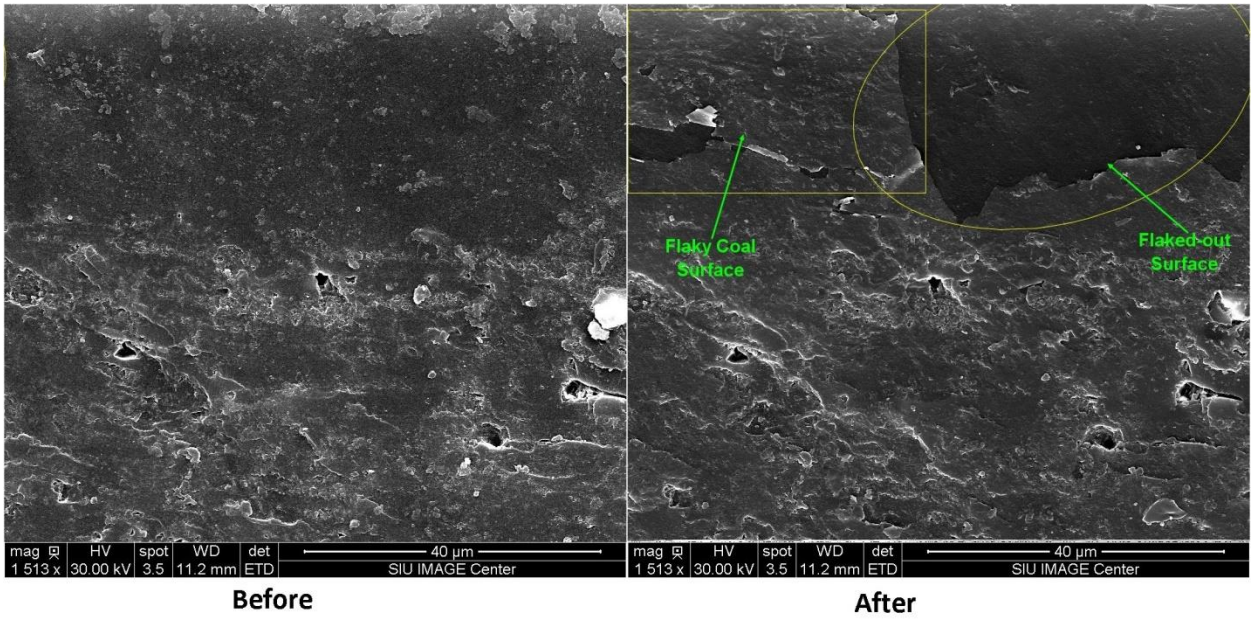

Figure 16: Before and after bioconversion images of S3_L1 at 40 micron resolution.

3.3 Fractal Dimension

As discussed previously, coal has a dual porosity structure. The complexity of such structure can be characterized by fractal dimension. The box-counting dimension used in this study can effectively characterize the coal surface geometry.

3.3.1 Image Processing

It is not possible to use the original gray-scale SEM images to conduct surface fractal analysis. Such analysis requires the image to be transformed into binary (black/white) images. A few studies have suggested direct conversion of gray-scale SEM images to binary after using the gray-scale global thresholding method (C. Liu et al. 2011; X. Liu and Nie 2016). The arbitrary thresholding affects the geometric patterns, resulting in an erroneous representation of the original image. Work presented by Perrotti et al (Perrotti et al. 2011) in 2011, also suggested skeletonizing the binary images, thereby resulting in easier pattern evaluation for fractal analysis.

Coal is massively heterogeneous at both macro-/microscopic scale. This results in a widely distributed gray-scale SEM images across all levels of magnification. The use of a bandpass filter, built into ImageJ, normalizes such variations, by removing the high and low spatial frequencies, which form a major fraction of noise associated with the images. The larger structures were filtered down to 3 pixels and the smaller structures up to 1 pixel using the bandpass filter. The resultant images post filtration contained the required surface characteristics, minus the noise associated with the data. The use of a single filter for global analysis (for all images) nullified the errors associated with manual image thresholding. Binary images were then obtained from the filtered image, which were subsequently converted to a skeletal form required for fractal analysis. Figure 17 illustrates the process for one image.

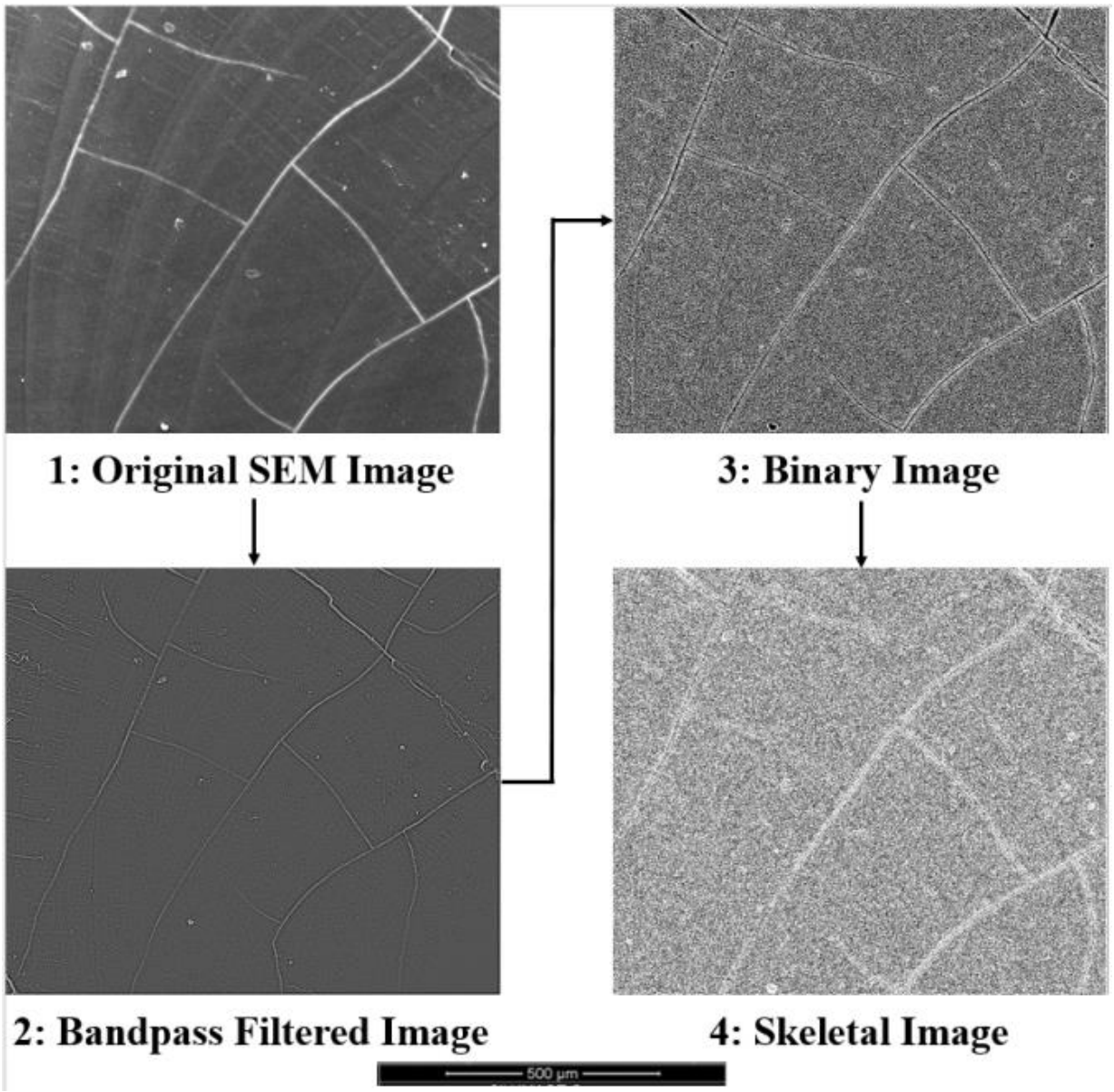

Figure 17: Image processing of a specific image required for fractal analysis.

3.3.2 Data Processing

Using the box counting method to calculate the fractal dimension of coal from the processed images, the dimension, D, was defined as:

$$D = -\lim_{\delta \to 0} \frac{\ln (N(\delta))}{\ln (\delta)},$$

where, δ is the box size, $N(\delta)$ is the number of boxes needed to completely cover the binary image. The slope of the plots of ln $(N(\delta))$ vs ln (δ) generates the fractal dimension D, which can vary from 1, for a perfectly smooth surface, to 2 for a surface with complex geometry. Figures 18 to 20 presents the results of the fractal analysis, where "Px Sy Lz" corresponds to pair X, sample Y and location Z. Samples 4, 5 and 6 had one specific location imaged. Each figure presents the dimensions obtained from the pairs of samples imaged. Images were obtained for increasing magnifications for a specific sample, at a specific location. The fractal dimension for each image was obtained by using the fractal box-counting tool built into ImageJ. All plots (not shown here) displayed good fits, with R^2 greater than 0.99.

Over the course of imaging a coal sample across increasing levels of magnification, often times there are features imaged that contribute to significant sources of error, such as, presence of sharp edges within the region of interest, neighboring (external) features being captured, or cases where intensity of light reflection from specific locations affected the image quality. The frequency of occurrence of these factors, resulting in noise (errors in image acquisition and processing), was primarily limited to images obtained at low magnification. The threshold for the samples imaged is marked by a green bar in figures 18 to 20. Images obtained at a magnification to the left of the threshold presented with significant errors. As images at increasing levels of magnification were obtained, we proceeded from imaging coal's macro-structure to imaging its micro-structure, which is the coal matrix. Across all graphs presented in figures 18 to 20, for all locations imaged, the calculated fractal dimensions approach a constant value with increasing magnification. The values of D obtained below the threshold vary significantly from the average values above the threshold. Few studies have suggested use of images at a specific magnification to characterize fractal dimensions of coals and shales (X. Liu and Nie 2016; Song et al. 2004),

which evidently associates errors with such measurements beyond statistical negligence. It is evident from the results obtained that *characterizing fractal dimension of coal from image analysis requires the sample to be imaged across multiple levels of magnification.*

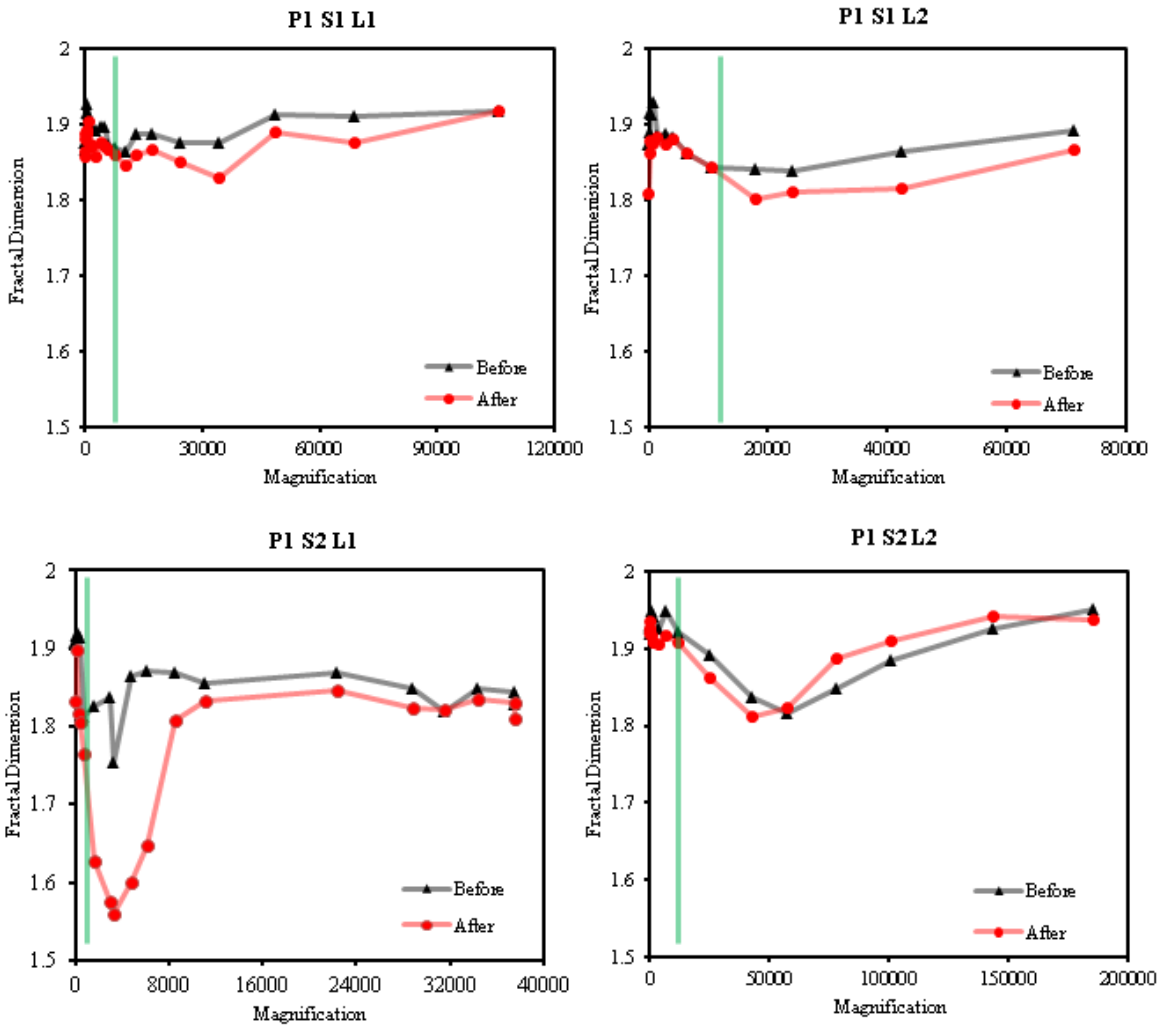

Figure 18: Change in fractal dimension of coal before and after bioconversion for Pair 1.

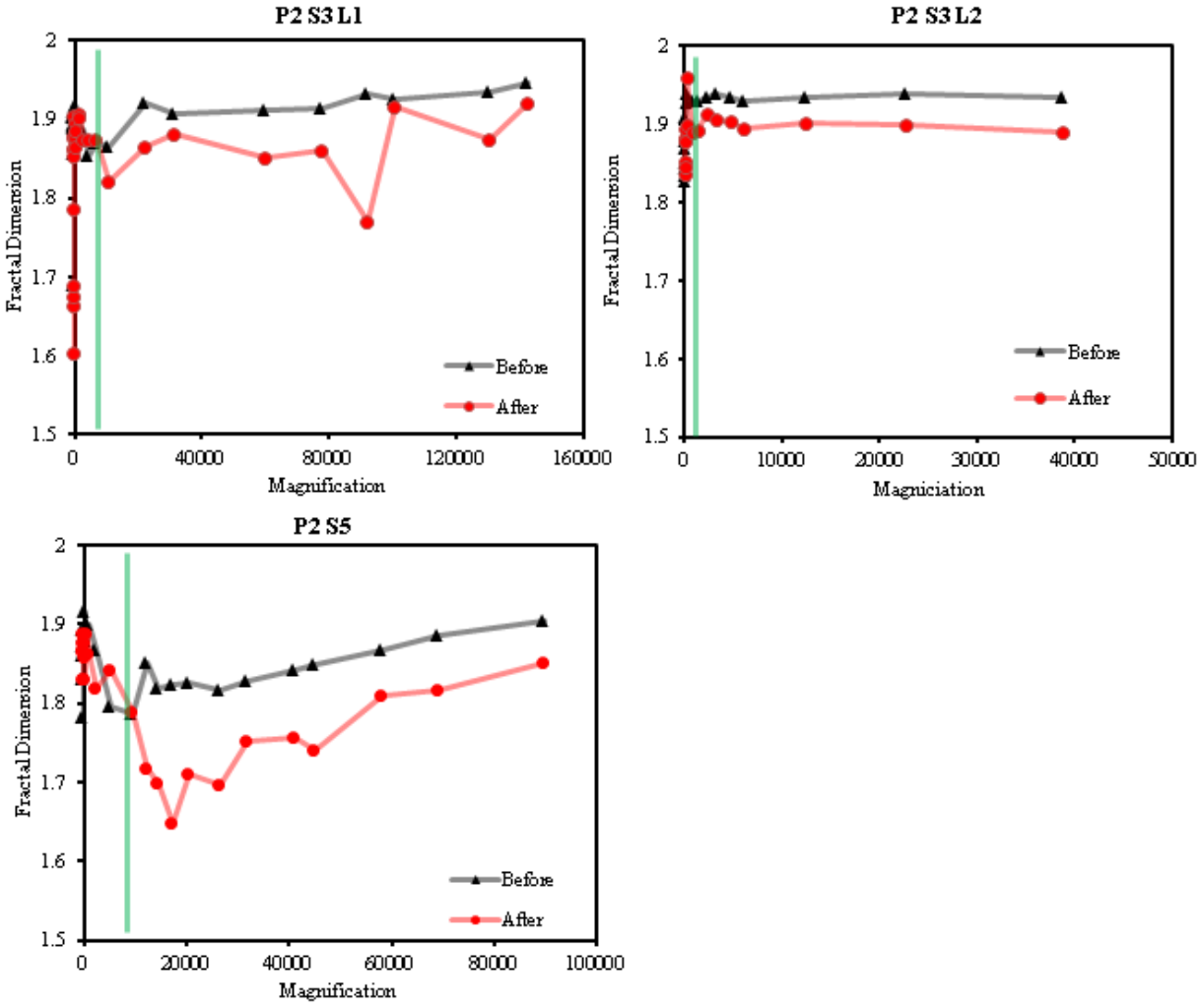

Figure 19: Change in fractal dimension of coal before and after bioconversion for Pair 2.

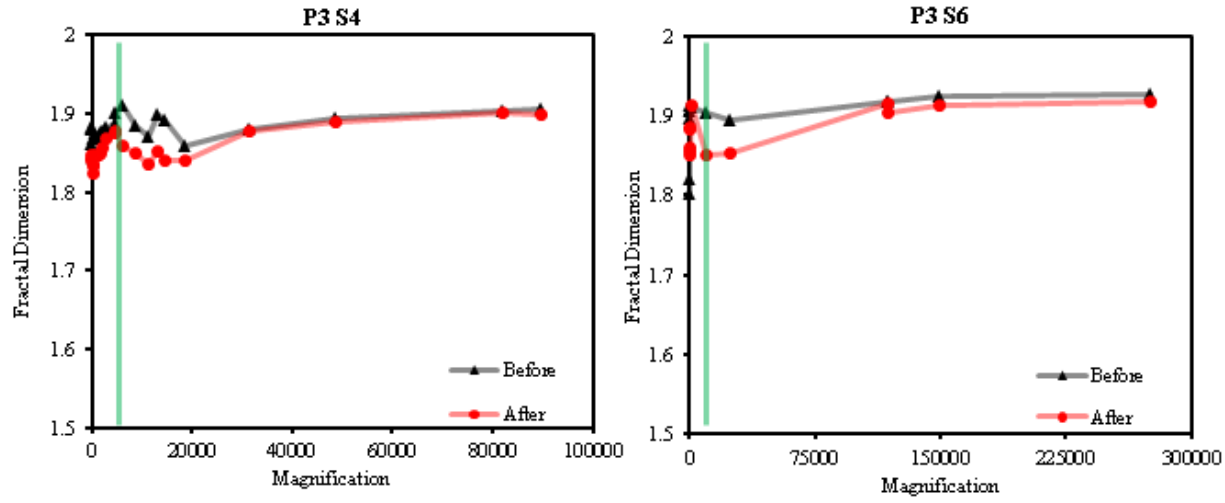

Figure 20: Change in fractal dimension of coal before and after bioconversion for Pair 3.

3.3.3 Fractal Data Interpretation

As evident from figures 18-20, bioconversion of coal resulted in decrease in its fractal dimension. This decrease bears relation with the volume of gas produced by coal. As seen in figure 20, samples 4 and 6, which produced the least amount of methane, had their fractal dimension decrease by 0.02 and 0.01 respectively. Dimensions of samples 3 and 5, presented in figure 19, decreased by 0.04 and 0.05 (initial – final) respectively. Samples 3 and 5 also had the maximum methane production. Decrease in the fractal dimension of sample 1 was 0.03. In sample 2, the first location had noticeable errors associated in the fractal dimensions obtained at low magnification. For the more reliable high magnification images that present a consistent trend in the observed values, the decrease in fractal dimension was 0.02. The general trend of decreasing fractal dimension was not observed in the second location of sample 2. Such aberration is attributed to the presence of molds in the sample. Coals or, locations with mold infestations, are not suitable locations for microbes to attach themselves to in order to produce methane. Moreover, presence of such infestations dictates the geometrical patterns in the images, and the change in fractal dimensions cannot be interpreted as a direct result of bioconversion. A reduction of fractal dimension post-bioconversion is indicative of a smoother matrix surface. The coal samples treated were arbitrarily selected after breaking down a larger block of coal. This resulted in samples with rough surfaces. It has become evident from the obtained images that, over the period of bioconversion, there is production of coal flakes, possibly fines. This suggests that, over the duration of bioconversion, consumption of organics at/around these rougher edges was preferential. Even in the images at submicron-nanometer level magnification, where samples did not demonstrate substantial loss of coal, the fractal dimension decreased. This

is indicative of a smoother boundary between micropores and coal. Swelling of the coal matrix, resulting in formation of numerous microfractures and pores corroborate the observed results.

3.4 Interpreting Results from a Reservoir Perspective

Measurement at specific locations within the matrix revealed swelling of the coal matrix due to bioconversion. Over a period of thirty days, maximum linear swelling strain measured in sample 2 ranged between 0.01 and 0.02. Matrix swelling resulted in reduction of cleat widths less than 5 micron wide, which is directly associated with the permeability of fluids in the coal reservoir. It was established by Sawyer et al. (Sawyer, Paul, and Schraufnagel 1990), and later by Harpalani and Chen (Harpalani and Chen 1995), that the permeability and porosity of coal can be determined from physical properties of coal structure, such as, aperture width cleat spacing (a) and aperture width (b) using the relationship:

$\Phi = \frac{2b}{a}$ and, $k = \frac{b^3}{12a}$,

where, Φ is the cleat porosity and k is the permeability.

The cleat structure of coals tested is well captured in Sample 2. The values obtained before and after bioconversion from S2_L2 would constitute a sample calculation illustrating the changes in porosity and permeability of coal due to bioconversion. The results are illustrated in table 3.

Table 3: Variation of porosity and permeability due to bioconversion.

S2_L2	Spacing (m)	Aperture (m)	Cleat Porosity (%)	Permeability (md)
Before	5.41E-04	6.50E-07	0.24%	0.0429
After	5.48E-04	4.00E-07	0.15%	0.0099

As evident from the images obtained, and the results presented in Table 3, bioconversion of coal caused development of un-recoverable swelling strains. Matrix strains are traditionally associated with ad-/de-sorption of methane in CBM reservoirs. Differentiating a CBM reservoir from other natural gas reservoirs is its sorption-induced-swelling property. Sorption of methane in the coal matrix results in swelling of the matrix. Extensive laboratory investigations have revealed that the strain developed due to sorption of methane on coal is a reversible process, where the developed strains are recovered with subsequent desorption (Levine 1996a; S. Liu and Harpalani 2013; Palmer and Mansoori 1998; J.-Q. Shi and Durucan 2005; J. Q. Shi and Durucan 2004). Liu et al (S. Liu, Wang, and Harpalani 2016) characterized the volumetric strain behavior of Illinois coals, where maximum sorption induced volumetric strain was measured to be 0.0096. Volumetric strain is the summation of the linear strains obtained in the three principal: X, Y and Z directions. The linear swelling strain due to bioconversion, measured (in one direction) in this study ranged from 0.01 to 0.02. Thus, the unrecoverable matrix strain developed due to bioconversion, was higher than the (recoverable) sorptive strains developed in Illinois coals only due to sorption of methane. It is difficult to identify the specific factors that resulted in the development of such unrecoverable strains. Loss of elastic constituents of coal, especially the highly organic and elastic macerals due to biodegradation (Xie 2015) or, imbibition of water and/or moisture sorption during treatment in a saturated environment, are some probable factors which could influence such behavior. Investigating these factors was beyond the scope of this study, but provide a direction for future research.

At the end of the treatment, swelling of the matrix resulted in a narrower cleat width for cleats less than 5 microns in width. Given that permeability is directly proportional to the cube of cleat width, the calculated permeability of the sample decreased by 77%, from 0.043 mD to 0.01

mD. Such decrease in permeability would directly affect production rates in the reservoir. Andrew Scott in his introductory paper on MECBM envisioned increase in cleat aperture/width as a result of bioconversion, resulting in increased flowrates in the reservoir. However, swelling of the coal matrix due to bioconversion was not accounted for. The effect of bioconversion induced swelling of coal clearly reduces the Darcian flow through coal. Hence, *bioconversion of coal, based on current techniques, is detrimental to a CBM reservoir from a production perspective*.

As a result of the localized reservoir stress history, there also exist natural fractures which are wider (>5 microns) and less frequent than cleats in Illinois coals. A number of these wider fractures increased in their aperture post-bioconversion, contrary to what was observed in the commonly occurring narrow cleats. Increase in fracture width translates to increase in permeability. However, since permeability bears a cubic relationship with cleat width/porosity, a 99% decrease in cleat width results in 6 orders of decrease in permeability, whereas 99% increase in cleat width, increases permeability by only one order of magnitude. The variation of permeability for constant cleat spacing with change in cleat width is shown in figure 21. Given that reduction of cleat width is the more commonly occurring outcome of bioconversion, although increase in fracture/cleat width results in increased flowrates, the overall effect of treatment is still negative.

It is possible that, given the wide fracture/cleat aperture existing before treatment (as seen in figure 15), additional surface area around the fracture was available to the microbes. Wider aperture also makes movement of the microbes within coal fractures easier. The microbes associated with bioconversion measure a few microns in their smallest dimension (Jabłoński, Rodowicz, and Łukaszewicz 2015). Cleats with submicron apertures restrict the movement of

microbes, thus hindering the ability of microbes to consume more coal to produce methane. The behavior of larger fractures to bioconversion opens up the possibility of using artificially induced fracturing techniques to enhance *in situ* biogenic methane production. However, the current experimental work was conducted under unconstrained (absence of horizontal and vertical stresses acting on *in situ* coal) conditions. The effect of *in situ* horizontal stresses to the entire process is unknown.

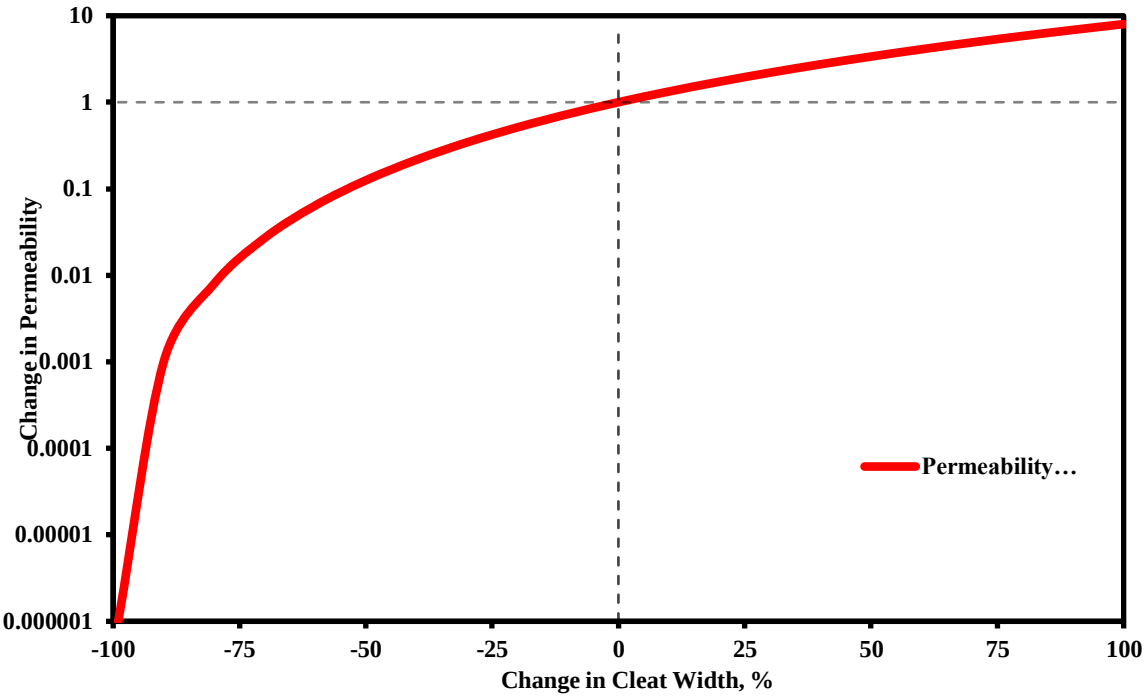

Figure 21: Variation in permeability with change in cleat width. (Intersection of dashed lines provides the starting reference point for permeability and cleat width)

Matrix swelling due to bioconversion resulted in the formation of new sub-micron wide micro-fractures/pores in coal. Formation of such fractures post-bioconversion was captured in numerous images across all samples imaged. As seen in figures 11 and 13, a number of these new pores were only a few nanometers wide, and discontinuously scattered across the coal matrix. Given the discontinuity and size of these pores/fractures, its impact in potentially

boosting Darcian flow through the coal would be negligible. However, for sample 4, treated for the longest duration (120 days), as seen in figure 14, a number of continuous sub-micron wide fractures developed post-treatment. This opens up the possibility of increased Darcian flow post long treatment periods, and provides an avenue for future research.

Although swelling of the matrix resulted in narrower cleats, its effect on the coal microstructure can be well understood from figure 12. As observed in the set of images, a submicron wide pore doubled in its size from 0.2 to 0.4 microns. Previous studies investigating the microporous properties of coal concluded that bioconversion increases the pore surface area of the coal by consuming coal, thereby creating new pores (R. Pandey et al. 2016; R. Zhang et al. 2017). The possibility of bioconversion induced matrix swelling, possibly resulting in increased pore surface areas, was not envisioned. Figure 12 clearly exhibits a swollen matrix, increasing the size of the visible pore and, in turn, increasing the microporous surface area. Pandey et al (R. Pandey et al. 2016) also reported higher diffusion rates for methane post-bioconversion. Diffusion of methane in coal is a function of the pore geometry. A narrower micropore entry would restrict the movement of gas in comparison to a wider micropore entry. As seen in figure 12, the micropore entry that was less than 0.1 micron increased in its width to 0.14 microns post treatment, thereby facilitating higher rates of diffusion in bioconverted coal.

Bioconversion resulted in flaking of the coal surface along the bedding plane. This is indicative of weakening of coal, potentially leading to formation of fines due to bioconversion. Fines in a coalbed methane reservoir block cleats and fractures, slowing down the flow of gas/water through them. Along with formation of fines, extensive polymer/organic deposition was also observed in the images obtained post-bioconversion. Such depositions, along with reduction in cleat width, serve to block the matrix micropores, potentially reducing the sorption

capacity, permeability and bioavailability of coal to the microbes. There potentially exists an encouraging result of the formation of fines, as they provide additional surface areas for the microbes to feed on. Experiments conducted by Zhang et al (Ji Zhang and Liang 2017) measured methane production exceeding 1000 scft from powdered coal. Methane production from the samples in this study was an order magnitude lower than the values reported for powdered coal. Hence, coal fines generated as a result of bioconversion failed to have a significant impact to boost methane production.

Liu and Nie (X. Liu and Nie 2016) (2016) extensively studied different types of coal from a fractal and sorption perspective. They concluded that fractal dimension of coal is inversely proportional to the Langmuir pressure constant (P_L). Decrease in fractal dimension due to bioconversion results in an increase in the P_L value of biotreated coal. This trend is in agreement with the experimental results published by Pandey et al (R. Pandey et al. 2016), where sorption trend of Illinois coals post-bioconversion resulted in substantial increase in the values of P_L. Change in P_L can be well understood by understanding it from a pore complexity perspective: a molecule of methane can ad/de-sorb on a perfectly flat surface of coal relatively easily. Any increase in surface roughness/complexity will make it harder for the sorbing molecule to find a location for sorption, resulting in higher values of P_L. Bioconversion of coal results in the formation of new pores/fractures, adding to the complexity of the porosity, thereby increasing the P_L. Hydrostatic pore pressures existing in the Illinois basin is a maximum of ~500 psi, which is relatively low. Such conditions are suitable for coals with low P_L, where volume of gas desorbed at lower pressures is significant. Thus, for basins such as Illinois, bioconversion fails to boost potential desorption rates. However, if the drop in P_L is a consistent trend, deeper coal

seams might be better suited for bioconversion, where early methane desorption with depletion would boost economic turnaround time.

3.5 Conceptual Model of Coal during Bioconversion

The results presented above were used to develop a conceptual structural model of coal, illustrating the changes as a result of bioconversion. The matchstick model is a well-accepted representation of coals macrostructure, where individual matchsticks make up the matrix block, with face and butt cleats separating different matchsticks. Figure 22 illustrates the matchstick model in plan view (as seen perpendicular to the bedding plane). Theoretically, each matchstick extends over the height of the coal seam. The first section (A) of figure 22 shows a coal block before bioconversion. The second (B) and third (C) section illustrates the effect of bioconversion, where bioconversion of coal resulted in swelling of the matrix as seen in the second section. The strains experienced by the coal due to swelling are unrecoverable, and results in creation of nanometer scale cracks and microfractures in the coal matrix, which were discontinuous in coals treated for shorter period. Longer treatment periods resulted in sub-micron scale continuous fractures in the coal matrix.

Figure 23 presents a conceptual model of a coal's microstructure and presents the changes as a result of bioconversion. Bioconversion induced matrix swelling results in enlargement of the micropores that constitute the coal's matrix. Enlarged pores facilitate increased sorption capacity for treated coal and make diffusive movement of methane easier in the micropores. Such behavior is supported by the observation in the images presented in this study, and the changes in sorption-diffusion properties of bioconverted coal, as reported previously (R. Pandey et al. 2016). As indicated by the fractal analysis, bioconversion also resulted in the smoothening of the microporous coal surface, represented in figure 23. Although

bioconversion enhances the sorption-diffusion properties of coal, macro-scale effect of short-term (less than 60 days) bioconversion characterized by permeability through cleats proves to be the bottleneck from a feasibility perspective.

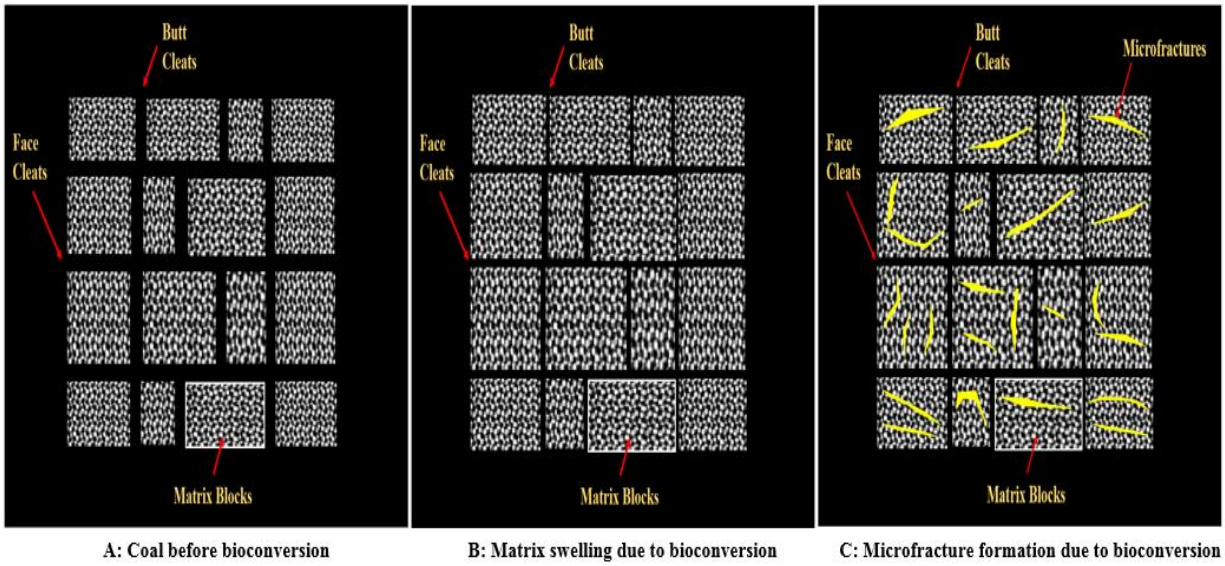

Figure 22: Conceptual model of coal *macrostructure* undergoing bioconversion.

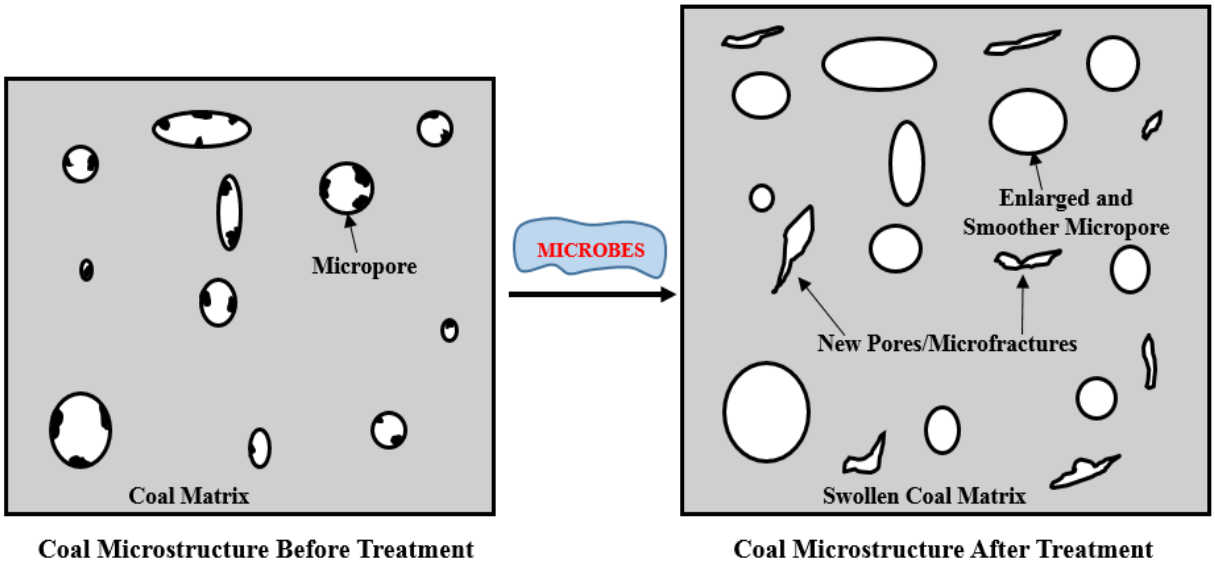

Figure 23: Conceptual model of coal *microstructure* undergoing bioconversion.

4. Conclusions

Imaging based techniques were used to study changes in the flow related physical characteristics of coal due to bioconversion. Based on the work completed, the following conclusions are made:

1. Coal bioconversion results in swelling of the coal matrix, thereby decreasing the cleat width/aperture. This bears direct relation to permeability of coal to fluid flow, as permeability is proportional to the cube of the cleat aperture. Results indicated ~77% reduction in permeability due to bioconversion.
2. Bioconversion resulted in flaking of the coal surface along the bedding plane. This would serve as a source of coal fines during bioconversion, which will potentially block cleats, thereby reducing fluid flow rates.
3. Coal bioconversion resulted in matrix swelling, and subsequent enlargement of existing pores, and creation of new pores, microcracks and fractures. Over a short period of time, these serve to increase matrix porosity, but do not contribute to fluid flow in the sample as they are discontinuous. Longer treatment periods indicated development of sub-micron wide continuous pores as a result of bioconversion.
4. Fractal dimensions reduced post-bioconversion. The reduction of fractal dimension was correlated with methane production from them. Reduction of D is indicative of a smoother matrix surface, and correlates inversely to the Langmuir pressure parameter, P_L.
5. Larger fractures present in the samples increased in width post-bioconversion, possibly due to increased microbial activity along the fractures, and thereby present a possibility of using artificially induced fracturing techniques to enhance biogenic methane production *in situ*.

6. Au-Pd ion sputtering on samples did not have any effect on methane production. Similar future studies should use sputtered samples to ensure high quality of images.
7. Accurate fractal analysis of coal from SEM images require imaging across multiple levels of magnification, contrary to what is reported earlier. Images acquired at matrix scale provide an accurate representation of the fractal dimension of the sample.

Acknowledgement

We gratefully acknowledge support from the US Department of Energy, award number DE-FE0026161. The authors would also like to thank Dr. Yanna Liang and Ji Zhang for providing optimized microbial media for bioconversion, and Nathalie Becerra Mora and Milinda Wasala from the SIU Image Center for assisting in imaging the coal samples.

CHAPTER 3

EXPERIMENTAL WORK

This chapter presents an exact copy (except for format change) of the journal paper entitled “Impact of bioconversion on matrix strain response of coal reservoirs: Part 1- Experimental insights.” published in *Fuel*, 2019. DOI: doi.org/10.1016/j.fuel.2018.10.009. Elsevier holds the copyright for this paper. This material may be downloaded for personal use only. Any other use requires prior permission of Elsevier.

Authors:

Rohit Pandey, Satya Harpalani

Abstract

The technical feasibility of commercial gas production from microbially enhanced coalbed methane (MECBM) reservoirs can be divided into two broad categories: microbial treatment procedures and reservoir suitability. At this time, studies investigating the changes in reservoir-scale properties of coal as a result of bioconversion are lacking. This paper, first of a two-part series, presents the experimental work aimed at investigating the changes in sorption-induced strain response of coal to helium and methane flooding as a result of bioconversion. The strain and its variation, critical to producing methane after bioconversion, were established for coal treated for three periods, 15, 30 and 60 days. The results indicated a softer coal post-bioconversion which, in turn, resulted in inelastic strain with initial helium injection. However, past this initial compression, the bioconverted coal behavior was similar to untreated coal during continued helium injection/depletion. Methane flooding resulted in decreased sorption-induced shrinkage post-treatment, the decrease in Langmuir pressure and volume constants becoming larger with continued treatment. The observed results were used to understand the changes in

coal structure for production of biogenic coalbed methane (BCBM) from depleted CBM reservoirs, recharged with methane using the bioconversion technology. The second part presents a detailed analysis of the experimental results to evaluate the behavior and performance of BCBM reservoirs.

Keywords: Coal bioconversion, Reservoir strain response, Reservoir recharge.

1. Introduction and Background

The year 2020 marks the start of the implementation period of the greenhouse gas emission control plan rolled out during the 2015 Paris agreement on climate change worldwide. This has led to an increased interest in reducing the carbon footprint of human activities, notably in the energy-sector. Natural gas, given its low carbon footprint provides a suitable alternative to traditional sources of energy like oil and coal. Although, methane stored in natural reservoirs like shale and sandstone, have been extracted over the past few decades, present geo-political scenarios call for severely ramping up production rates to meet the environmental demands. Such increased demands have led to the hunt for alternate sources of natural gas.

Coalbed methane (CBM), which has been commercially extracted since the late 1980's, refers to the naturally occurring methane extracted from coal seams, provides one such alternate source of natural gas. Isotopic analysis of the produced methane from CBM reservoirs associate biogenic and thermogenic sources of origin (Flores et al. 2008; Midgley et al. 2010; Moore 2012b; Penner, Foght, and Budwill 2010; Strąpoć et al. 2008). Thermogenic methane is produced due to the thermo-catalytic conversion of coal at higher temperatures existing during the process of coalification. Biogenic methane is produced from the microbial breakdown of the organic content of coal over time. Andrew Scott (Scott 1999a) in the 1990's, proposed replicating the natural process of biogenic methane production under controlled conditions in

order to increase the methane yield of CBM reservoirs over time. This technology was termed as microbially enhanced CBM (MECBM), and will be referred to as biogenic CBM (BCBM) in this manuscript.

Significant technological development of coal bioconversion, since its initiation has been from a microbial perspective. Several experimental studies have reported biogenic methane production, primarily from coal fines in excess of 500 standard cubic feet of methane per ton of coal (scft) (Jones et al. 2010; Opara et al. 2012; Suman Saurabh and Harpalani 2018; Strąpoć et al. 2008; J. Zhang, Liang, Pandey, et al. 2015; J. Zhang, Liang, Yau, et al. 2015; Ji Zhang and Liang 2017). Given that the coal seam would serve as a source and reservoir rock for the produced methane, it is important to characterize the effect of bioconversion on the reservoir scale behavior of BCBM reservoirs.

Characterization of CBM reservoirs require understanding of the dual: micro- and macro-porosity of coal, which dictates transport of fluids in the reservoir. The micro-pores, less than 2 nm in size, make up the coal matrix, and is surrounded by the macro-porous fracture network, known as cleats, whose width exceeds 50 nm. The micro-pores serve as the storehouse for over 95% of the gas in an adsorbed form (Gray 1987). In course of CBM production, as the pore pressure of the reservoir is reduced by pumping out water, the adsorbed methane molecules start to desorb from the micro-porous coal surface. This is the first transport phenomenon associated with a CBM reservoir. Once desorbed, the methane molecules diffuse through the micro-porous coal matrix, until it reaches the wider cleats. This is the second step of the three-step process. Finally, once the methane molecule reaches the wider cleats, it flows in accordance to Darcian law, characterized by the permeability of the reservoir, and is the third and final transport phenomenon.

A distinctive feature of CBM reservoirs, setting it apart from traditional natural gas reservoirs, is the competing mechanisms of poro-mechanical cleat compression and desorption-induced matrix shrinkage governing the Darcian flow. Over the life of a CBM reservoir, removal of water to start production results in decreased pore pressure that keeps the cleat apertures open. As a result, the effective stress acting on the cleats increases, resulting in their closure and decreasing the flowrates. On the other hand, as methane desorbs from the micro-porous coal surface, it results in shrinkage of the coal matrix. This shrinkage results in widening of the cleat/fracture apertures in coal, thereby boosting flowrates. The shrinkage behavior competes with the changes in effective horizontal stress to dictate the overall flow patterns in CBM reservoirs. A sound knowledge of coal's volumetric response to pressure variations is, therefore, critical given its impact when interpreting gas production data as well as projecting future production.

Shrinkage of coal matrix as a result of gas desorption has been widely reported by several researchers (Harpalani and Chen 1995, 1997; Levine 1996b; Moffat and Weale 1954; Seidle and Huitt 1995). It has been recognized that the shrinkage behavior of coal is a reversible process, where coal matrix swells upon adsorption of methane in its micro-pores and shrinks with desorption. Moffat and Weale (Moffat and Weale 1954) were the first to report a volumetric increase ranging from 0.2% to 1.6% for coals of different ranks, when subjected to a pressure of 2716 psi (15 MPa). Harpalani and Schraufnagel (Harpalani and Schraufnagel 1990) studied the volumetric strain of coal in methane and helium environments. For helium, coal matrix was found to decrease with increase in gas pressure as a result of compression of solid grains of coal matrix. For methane, swelling of the coal matrix was reported with increase in gas pressure, the measured increase in matrix volume being approximately 0.5% at 1000 psi (6.9 MPa). They also

reported that the sorption-induced strain exhibited a curvilinear form, with a steep slope at lower pressure, which became gentler at higher pressures (Harpalani and Chen 1995; Harpalani and Schraufnagel 1990). Levine (Levine 1996b) later characterized such strain behavior by proposing a Langmuir-type model to fit volumetric strain-pressure relationship, as follows:

$$\epsilon = \epsilon_l \frac{p}{p + P_\epsilon} \quad (1)$$

where, ϵ is the sorption-induced volumetric strain at pressure, **p**; ϵ_l represents the maximum strain, which can be achieved at infinite pressure; and P_ϵ is the pressure at which coal attains 50% of the maximum strain.

There is a dearth of studies investigating reservoir scale implications of coal bioconversion and its impact on expected flowrates. Experimental work conducted on powdered coal to characterize changes in sorption properties due to bioconversion was first reported by Pandey et al in 2016 (R. Pandey et al. 2016), and more recently by Zhang et al in 2017 (R. Zhang et al. 2017). It was reported that increase in micro-porous surface area post-bioconversion resulted in the observed increase of the coal's sorption capacity. Bioconversion also resulted in increased diffusion rates for methane and carbon dioxide. Such variation translates to increased micro-porous surface area available for sorption and altered pore geometry, resulting in increased flowrates (diffusive) at the microscopic scale. Increase porosity of coal, post-bioconversion, was also evident in the images presented by Zhang et al (Ji Zhang et al. 2018) from the results of a year-long bioconversion study, where ~5000 scft of methane was produced over the treatment duration. The two reported studies remain to be the only investigations reporting changes in reservoir scale properties of coal due to bioconversion. More recently, a detailed imaging study was presented by Pandey and Harpalani (R. Pandey and Harpalani 2018) which reported changes in the physical structure of coal due to bioconversion. Variation in the

physical structure of coal was then interpreted from a reservoir perspective, however no direct measure of flow-related properties was presented. Evaluating production potential of a BCBM reservoir requires a sound understanding of the changes in the strain behavior of coal, an aspect missing in current literature, providing the motivation for the work presented in this paper.

The major goal of the study presented in this paper was to document the sorption-induced strain behavior of bioconverted coals in order to evaluate the technical feasibility of methane production from depleted CBM reservoirs, re-charged with methane using bio-conversion. Such strain-evaluations are required in prior to setting up extensive experimental studies, in order to optimize design parameters and identify boundary conditions for experiments investigating properties of biogenic CBM reservoirs under replicated *in situ* conditions under confining stresses, and to assess/decide field-scale approaches to implement this technology. As a first step, changes in the sorption-induced shrinkage/swelling behavior of coal as a result of bioconversion were established. The results were used to understand the dynamic behavior of a depleted CBM reservoir subjected to biogenic recharge and then followed by production of biogenic methane, referred to as biogenic coalbed methane (BCBM) reservoirs. Furthermore, the observed/measured changes were translated to expected changes in several reservoir parameters, a topic discussed in detail in the second part of this two-part series. Given that the overarching goal of BCBM is to produce biogenic methane from *in situ* coal, this study focused on the technical pre-feasibility of BCBM reservoirs, along with providing an in-depth understanding of the transport processes associated with it.

2. Experimental Work

In order to estimate the shrinkage/swelling characteristics of bioconverted coal and monitor changes due to bioconversion, a three-step experiment was conducted. First, the baseline

sorption induced shrinkage/swelling behavior of untreated coal was established. Second, the coal samples were treated with microbial solutions aimed to produce methane. Details of the treatment procedures and conditions for the coal type studied can be found in paper by Zhang et al. (Ji Zhang, Liang, and Harpalani 2016). Three coal samples, for which the baseline characteristics were established, were then treated for 15, 30 and 60 days respectively. Gas content was measured at the end of the treatment periods for the three samples tested. Finally, the sorption-induced strain behavior of the treated samples was established.

2.1 Sample Procurement and Preparation

Coal samples for the experimental work were obtained from blocks of coal, retrieved from an underground mining operation, mining the Illinois 6 seam in southern Illinois. Sample quadrants, ~2-inch side, were then prepared from one coal block and three samples with the fewest cleats were selected. Quadrant shaped samples allowed placement of three linear gauges on each sample to monitor strains in the three orthogonal directions, with the z- direction being perpendicular to the bedding planes. The sample size was also limited to 2 inches to ensure strain equilibrium time was not prolonged, as it is with larger coal samples. Prior to starting the tests (strain and treatment), the prepared samples were kept in an environmental chamber under controlled conditions of temperature and humidity.

2.2 Experimental Setup

The experimental study had two aspects, establishing the sorption induced strain behavior and carrying out coal bioconversion.

2.2.1 Shrinkage/Swelling Setup

The experimental setup consisted of three vessels capable of withstanding high pressures. To continuously monitor the volumetric behavior, linear deformation strain gauges were used.

These strain gages measure linear strain over a small area, and the results are then interpreted to represent the strain observed by the entire sample. A data acquisition system (DAS) was used to collect and record the pressure and strain data continually every minute. The obtained data was then reduced to a single point data corresponding to a particular pore pressure. To eliminate thermal-induced effects on coal matrix strain, the high-pressure vessels were kept in a constant temperature water bath, capable of maintaining the temperature to within 0.1^{o}C of the desired *in* situ temperature (32^{o}C). A schematic of the experimental setup is shown in Figure 24A. Figures 25A and 25B show one coal sample with affixed strain gages and the entire experimental setup respectively.

2.2.2 Treatment Setup

The coal samples were treated in the same vessel used for the shrinkage/swelling experiment. Once the baseline strain characteristics were established, the strain gages attached to the samples were removed, and the sample surface was polished to remove any remaining bonding glue. The samples were then added to the microbial solution in the high-pressure assembly, and the headspace was purged with helium. The samples were subjected to a hydrostatic pore pressure (unconstrained) of 480 psi using helium in the headspace. A schematic of the experimental setup is shown in Figure 24B.

Microbial solutions for the particular type of coal were developed over the last two years, and are extensively reported in prior publications (Suman and Harpalani 2018; J. Zhang, Liang, Pandey, et al. 2015; J. Zhang, Liang, Yau, et al. 2015; Ji Zhang and Liang 2017; Ji Zhang, Liang, and Harpalani 2016). Since the coal samples used in this study were obtained from the same block of coal as used in these studies, details of the treatment procedure along with the associated changes in proximate and ultimate analysis are not included here. These can be found

in Zhang et al. and Pandey et al. respectively (Pandey et al. 2016; Pandey 2015b; J. Zhang, Liang, Pandey, et al. 2015).

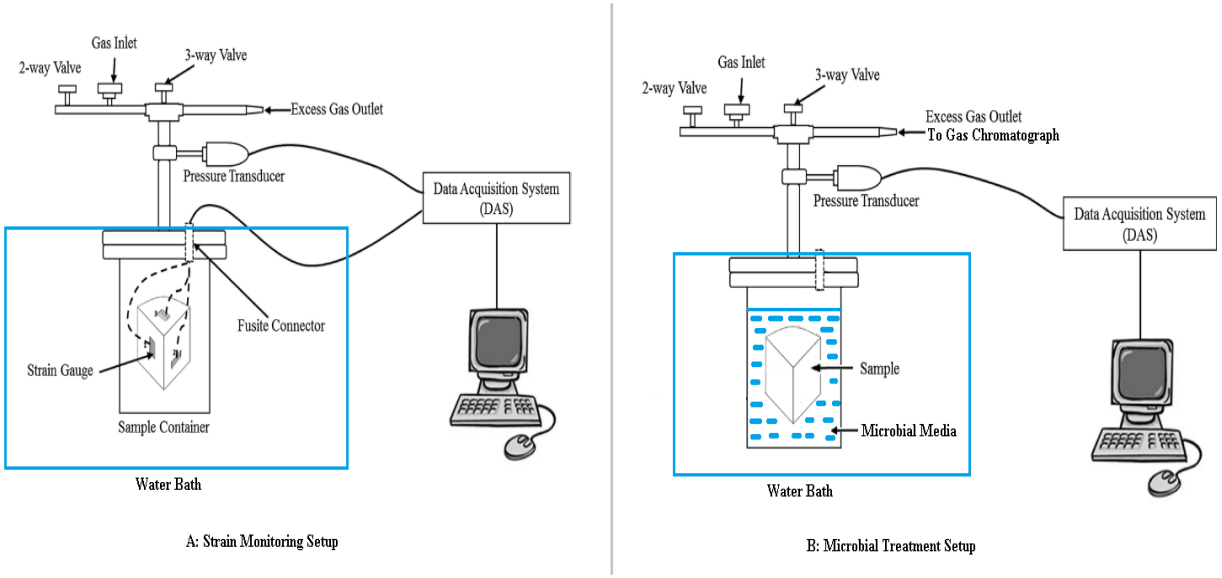

Figure 24: Schematic of experimental setup for measurement of coal matrix strain (A), and microbial treatment (B).

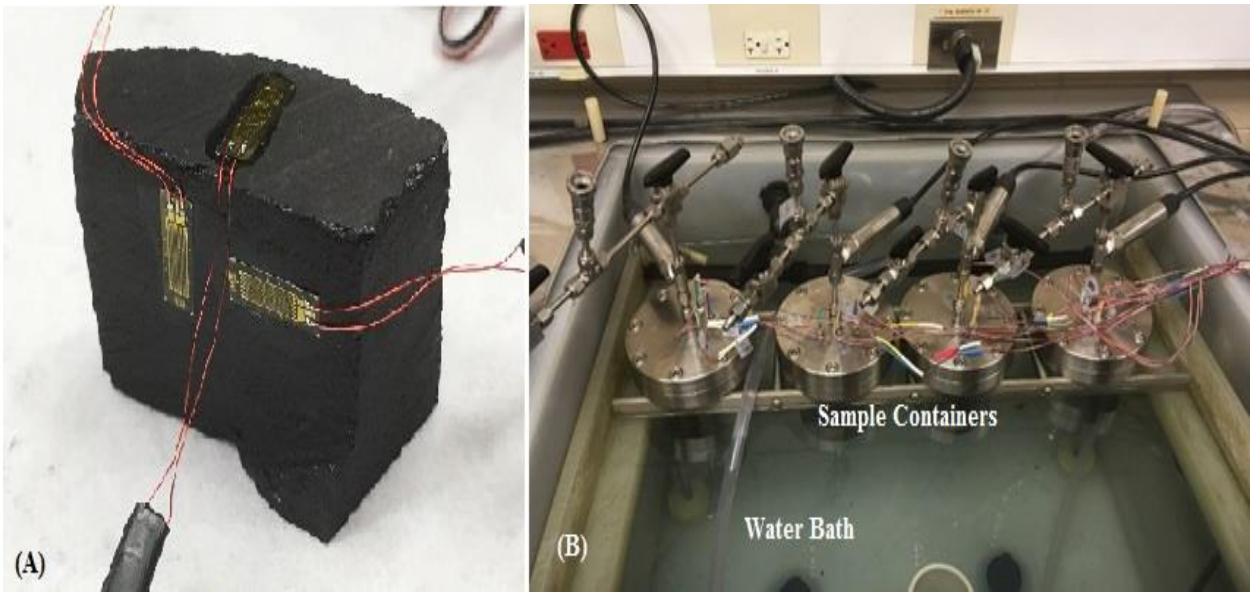

Figure 25: (A) Coal sample with attached strain gages, (B) Complete experimental setup.

2.3 Experimental Procedure

To obtain shrinkage and swelling strain in the laboratory, helium and methane were used. The specimens were first subjected to increasing helium pressure in a stepwise manner (150-300 psi steps). For helium, a non-sorbing gas, the measured volumetric strain was purely the result of mechanical compression of solid coal. Once the samples equilibrated at the maximum pressure of 1500 psi (1200 psi for treated coal), helium was bled out in a stepwise manner while monitoring the strains during depletion. The samples were then subjected to methane flooding, in similar steps to a final pressure of 1200 to 1500 psi, followed by stepwise depletion down to atmospheric pressure. Two strains are associated with injection of methane, mechanical compressional effect and the sorption-induced strain. Thus, the "true" shrinkage or swelling strain due to methane alone was estimated by subtracting the strain measured during helium flooding from the strain measured during methane flooding. The true strain values were then used to model reservoir scale parameters to determine the effect of bioconversion of coal, presented in detail in the second part of this two-part series. Each coal sample was subjected to this procedure twice, before and after treatment.

3. Results and Discussion

The following section presents the experimental data obtained, along with a discussion of the observed trends.

3.1 Baseline Characteristics (*untreated coal*)

3.1.1 Helium Injection Results

The volumetric strain of the sample was calculated as the summation of the linear strains in three orthogonal directions, and the sample is assumed to be isotropic:

$$\epsilon_V = \epsilon_{XX} + \epsilon_{YY} + \epsilon_{ZZ} \quad (2)$$

where, ϵ_V is the volumetric strain, and ϵ_{XX}, ϵ_{YY} and ϵ_{ZZ} are the linear strains in x-, y- and z-directions respectively.

Figure 26 presents the results of the volumetric strain for the samples tested for increasing helium pressure. Decreasing helium pressures resulted in the coal sample exhibiting a similar path as that observed during injection. Therefore, only the results measured during injection are presented. As expected, the volume of coal matrix decreased with increasing pressure due to compression of the solid coal. During depletion, the volume of coal matrix increased due to de-compression of the solid coal. This enabled estimation of the coal matrix/grain compressibility, obtained from the slope of the pore pressure-volumetric strain plot. The compressibility of the samples was measured to be 1.20 E^{-6} psi^{-1}, 1.08 E^{-6} psi^{-1} and 1.43 E^{-6} psi^{-1} for samples 1, 2 and 3 respectively.

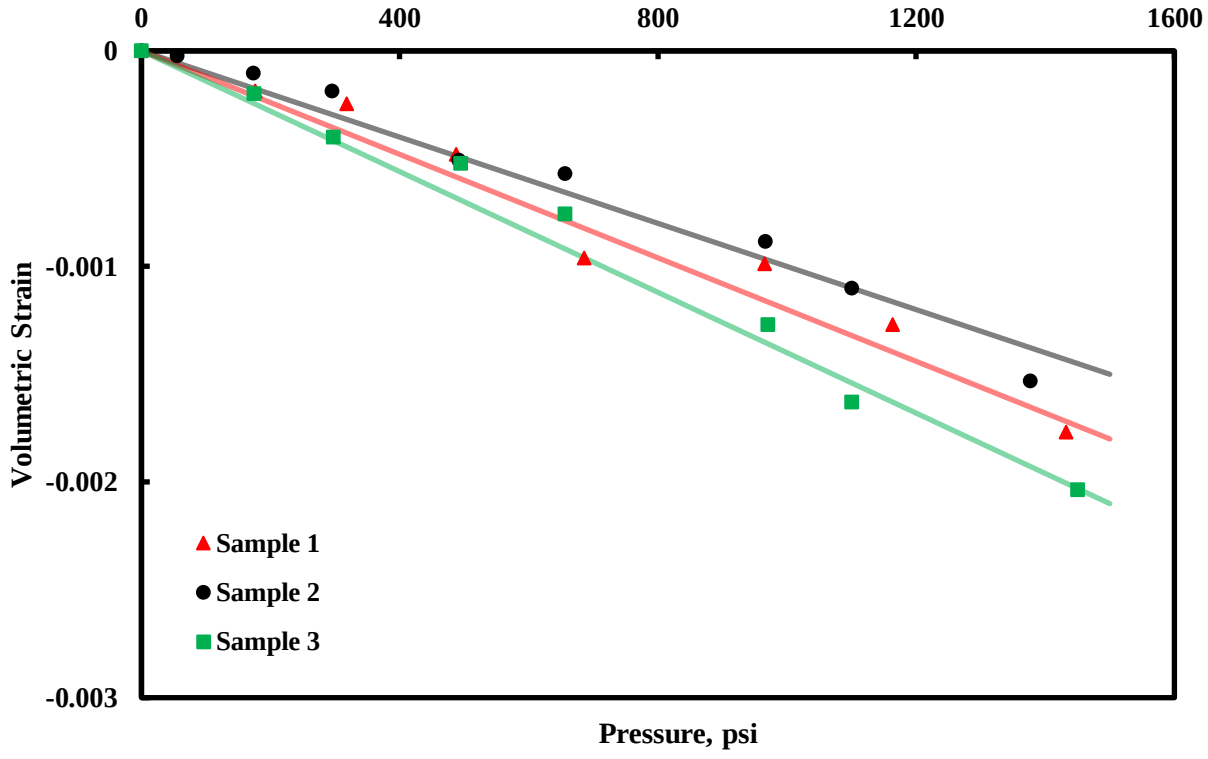

Figure 26: Matrix strain with helium injection for untreated coal.

3.1.2 Methane Injection/Depletion Results

After completing the helium cycle, gas was bled out from the pressure vessel. This was followed by methane injection, as described in section 2.3. The volumetric strain induced with methane injection was calculated for each pressure equilibrium step. As expected, the coal matrix swelled with increasing methane pressure, and shrunk with decreasing methane pressure. The three samples tested presented similar strain behavior and this was expected. Figures 27, 28 and 29 present the experimental results for the three samples along with the best fitted Langmuir model. The Langmuir's constants obtained using equation 1 for adsorption-induced swelling are presented in table 4.

Given that swelling strain developed due to adsorption is a reversible process, desorption-induced shrinkage should ideally be identical to adsorption-induced swelling. However, under laboratory conditions, slight hysteresis is often observed between shrinkage and swelling behavior. Residual strains of 0.00065, 0.00062 and 0.0008 were observed upon complete depletion of methane in the three samples.

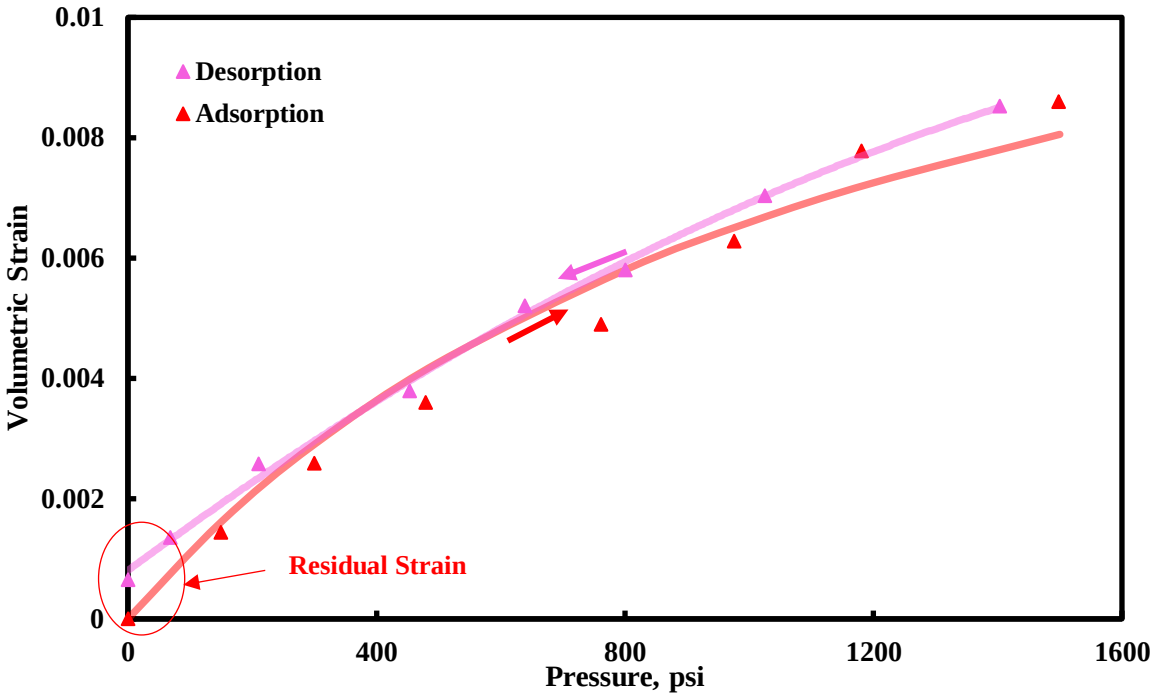

Figure 27: Shrinkage-swelling strains with methane sorption in untreated sample 1.

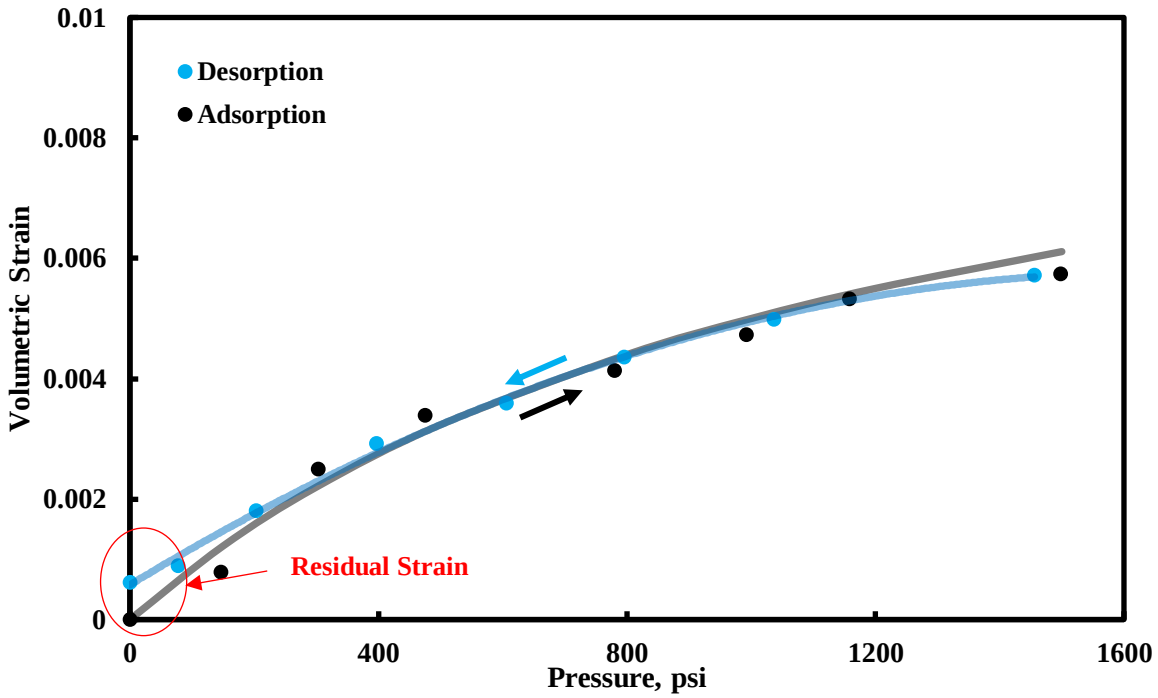

Figure 28: Shrinkage-swelling strains with methane sorption in untreated sample 2.

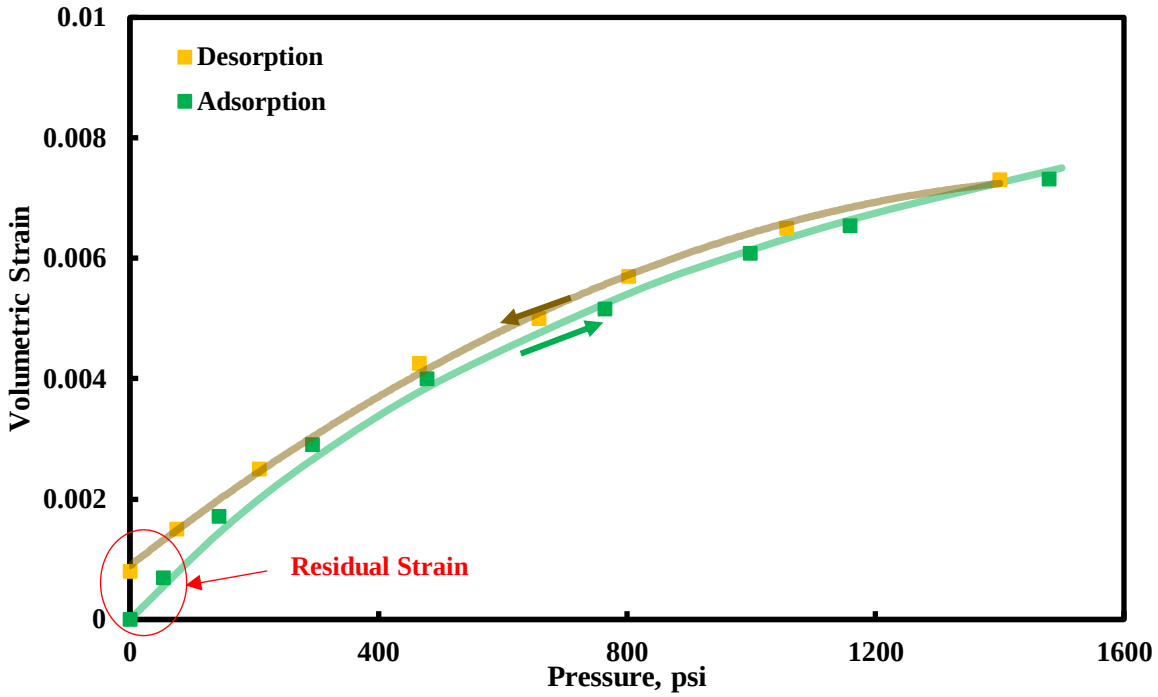

Figure 29: Shrinkage/swelling strains with methane sorption in untreated sample 3.

Table 4: Langmuir strain constants for untreated coal.

Sample Number	Langmuir Strain ϵ_l	Langmuir Pressure P_ϵ (psi)
1	0.0145	1200
2	0.0115	1250
3	0.0135	1200

3.1.3 True Shrinkage/Swelling Results

When coal is flooded with methane, both mechanical compression and shrinkage/swelling strain govern its overall volumetric response. However, when the coal is exposed to helium, mechanical compression effect alone is responsible for the observed strain. Therefore, the "true" sorption- induced volumetric strain was calculated by subtracting the

mechanical induced strain from the measured methane-injection induced strain. Figure 30 is an example of the calculated true shrinkage/swelling behavior for sample 3. Figure 31 presents the true shrinkage/swelling behavior for all the three samples tested. Mathematically, the true shrinkage is represented by the following equations, where ϵ_{Vx} is the volumetric strain induced in sample x (=1, 2, 3), and p is the pore pressure.

$$\boldsymbol{\epsilon_{V1} = 0.0145 \frac{p}{p+1200} - (-1.2E^{-6}\, p)} \quad (3a)$$

$$\boldsymbol{\epsilon_{V2} = 0.0115 \frac{p}{p+1250} - (-1.08E^{-6}\, p)} \quad (3b)$$

$$\boldsymbol{\epsilon_{V3} = 0.0135 \frac{p}{p+1200} - (-1.43E^{-6}\, p)} \quad (3c)$$

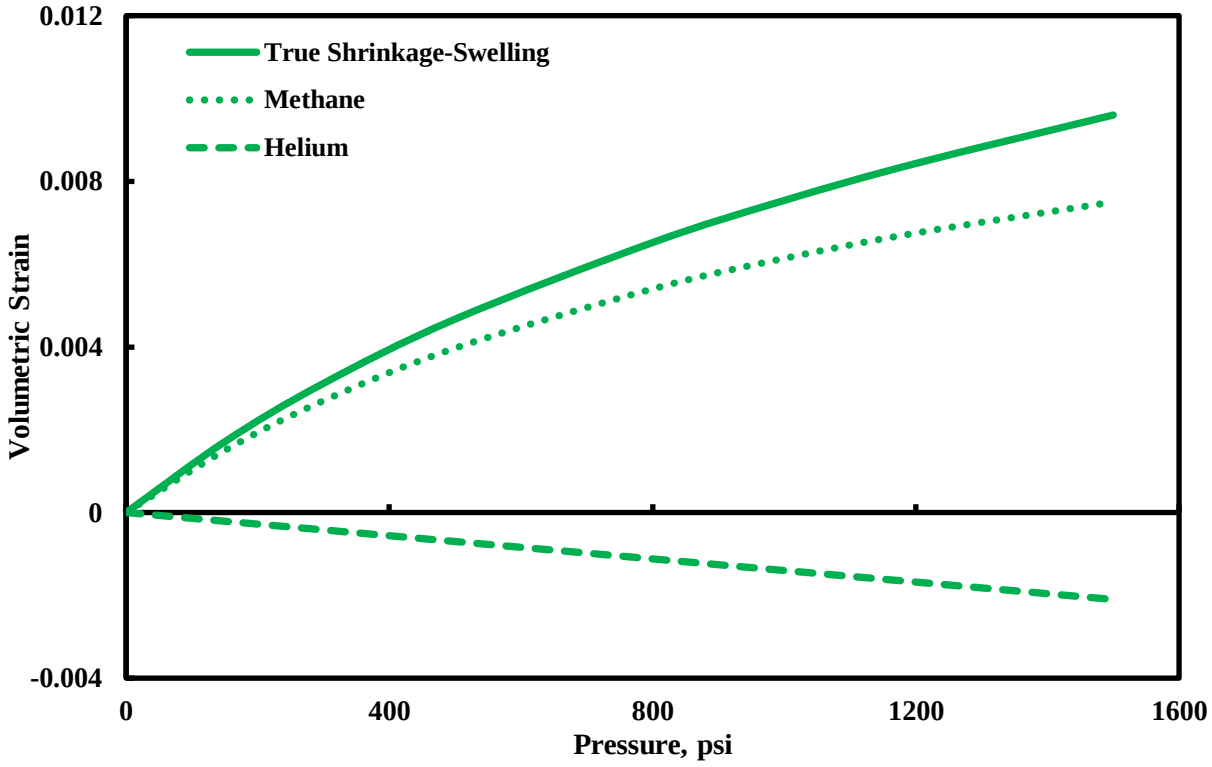

Figure 30: True shrinkage swelling behavior calculated for sample 3 (untreated).

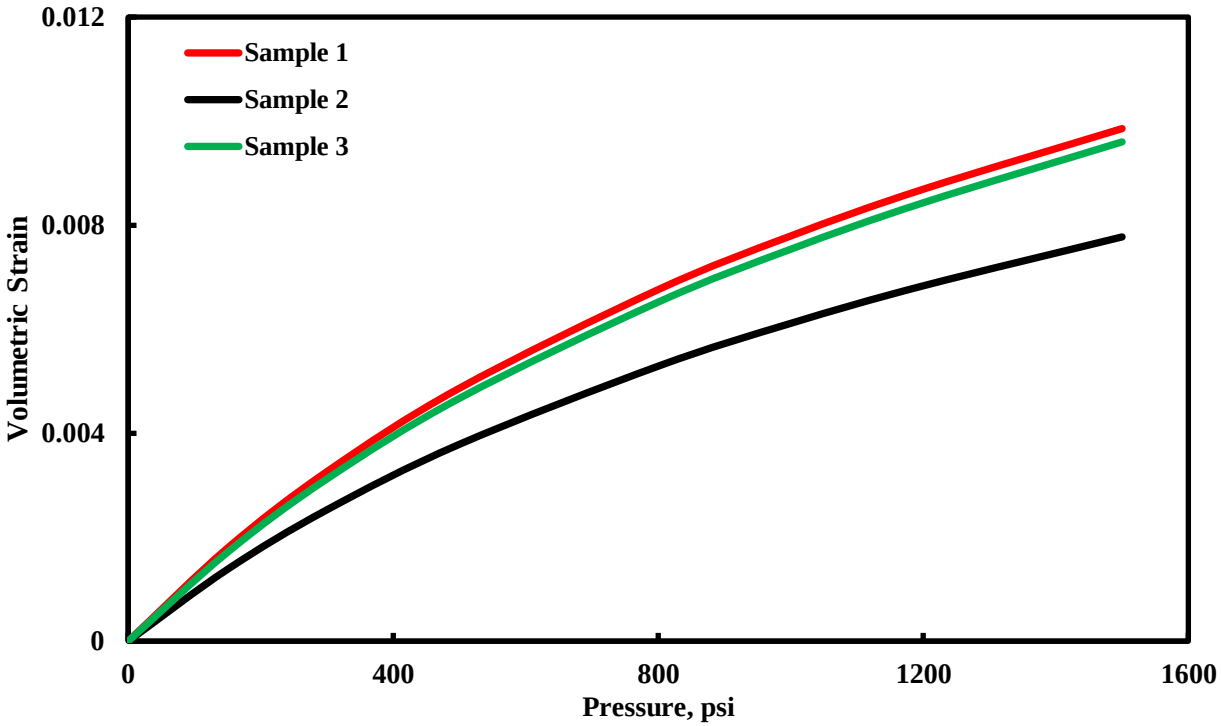

Figure 31: True shrinkage-swelling behavior for the three untreated coal samples.

3.2 Gas Production

Methane production from the three samples, listed in table 5, was measured at the end of 15, 30 and 60 days from samples 1, 2 and 3 respectively. Gas production was measured in moles of methane/gram of coal, and then scaled up to standard cubic feet of methane per ton of coal (scft).

Table 5: Biogenic methane production from Illinois coals.

	Sample 1	**Sample 2**	**Sample 3**
Time (days)	15	30	60
Methane Production (scft)	172	568	689

Production of biogenic methane by microbial consortia was first modeled by Saurabh and Harpalani (Suman and Harpalani 2018) using a population logistic equation expressed as:

$$\boldsymbol{V(t)} = \frac{\boldsymbol{K\,V_0}}{\boldsymbol{V_o + (K - V_o)e^{-rt}}} \quad (4)$$

where, $\boldsymbol{V(t)}$ is the volume of methane produced during time $\boldsymbol{t}$ (days) in scft, $\boldsymbol{K}$ is the carrying capacity expressed as a % (v/v) which is a measure of the maximum volume of methane that can be generated in the given environment, $\boldsymbol{V_0}$ is the methane volume generated by the initial population of microbes at the start of the experiment, $\boldsymbol{r}$ is the microbial population growth parameter in day^{-1}. Figure 32 shows methane production over the duration of treatment, as tabulated in table 2. The volume of methane produced was significant, given that virgin Illinois basin reservoirs have less than 300 scft gas-in-place (Demir, I; Damberger 2000). Also graphed is the modeled production, obtained by a fitting exercise where, for the particular coal type, $\boldsymbol{K}$ = 701 (%), $\boldsymbol{V_0}$ = 25.3 scft and $\boldsymbol{r}$ = 0.1547 day^{-1}. Maximum methane production of ~700 scft was modeled at ~64 days although only 172 scft of biogenic methane was produced over the initial 15 days. The generation rates increased over the next 15 days, where 568 scft of methane was produced over 30 days. This rate of increase slowed down past the 35 day mark, as seen in the modeled production. The cumulative methane was produced at the end of 60 days of treatment was 689 scft. Such decrease in the methane generation rates is attributed to decreasing microbial population and availability of bio-nutrients over time (Suman and Harpalani 2018; Ji Zhang, Liang, and Harpalani 2016). It needs to be pointed out here that methane production recorded over 15, 30 and 60 days was from three different samples. The samples were however sourced from the same larger block of coal, and the obtained data can be assumed to be representative of methane production from a single sample over a continuous treatment period of 60 days. The modeled production matches well with data in existing literature, which reported continual gas

production from single bioreactors (Suman Saurabh and Harpalani 2018; Ji Zhang et al. 2016; Ji Zhang, Bi, and Liang 2018; Ji Zhang and Liang 2017). In the second part of this two-part series, the modeled production will be used to characterize the changes in reservoir parameters due to bioconversion.

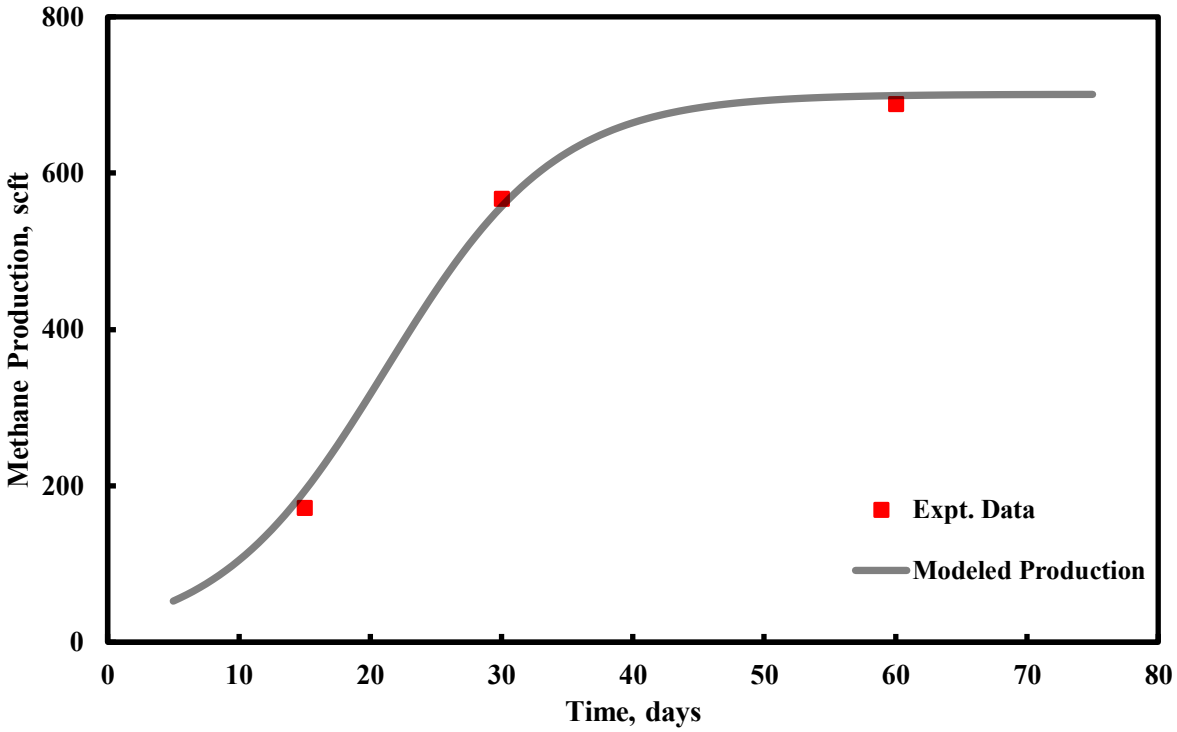

Figure 32: Biogenic methane production from coal over time.

3.3 Treated Coal

Treatment of coal required removal of the affixed strain gages. Post-treatment, strain gages were re-affixed before initiating the experiment. Results of helium and methane flooding along with true shrinkage results are presented below.

3.3.1 Helium Injection/Depletion Results

All three treated samples were subjected to step-wise helium injection and then depletion, while recording the resulting strains. Figures 33, 34 and 35 present the results obtained for

treated samples 1, 2 and 3 respectively. For the sake of reference, the strains measured pre-treatment are included.

Post-treatment results present an aberration to the expected linear trend. Two specific types of strains were observed with helium injection: inelastic and elastic strains. Upon initial injection of helium, a larger volumetric contraction was observed, contributing to the nonlinearity. Continued flooding, however, resulted in linear compression of coal. The initial inelasticity of the bioconverted coal samples implies a softer coal matrix post-treatment, with the solid matrix compressibility almost an order magnitude greater than that of untreated coal. However, subsequent to initial compression, the compressibility of the coal matrix decreases and remains constant over the duration of helium injection. For helium depletion, the samples decompressed linearly, with a similar slope to that observed during compression. However, the initial inelastic behavior during helium injection was not recovered at the end of flooding, an obvious outcome of bioconversion. Inelastic strains of 0.0005, 0.0014 and 0.0023 were measured in the three samples respectively. The compressibility of the solid coal matrix for the samples post-treatment, for both the inelastic and elastic zone, along with the compressibility pre-treatment are presented in table 6. As seen in the table, the solid matrix compressibility of coal decreased by an order of magnitude in the inelastic region. However, for the remaining period of helium injection and depletion, the compressibility of the solid coal matrix increased, and the coal matrix became stiffer as a result of bioconversion.

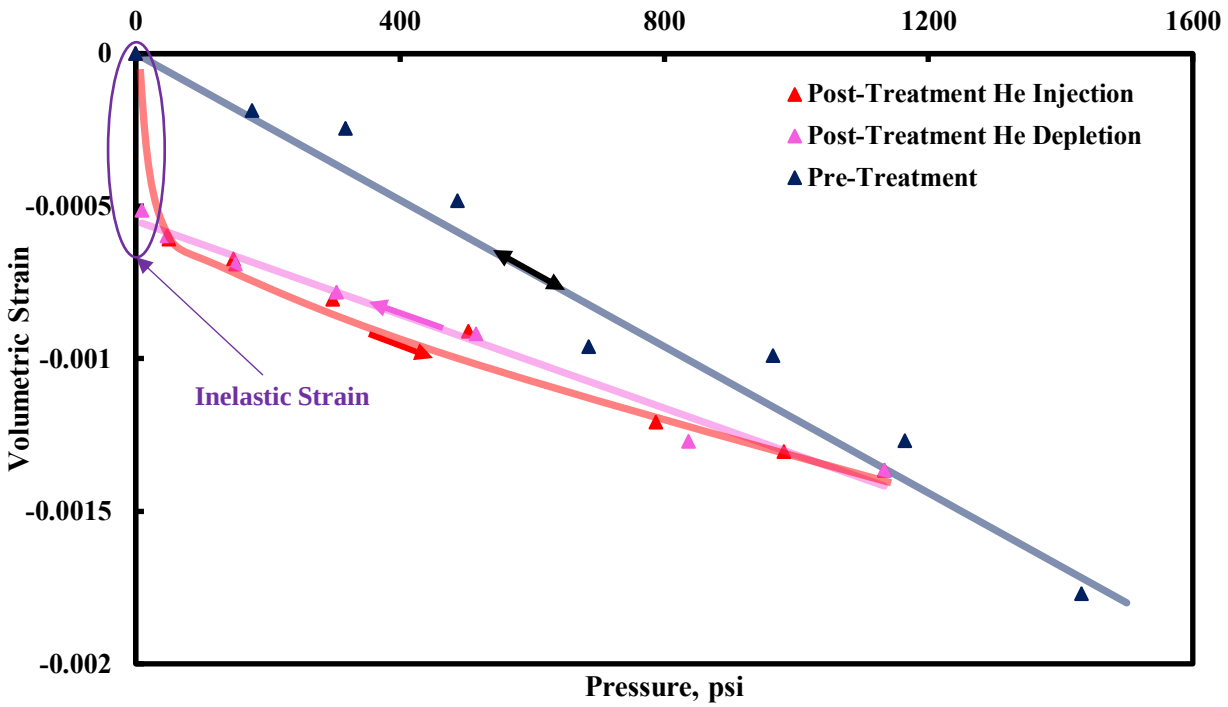

Figure 33: Strains developed due to helium flooding pre-and post-treatment (Sample 1).

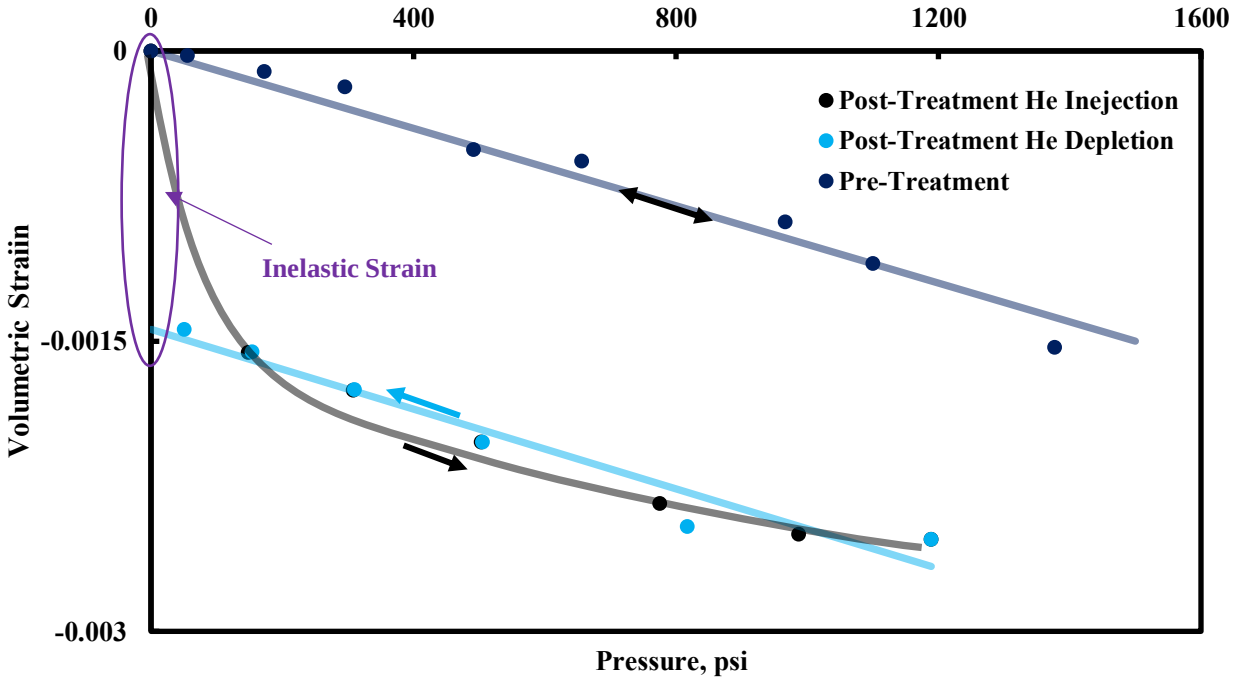

Figure 34: Strains developed due to helium flooding pre-and post-treatment (Sample 2).

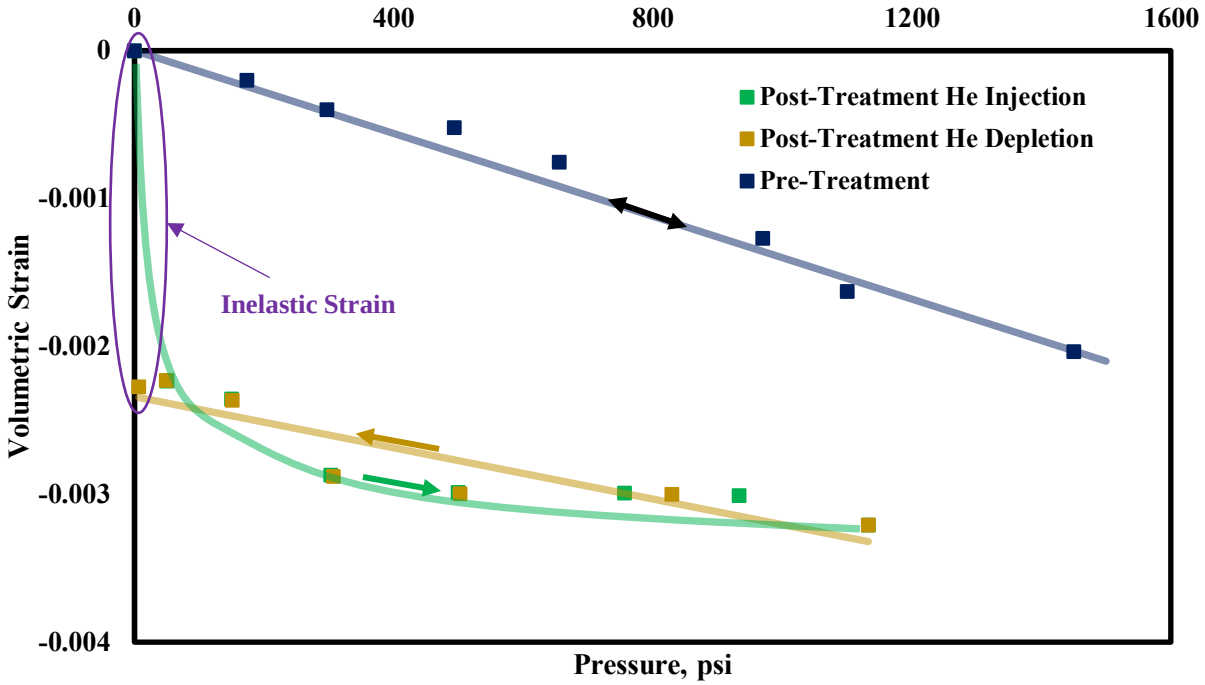

Figure 35: Strains developed due to helium flooding pre-and post-treatment (Sample 3).

Table 6: Solid matrix compressibility (psi^{-1}) of the coal samples pre- and post-treatment

Sample #	Pre-treatment	Post-treatment	
		Inelastic	Elastic
1	$-1.2E^{-6}$	$-1.21E^{-5}$	$-0.77E^{-6}$
2	$-1.08E^{-6}$	$-1.05E^{-5}$	$-1.03E^{-6}$
3	$-1.43E^{-6}$	$-4.47E^{-5}$	$-0.87E^{-6}$

3.3.2 Methane Injection/Depletion Results

Figures 36, 37 and 38 present the results of strains during methane injection and depletion in the treated samples 1, 2 and 3 respectively. Langmuir parameters for the three treated coals are presented in Table 7, showing a decrease in the values of ϵ_l and P_ϵ post-treatment. Such an observation confirms the results presented by Pandey et al (R. Pandey et al.

2016), where sorption capacity of coal reduced post-treatment. Lower volumes of sorbed gases would result in smaller volumetric strain. Evidently, bioconversion of coal reduces the sorption capacity of coals, thereby suppressing the sorption-induced shrinkage/swelling behavior. The Langmuir strain reduced by 0.004, 0.0065 and 0.008 and the Langmuir pressure reduced by 200 psi, 450 psi and 600 psi at the end of 15, 30 and 60 days respectively. Unlike the untreated samples, desorption showed excess volumetric shrinkage after complete methane depletion. That is, the samples shrunk more in volume in comparison to its initial state at the end of injection-depletion cycles. The measured excess (shrinkage) volumetric strains were 0.000492, 0.000290 and 0.000335 for the three samples.

Table 7: Langmuir-type constants for bioconverted coal.

Sample Number	**Langmuir Strain** ϵ_l	**Langmuir Pressure** P_ϵ **(psi)**
Sample 1	0.0105	1000
Sample 2	0.005	800
Sample 3	0.0055	600

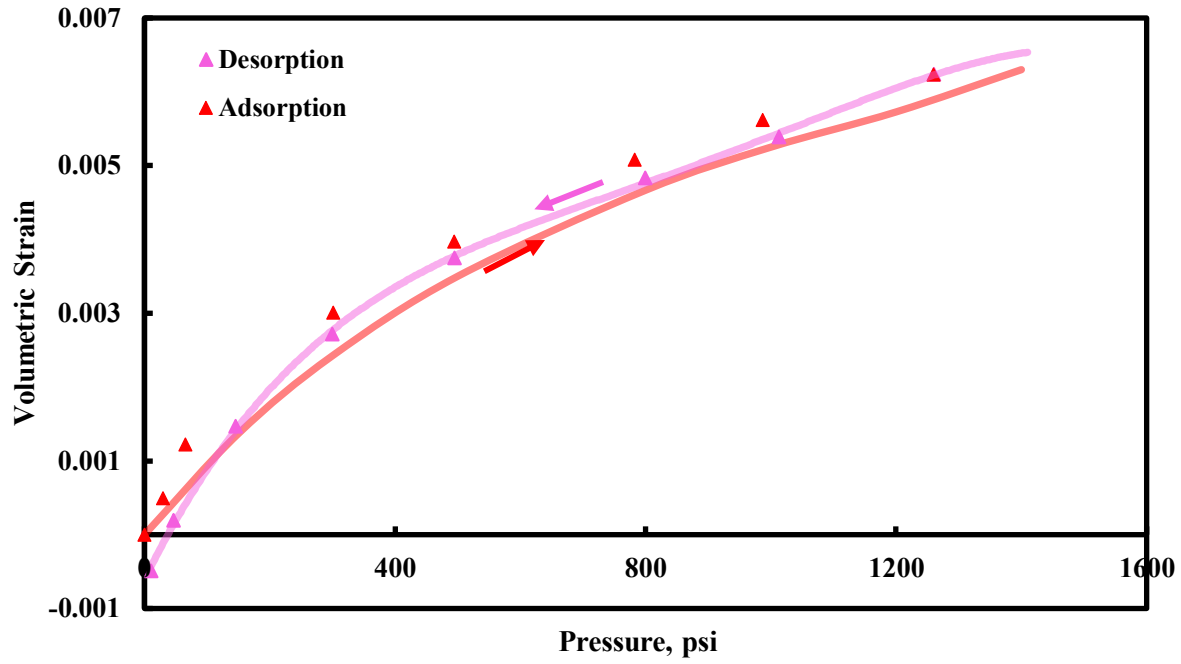

Figure 36: Shrinkage-swelling strains with methane sorption in treated coal (sample 1).

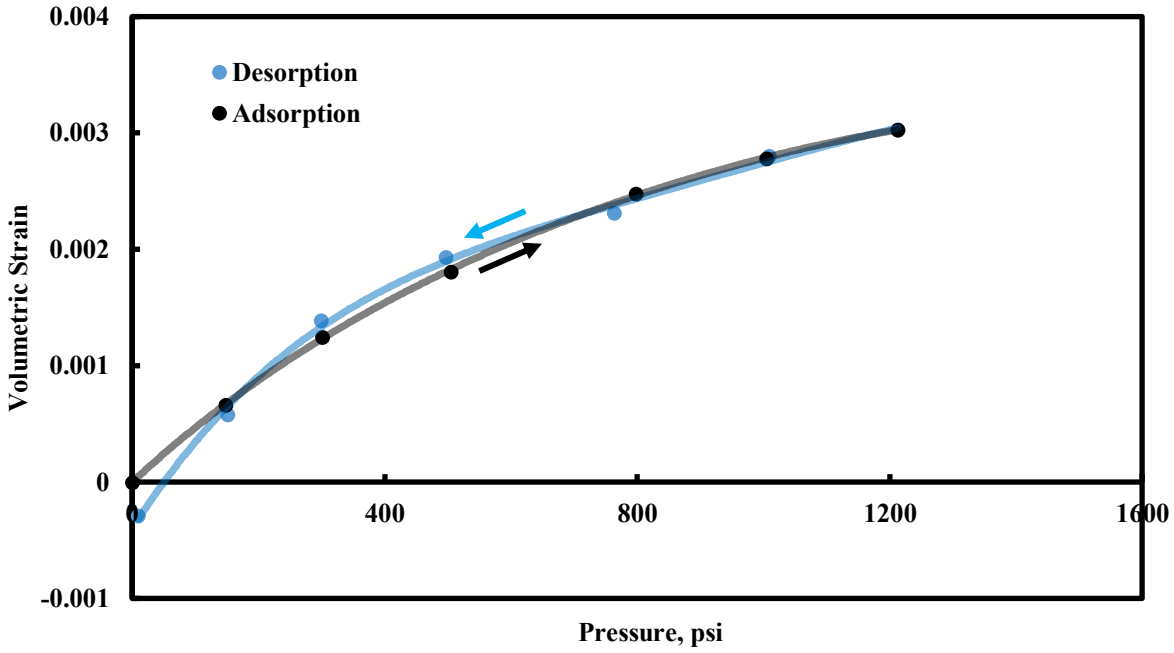

Figure 37: Shrinkage-swelling strains with methane sorption in treated coal (sample 2).

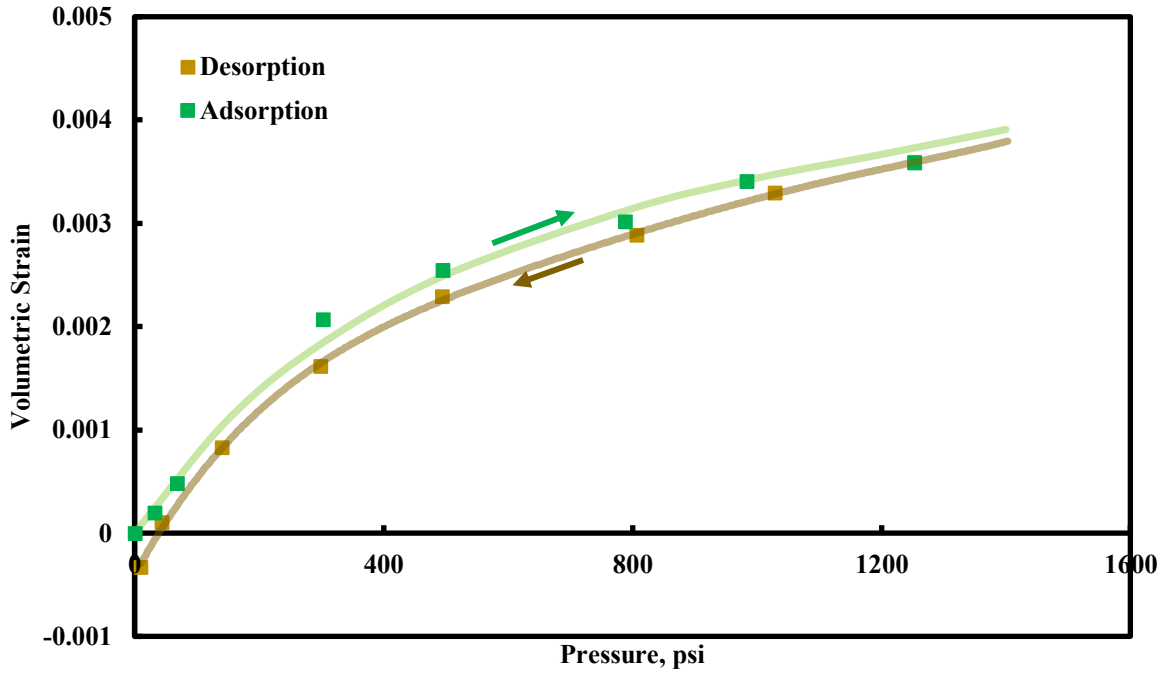

Figure 38: Shrinkage-swelling strains with methane sorption in treated coal (sample 3).

3.3.3 True Shrinkage/Swelling Results

The results of helium and methane flooding were used to obtain the true shrinkage/swelling behavior of treated coals, modeled using the following equations (5 a, b, c), where the superscript T, denotes treated coal:

$$\epsilon_{V1}^{T} = \mathbf{0.0105}\frac{p}{p+1000} - (\mathbf{-7.67E^{-7}}\,p) \quad (5a)$$

$$\epsilon_{V2}^{T} = \mathbf{0.005}\frac{p}{p+800} - (\mathbf{-1.03E^{-6}}\,p) \quad (5b)$$

$$\epsilon_{V3}^{T} = \mathbf{0.0055}\frac{p}{p+600} - (\mathbf{-8.65E^{-7}}\,p) \quad (5c)$$

The strain behavior of the three samples pre- and post- bioconversion is graphically illustrated in figure 39. The results clearly show that, post-bioconversion, true sorption-induced strain in coal is suppressed. Furthermore, longer the treatment duration, greater is the suppression. The results presented in figure 39 show that the areas bound by the pre- and post-

treatment plots (solid and dotted plots) of sample 1 was the least, and sample 3 was the highest. The sorptive-strain in coal originates in the macerals, which is the organic fraction of coal. Microbial bioconversion results in loss of organic fraction, which results in reduced sorption of methane, thereby suppression of the sorptive strains.

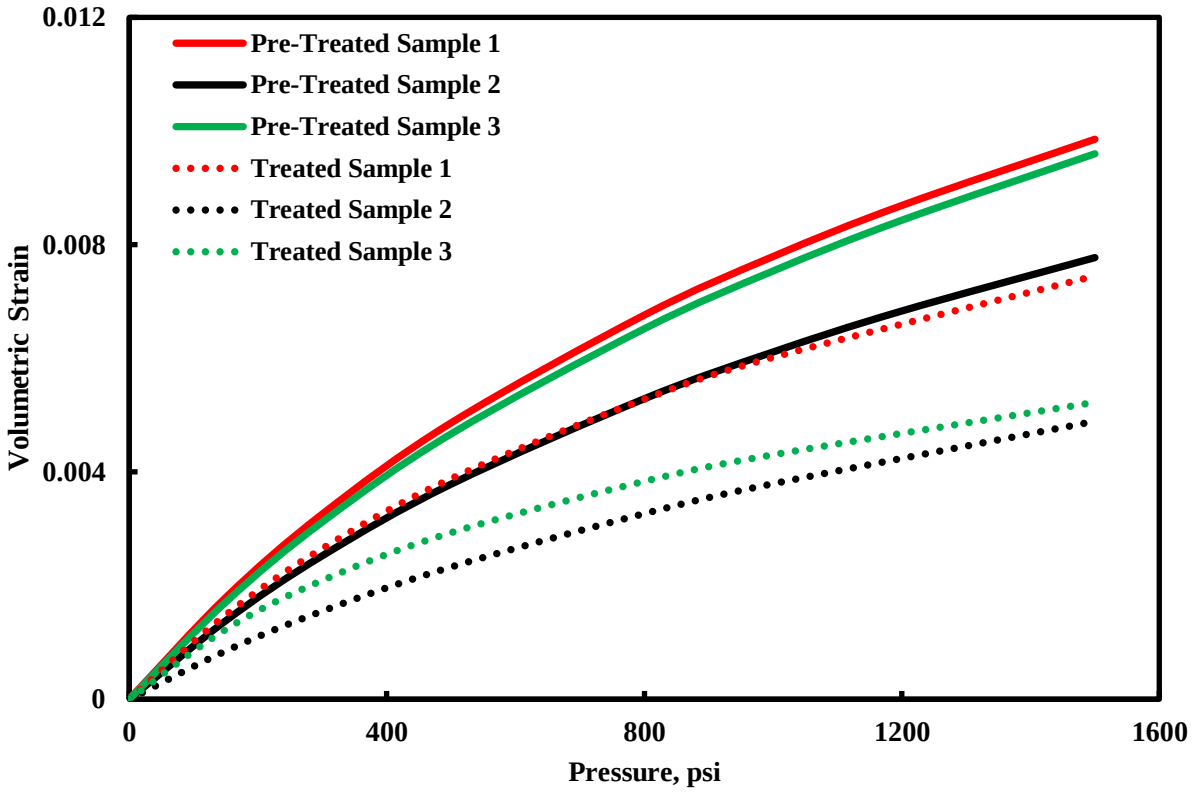

Figure 39: True shrinkage/swelling behavior of coals pre- and post-treatment.

3.4 Practical Implications

As mentioned earlier, flow in the cleat (fracture) network is governed by Darcy's law. The two primary factors controlling Darcian flow in coal are the cleat aperture (width) and cleat spacing. The cleat aperture in coal varies over the life of a producing reservoir due to the sorption-induced matrix shrinkage and varying effective stress. The permeability behavior, describing the Darcian flowrates of a reservoir is, therefore, modeled considering these two effects as a function of pressure. The strain responses to helium and methane flooding on pre-and

post-treated coal, as established here, provide vital insights to the predicted behavior of a BCBM reservoir, as discussed below.

Hypothetical case: Biogenic re-charge and production from a depleted CBM reservoir:

Here, we consider production from a re-charged CBM reservoir, represented by sample 3 in this study, which is bioconverted post-depletion. The starting point of the process is a saturated CBM reservoir, which was depleted of its original *in situ* methane content. Post-depletion, microbially amended nutrient solution was injected into the reservoir at formation pressure and treated. Post-treatment, the biogenic methane generated was then produced in a manner similar to the original CBM reservoir. Figure 40 presents the strain response of the reservoir over the entire process, and figure 41 is a schematic of the resultant changes in coal structure. The coal structure is presented as a matchstick model, where the coal matrix is represented by individual matchsticks, surrounded by natural fractures (cleats). The matchsticks are assumed to be continuous in the vertical axis, and illustration (figure 41) shows the plan view of a horizontal cross-section through coal. In figure 41, part **AB** represents the structure of original coal pre-depletion (baseline). Parts **A1** and **B1** (column 1) represent the structure of coal post-depletion. Parts **A2** and **B2** (column 2) represent the structure of coal post-bioconversion. Parts **A3** and **B3** (column 3) represent the structure of coal post-depletion of biogenic methane. The prefix A (row) corresponds to change in the structure of coal due to mechanical effects, and prefix (row) **B** corresponds to the change in coal structure as a result of the combination of the sorption and mechanical effect. Hence, the actual state (sorptive and mechanical state) of the reservoir is represented by the row **B**. Row **A** simply corresponds to an intermediate (mechanical effect) step, analyzed in isolation. To summarize, (i) a saturated CBM reservoir is first depleted, (ii) then recharged biogenically until the reservoir is saturated with methane, following which

(iii) the biogenic methane generated is depleted from the BCBM reservoir. Volumetric data obtained in this study was used to understand the changes in coal structure over these three stages.

(i) Initial Depletion: During initial depletion, as the pore pressure decreases, the roles of increased effective stress and desorption induced shrinkage come into play. Continued reduction in pore pressure results in increased effective stress acting on the cleats, reducing its width. This is understood by the helium flooding results of untreated coal, presented in figure 40 (helium quadrant - baseline) and Part **A1** of figure 41. At the same time, reduction in pore pressure results in desorption of methane molecules, resulting in matrix shrinkage. The shrunken matrix results in increased cleat apertures during depletion, thereby boosting the permeability. The combined effect of sorptive strain and mechanical compression due to increased effective stress of the CBM reservoir during depletion is illustrated by the baseline depletion plot (green) in the methane quadrant of figure 40, illustrated as **B1** in figure 41.

(ii) Coal bioconversion: Post-depletion, the reservoir will be injected with amended microbial solution, increasing the reservoir pressure. The produced methane will then adsorb in the coal matrix. There are two aspects to this overall process. First, helium flooding on bioconverted coal revealed a softer coal matrix post-bioconversion, as evident in the helium (treated) injection results presented in figure 40. The volumetric strain measured at the highest helium pore pressure for bioconverted coal was 36% higher than for untreated coal. The implication of a softer coal matrix is that, during formation of biogenic methane, the increase in pore pressure and coal matrix softening would result in matrix compression, shown as **A2** in figure 41. Thus the matrix volume reduces, enlarging the cleats compared to the structure presented in **B1**. The second aspect considers the adsorption of produced biogenic methane in the

coal matrix, resulting in matrix swelling. However, since bioconversion suppresses the sorption-induced strain, matrix swelling will be smaller. Even at complete saturation, the sorptive strain in bioconverted coal would be less (~27%) than the original CBM reservoir. The swelling would follow the volumetric strain behavior as indicated by the treated injection plot in the methane quadrant in figure 40. Schematically, **B2** of figure 41 shows this effect. Since the volumetric strain of treated coal is lower than that for untreated coal, the bioconverted coal would have wider cleat apertures at the end of bioconversion compared to the original CBM reservoir or, a higher permeability.

(iii) Biogenic methane production: Bioconversion will be followed by production of biogenic methane. Similar to a traditional CBM reservoir, BCBM production would also be affected by its coal matrix compressibility and desorption-induced shrinkage behavior. Helium depletion of treated coal revealed a (~39%) stiffer coal matrix. A stiffer coal matrix would limit its deformation due to increased effective stress. This effect is seen in figure 41, where the decrease in cleat apertures in part **A3** (bioconverted coal) is less than in part **A1** (untreated coal).

The sorptive strain trends for methane injection and depletion, as seen in figure 40, were similar for treated coal. Compared to untreated coal (baseline), volumetric response of coal to methane flooding was suppressed. Hence, during depletion, shrinkage of bioconverted coal matrix (**B2** to **B3**) is smaller than that observed for untreated coal (**AB** to **B1**). However, methane depletion revealed excess shrinkage of 0.00034 in bioconverted coals. This implies that the coal matrix of BCBM reservoirs post-depletion (**B3**) would be slightly smaller than the coal matrix post-depletion of an untreated reservoir (**B1**). This would result in a higher final permeability of a biogenic reservoir post-depletion (**B3**) at the end of BCBM production. It is important to mention that the final reservoir permeability is not of much consequence from an operator's

perspective. However, the depleted stress-permeability state of the BCBM reservoir will be crucial for subsequent cycles of bioconversion, where a depleted BCBM reservoir can be bioconverted multiple times, depending on the availability of organic carbon fraction to the microbial community. The factors affecting such a permeability increase would depend on increase in the coal matrix compressibility post-bioconversion, decrease in sorption-induced strains and the magnitude of excess shrinkage. This is further analyzed and presented in part-2 of this two-part paper.

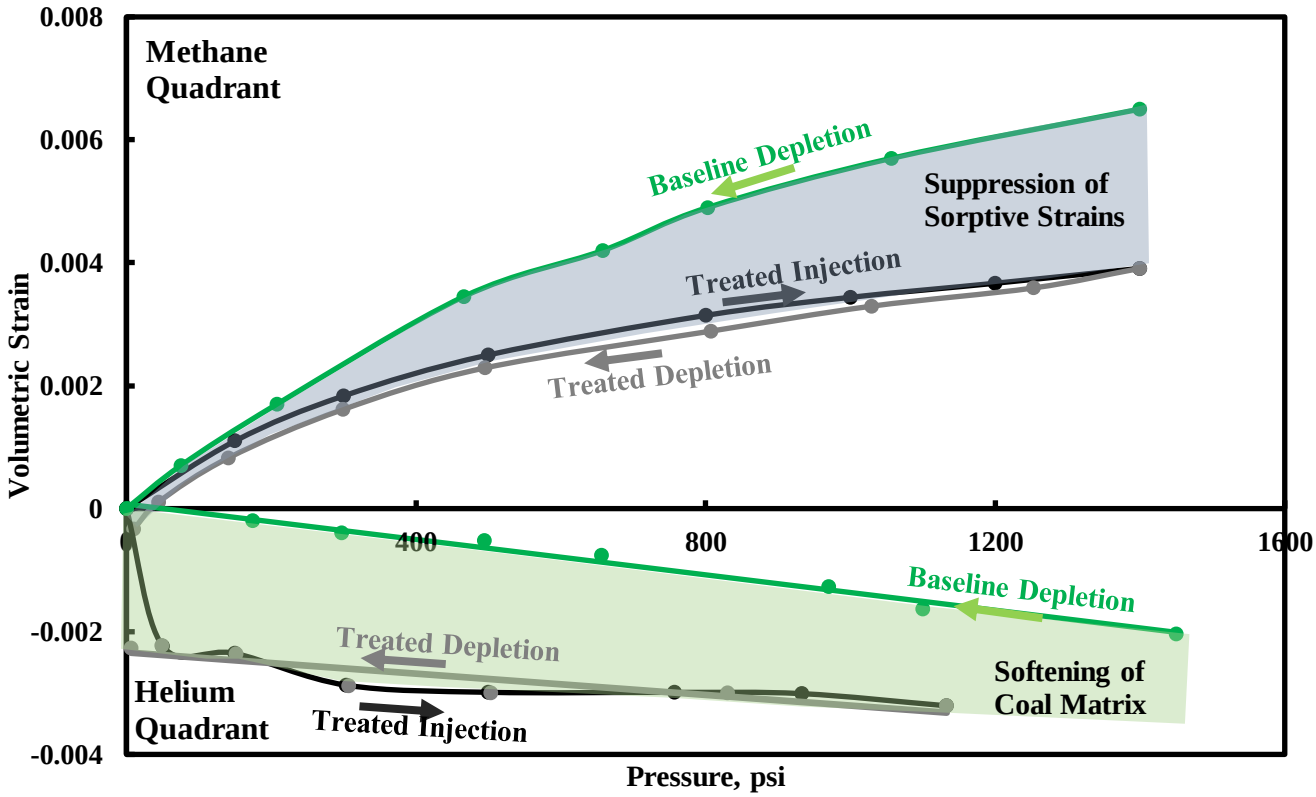

Figure 40: Strains measured pre-and post-bioconversion during helium and methane flooding (sample 3).

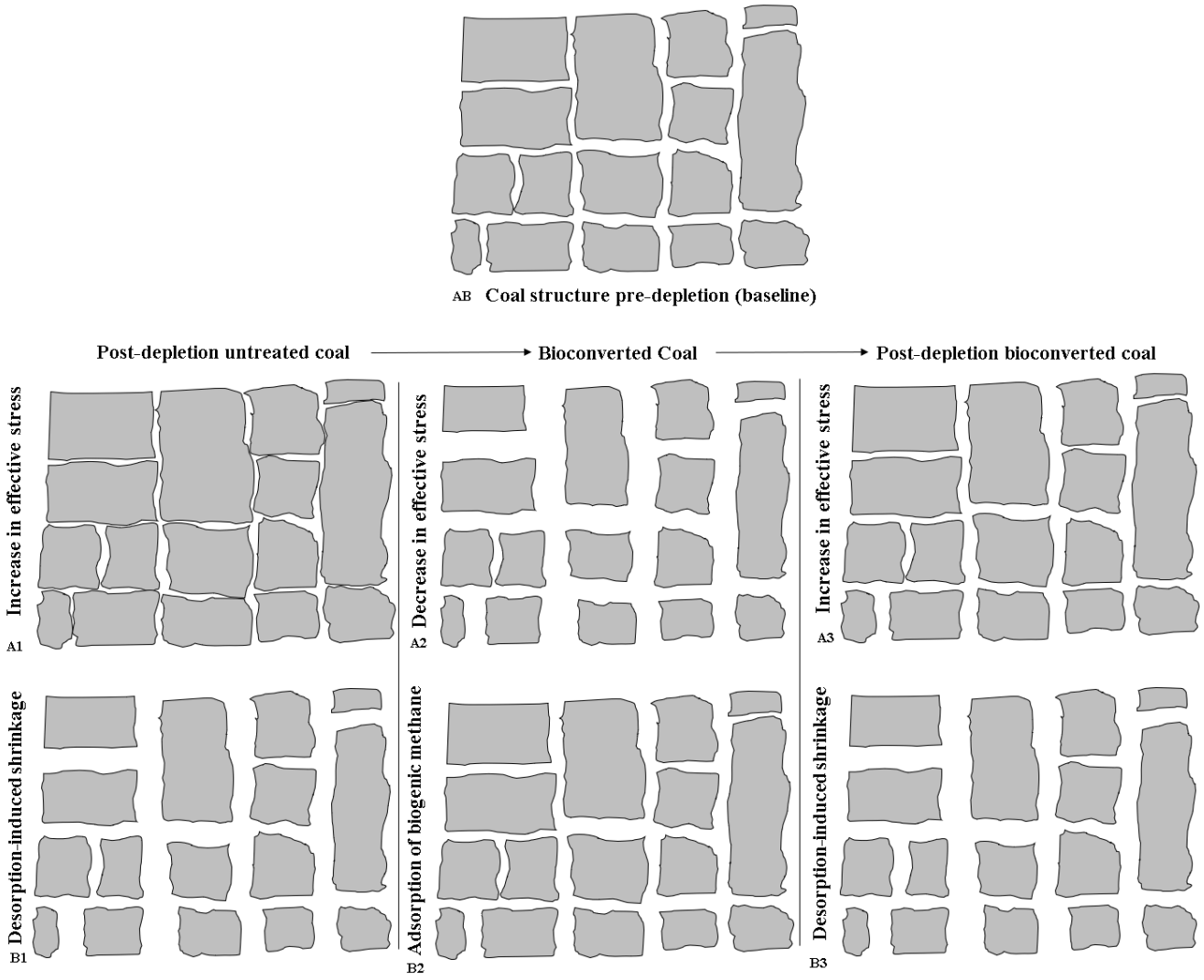

Figure 41: Conceptual model of coal illustrating the effect of bioconversion induced recharge on structure of coal.

4. Conclusions

Variation in the strain response of a coal reservoir due to bioconversion was measured experimentally for helium and methane flooding. Based on the work completed, the following conclusions are made:

a) Helium injection post-treatment revealed a two-step strain variation. Upon initial compression, the treated sample revealed a softer coal matrix, with an order of magnitude

increase in the solid matrix compressibility. However, continued flooding, followed by depletion, showed that the coal matrix became stiffer compared to pre-treated coal. Also, upon complete depletion, the initial strain observed during injection was not recovered, contributing to the inelasticity. This suggests that the process of bioconversion results in unrecoverable matrix compression, enlarging the cleat/fracture apertures, thereby increasing the permeability of the reservoir. Additionally, a stiffer coal matrix during depletion would reduce the negative impact of increased effective stress on the permeability evolution of a reservoir. Hence, qualitatively speaking, the effect will have a positive impact on coal permeability.

b) Methane injection and depletion revealed suppression of the sorption-induced strain behavior post-bioconversion. Reduction in the Langmuir's pressure and volume constants was progressively greater for longer duration of treatment. Such variations have a two-fold impact. First, during biogenic re-charge, adsorption of the produced biogenic methane would result in swelling of the matrix, which would reduce the permeability. Suppressed strains would limit the swelling, thereby limiting the permeability decrease. Second, during production of biogenic methane, desorption-induced shrinkage during depletion helps increase the reservoir permeability. Suppressed strain response would limit this permeability increase. However, methane injection-depletion cycles revealed excess volumetric shrinkage of the coal matrix at the end of the cycle, which will increase the absolute permeability of a depleted BCBM reservoir. This aspect becomes important when considering the possibility of multiple cycles of bioconversion and depletion.

Availability of strain data from helium and methane flooding, pre- and post-bioconversion, enables conducting an in-depth analysis of the reservoir behavior. Further

insights to reservoir performance from a compressibility, effective stress, recovery and rebound pressures, and permeability evolution perspectives; along with sensitivity to variation in geo-mechanical parameters is discussed in part-2 of the manuscript.

Acknowledgement

We gratefully acknowledge support from the US Department of Energy, award number DE-FE0026161. The authors would also like to thank Dr. Yanna Liang and Ji Zhang for providing optimized microbial media for bioconversion.

CHAPTER 4

RESERVOIR INSIGHTS

This chapter presents an exact copy (except for format change) of the journal paper entitled "Impact of bioconversion on matrix strain response of coal reservoirs: Part 2- Reservoir insights." published in *Fuel*, 2019. DOI: doi.org/10.1016/j.fuel.2018.10.008. Elsevier holds the copyright for this paper. This material may be downloaded for personal use only. Any other use requires prior permission of Elsevier.

Authors:

Rohit Pandey, Satya Harpalani

Abstract

Experimental data obtained for the strain response of coal to helium and methane flooding, pre-and post-bioconversion, was used to evaluate the reservoir-scale implications of coal bioconversion. Analysis showed that reservoir parameters, Langmuir-type strain **(ϵ_l)** and pressure **(P_ϵ)**, rebound **(P_{rb})** and recovery **(P_{rc})** pressures decreased post-bioconversion non-linearly with the volume of biogenic methane produced. Also, the solid-matrix compressibility **(C_S)** increased and shrinkage/swelling **(C_m)** compressibility decreased post-bioconversion. The effective stress and permeability response of coal to depletion was suppressed after microbial treatment. Finally, bioconversion resulted in softening of the coal matrix as well as 'excess' volumetric shrinkage post-methane depletion, enhancing the reservoir permeability. However, the increase was insignificant and was overshadowed by the effect of bioconversion induced swelling, which resulted in a significant reduction in reservoir permeability. The non-linear dependence of C_m to pore pressure resulted in its rebound past an inflection pressure **(P_I)**, identifiable for coal treated for longer durations. This was used to define an ideal condition,

beyond which there was some improvement in reservoir performance. Effective stress response of coals before and after treatment was then used to rate the suitability of coals to bioconversion from a reservoir perspective.

Keywords: Coal bioconversion, compressibility, stress state, permeability, reservoir suitability.

1. Summary of Experimental Work

The experimental work investigating the strain response of coal to helium and methane flooding as a result of bioconversion was presented and discussed in part 1 of this two-paper series. Coal treated with nutrient amended microbial solutions, engineered to produce biogenic methane over 15, 30 and 60 days, revealed significant changes in the strain response to helium and methane flooding (step-wise injection and depletion). Results of helium flooding revealed a softer coal matrix post-bioconversion, with the calculated values of solid-matrix compressibility ($\mathbf{C_s}$) an order magnitude lower than that of pre-treated coal. However, such behavior was only observed during initial helium flooding. Subsequent increase in helium pore pressure, and eventual depletion revealed an overall stiffer coal matrix post-bioconversion. Methane flooding revealed a significant suppression of ad-/de- sorption induced matrix swelling/shrinkage characteristics, longer treatment duration resulting in larger suppression of the Langmuir-type pressure $(\boldsymbol{P_\epsilon})$ and strain $(\boldsymbol{\epsilon_l})$, typically used to characterize sorption-induced strains. The experimental results reported in part-1 are summarized in table 8. In this paper, the complementing theoretical/ numerical modeling to understand the reservoir scale behavior of a biogenic coalbed methane (BCBM) reservoir is presented.

2. Background

Transport of fluids in CBM reservoirs is dictated by the dual porosity nature of coal. With depletion, reduced pore pressure results in desorption of methane, initiating diffusion of gas in

the coal matrix towards the cleat network. Hence, diffusion is the first transport process. Once gas reaches the cleats, the flow becomes Darcian, characterized by fluid permeability in the cleats, which is the second transport process. To add to the complexity of the two-staged flow, coal possesses a unique characteristic of sorption-induced matrix swelling/shrinkage. As methane molecules desorb in the matrix, the matrix volume starts to shrink, resulting in opening of the cleat aperture, thus affecting flow rates positively. Simultaneously, decreasing pore pressure reduces the resistance to the tectonic stresses acting on the coal formation. With the tectonic horizontal stresses remaining fairly constant, reduced pore pressure increases the effective horizontal stress, defined as the difference between tectonic stress and pore pressure, acting on the reservoir. This increase in effective stress works to clamp down on the open fractures, thereby reducing the flow rate. The overall resultant flow rate in a CBM reservoir is, therefore, the combined effect of depletion induced increase in effective stresses and desorption-induced matrix shrinkage. Consequently, fluid flow rate varies, depending on the sorptive and geomechanical nature of coal over the producing life of a CBM reservoir.

Table 8: Experimental results of strain response of coal pre-/post- bioconversion.

Sample	Time (days)	Gas Prod (scft)	ϵ_l		P_ϵ (psi)		C_s (psi^{-1})		
			Pre-	Post-	Pre	Post	Pre-	Post-	
								Inelastic	Elastic
1	15	172	0.0145	0.0105	1200	1000	-1.2 E^{-6}	-1.21 E^{-5}	-0.77 E^{-6}
2	30	568	0.0115	0.005	1250	800	-1.08 E^{-6}	-1.05 E^{-5}	-1.03 E^{-6}
3	60	689	0.0135	0.0055	1200	600	-1.43 E^{-6}	-4.47 E^{-5}	-0.87 E^{-6}

A detailed insight of the flow-coupled-geomechanics requires both experimental and theoretical understanding. Typically, experimentally determined sorptive-strain data is used to model the flow behavior and stress conditions of a reservoir. In order to accurately represent the stress behavior of CBM reservoirs, Gray (Gray 1987) was the first to introduce the boundary conditions of uniaxial strain (coal is constrained laterally) and constant verticals stress (determined by the weight of overburden). The subsequent permeability models, particularly the ones presented by Palmer and Mansoori (Palmer and Mansoori 1998) and Shi and Durucan (J. Q. Shi and Durucan 2004), used this approach extensively to understand laboratory and field scale behavior of CBM reservoirs.

Given the advances made in the area of *in situ* coal bioconversion and its application to re-charge depleted CBM reservoirs, it is important to evaluate the effect of coal bioconversion on the state of effective stress and the resulting reservoir permeability variation. After all, *in situ* bioconversion not only requires economic rates of methane production, but also reservoir conditions suitable for economic recovery of the biogenic methane produced. One without the other serves no purpose beyond the science behind the technique/technology. For the sake of clarity, we define production from *re-charged* reservoirs as Biogenic Coalbed Methane production (BCBM). The major goal of the work presented here is to interpret the experimentally established sorption-induced strain behavior of bioconverted coals, reported in part-1, from a reservoir perspective. The improved understanding of reservoir response to bioconversion is then used to create a classification system, ranking coal reservoirs in accordance with their suitability to bioconversion. Three major aspects of reservoir analysis are presented: coal compressibility, effective stress and permeability behavior, all providing insights into the volumetric response of coal to pore pressure variation and aid in projection of long-term gas production from BCBM

reservoirs. Coal compressibility, as discussed in detail by Liu and Harpalani in a two-part paper (S. Liu and Harpalani 2014a, 2014b), provides the starting point for this study. Effective stress and permeability analyses are based on the model proposed by Shi and Durucan (J. Q. Shi and Durucan 2004), which has been successfully used to match laboratory scale (Mitra 2010a) and field scale (J. Q. Shi and Durucan 2004) observations.

3 Reservoir Impact

Given that the sorption-induced strain in coal greatly affects the reservoir performance of a CBM reservoir, we present a number reservoir implication of the strain results and behavior of coal due to bioconversion.

3.1 Compressibility of Coal

Volumetric behavior of reservoir rocks is complex, especially in sorbing gas environments. Extending the work of Zimmerman (Zimmerman 1991) to understanding the volumetric behavior of rocks using different compressibilities to sorptive reservoirs, Liu and Harpalani (S. Liu and Harpalani 2014a) introduced the concept of matrix shrinkage/swelling compressibility ($\mathbf{C_m}$), defined as the incremental change in the volume of coal matrix with respect to changes in sorbing gas pressure. The strains developed in a CBM reservoir during depletion can be split into two separate components: first, the elastic strain related to mechanical de-compression of the solid matrix (solid matrix compressibility, $\mathbf{C_s}$) with depletion and, second, the inelastic shrinkage/swelling strain induced by ad/de-sorption of gas(es). $\mathbf{C_m}$ is obtained from the slope of the true shrinkage/swelling strain vs pore pressure plots, and the solid matrix compressibility is obtained from the slope of the elastic strains recorded during helium flooding with respect to pore pressure. The calculated compressibility values are listed in table 9.

As seen in Table 2, the solid coal compressibility increased post-treatment by 36%, 4.6%

and 39% in the three coals tested respectively, that is, bioconversion resulted in stiffer coal matrix, which deformed less compared to untreated coal under application of mechanical stress.

Table 9: Change in compressibility of coal due to bioconversion

		C_s, psi^{-1}	C_m, psi^{-1}
Sample 1	**Pre-**	-1.2E^{-6}	$C_{m1}^{B} = 0.0145\frac{1200}{(p+1200)^2} + 1.2\text{E}^{-6}$
	Post-	-0.77E^{-6}	$C_{m1}^{A} = 0.0105\frac{1000}{(p+1000)^2} + 0.767\text{E}^{-6}$
Sample 2	**Pre-**	-1.08E^{-6}	$C_{m2}^{B} = 0.0115\frac{1250}{(p+1250)^2} + 1.08\text{E}^{-6}$
	Post-	-1.03E^{-6}	$C_{m2}^{A} = 0.005\frac{800}{(p+800)^2} + 1.03\text{E}^{-6}$
Sample 3	**Pre-**	-1.43E^{-6}	$C_{m3}^{B} = 0.0135\frac{1200}{(p+1200)^2} + 1.43\text{E}^{-6}$
	Post-	-0.87E^{-6}	$C_{m3}^{A} = 0.0055\frac{600}{(p+600)^2} + 0.887\text{E}^{-6}$

Figure 42 shows the variation in shrinkage/swelling compressibility, C_m, with depletion. For all three samples, there was a decrease in the value of C_m post-bioconversion. Thus, sorption-induced deformation in bioconverted coals is lower than in coals prior to bioconversion. Since desorption-induced shrinkage behavior of coal plays a critical role in boosting the permeability with continued production, a decrease in C_m along with an increase in C_s would eventually suppress the permeability evolution with pore pressure reduction in BCBM reservoirs compared to CBM reservoirs. This aspect is discussed further in section 3.3.

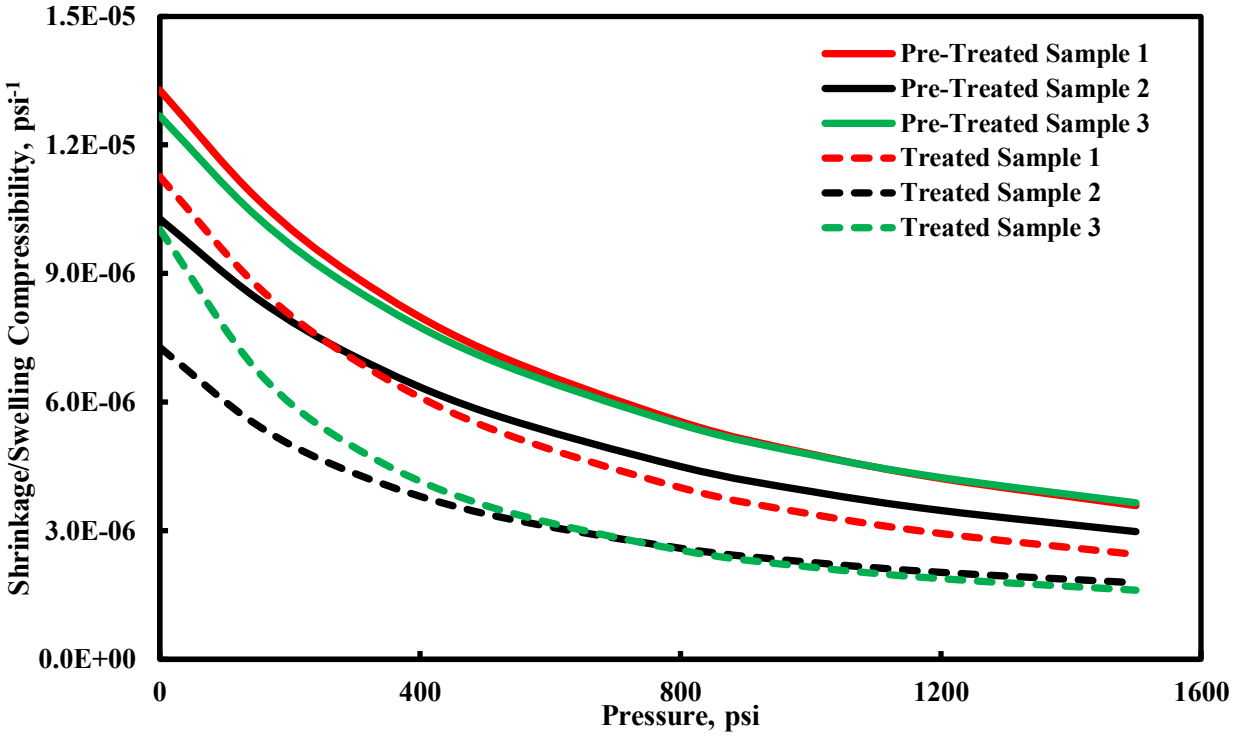

Figure 42: Shrinkage/swelling compressibility of coal pre- and post-treatment.

Figure 43 shows the *change in* C_m, represented by $\boldsymbol{\Delta C_m}$, as a function of pore pressure $\boldsymbol{(p)}$ for the three samples. $\boldsymbol{\Delta C_m}$ was calculated as the difference in the values of $\boldsymbol{C_m}$ pre- and post- treatment at a given pore pressure. It is clear that sample 1, which was treated for the shortest duration and produced the least quantity of methane, had the least reduction. Sample 3, which was treated for the longest duration and produced the maximum quantity of methane, showed the maximum decrease in the value of $\mathbf{C_m}$. However, in the lower pressure regime, the value of $\mathbf{\Delta C_m}$ decreased, past a point of inflection, and the compressibility started increasing. This behavior, distinct for sample 3, initially came across as an aberration, but was understood by analyzing the nature of the plots presented in figures 42 and 43.

In figure 42, $\boldsymbol{C_m}$ for sample 3 post-bioconversion (dashed green line) started increasing rapidly below ~250 psi. This sudden increase in compressibility was not observed for pre-treated coal. Further reduction in pore pressure partly recovered the compressibility lost due to

bioconversion. This can also be understood from figure 43, where past the point of inflection (~250 psi) for sample 3, the change in shrinkage/swelling compressibility decreased.

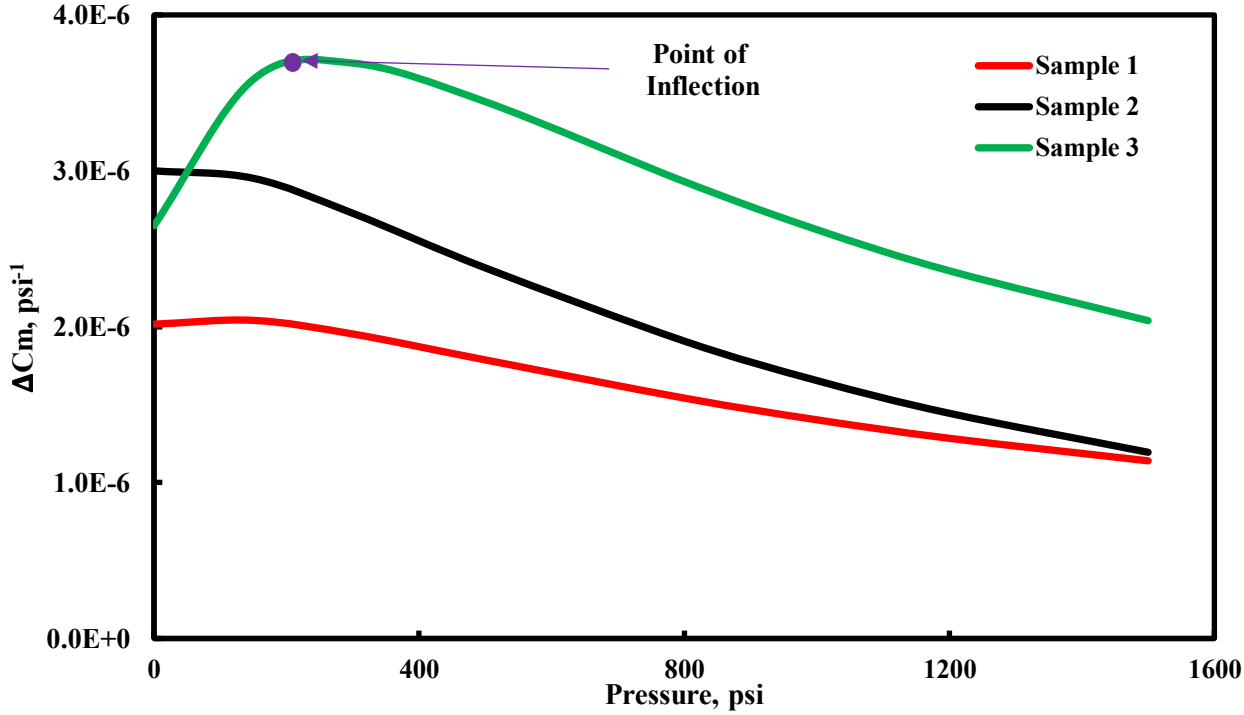

Figure 43: Change in shrinkage/swelling compressibility (ΔCm) of bioconverted coals.

In order to numerically characterize the behavior of bioconverted coal compressibility, we start with the experimental results, where bioconversion of coal resulted in decreased values of $\boldsymbol{C_s}$, $\boldsymbol{\epsilon_l}$ and $\boldsymbol{P_\epsilon}$ by $\boldsymbol{\Delta C_s}$, $\boldsymbol{\Delta \epsilon_l}$ and $\boldsymbol{\Delta P_\epsilon}$ respectively. The expression, $\boldsymbol{\Delta C_m}$, which is the change in shrinkage/swelling compressibility, is then expressed as:

$$\boldsymbol{\Delta C_m} = \left[\frac{\boldsymbol{P_\epsilon\, \epsilon_l}}{\boldsymbol{(p+P_\epsilon)^2}} + \boldsymbol{C_s}\right] - \left[\frac{\boldsymbol{(P_\epsilon - \Delta P_\epsilon)(\epsilon_l - \Delta \epsilon_l)}}{\boldsymbol{(p+P_\epsilon - \Delta P_\epsilon)^2}} + \boldsymbol{(C_s - \Delta C_s)}\right] \quad \textbf{(6)}$$

Recovery of lost compressibility due to bioconversion commences once the pore pressure reduces past the point of inflection. The point itself can be found by differentiating $\boldsymbol{\Delta C_m}$ with respect to pressure and equating it to zero. Additionally, post-bioconversion, $\boldsymbol{\Delta C_m}$ would continue to decrease with depletion once the slope exceeds zero. Thus, the ideal condition is defined by:

$$\frac{\mathbf{d}\Delta \boldsymbol{C_m}}{\boldsymbol{dP}} \geq \mathbf{0} \quad \textbf{(7)}$$

which reduces to the following:

$$\frac{(\boldsymbol{P_\epsilon}-\boldsymbol{\Delta P_\epsilon})(\,\boldsymbol{\epsilon_l}-\boldsymbol{\Delta\epsilon_l})}{(\boldsymbol{p}+\boldsymbol{P_\epsilon}-\boldsymbol{\Delta P_\epsilon})^3} \geq \frac{\boldsymbol{P_\epsilon}\,\boldsymbol{\epsilon_l}}{(\boldsymbol{p}+\boldsymbol{P_\epsilon})^3} \quad \textbf{(8)}$$

Hence, under ideal conditions, bioconversion of coal would result in values of $\boldsymbol{\Delta\epsilon_l}$ and $\boldsymbol{\Delta P_\epsilon}$ such that equation 8 is satisfied. Additionally, greater the difference between the two expressions (left and right-hand sides) in equation 8, greater will be the rebound of the compressibility of bioconverted coals, improving the suitability of coal to bioconversion from a reservoir perspective. However, there exists bounds to the values that $\boldsymbol{\Delta\epsilon_l}$ and $\boldsymbol{\Delta P_\epsilon}$ can attain, which is a function of the volume of methane generated and is discussed in detail in section 4.1. The above situation can also be understood in terms of pore pressure since, with reduction in pore pressure past the point of inflection (inflection pressure, $\mathbf{P_I}$), compressibility of treated coal starts increasing rapidly. Given the cubic nature of the denominator, additional increase in the value of $\boldsymbol{\Delta P_\epsilon}$ past the inflection point would only serve to exponentially increase the left-hand side of equation 8, thereby making a BCBM reservoir more ideal from a reservoir perspective. It also needs to be pointed out that bioconversion results in an increase in the value of $\boldsymbol{\Delta\epsilon_l}$, which bears a linear relationship to $\boldsymbol{\Delta C_m}$ and $\frac{\mathbf{d}\Delta \boldsymbol{C_m}}{\boldsymbol{dP}}$. However, given the relationship of the two Langmuir constants with compressibility components, the pressure parameter bears a greater sensitivity to $\boldsymbol{C_m}$ and $\boldsymbol{\Delta C_m}$. This effect is evident in the behavior of the three coals tested, as seen in figure 44. With increasing treatment duration, the inflection pressure reduced initially. Sample 1 had an inflection pressure of 100 psi, reducing to 40 psi for sample 2. This is due to the reduction in Langmuir parameters resulting from bioconversion. However, for sample 3, which was treated for the longest duration and produced the maximum quantity of methane, the

Langmuir parameters reduced further and the sensitivity to change in pressure parameter became evident, as the inflection pressure increased to ~250 psi. Such behavior of bioconverted coals would play a positive role in the governing Darcian flow *in situ*, since increase in $\boldsymbol{C_m}$ will increase the volumetric shrinkage of the coal matrix, enlarging the cleats and improving the flow rates. This aspect is discussed in more detail in the sections below. However, given that rebound of $\boldsymbol{C_m}$ past an inflection point is noticeable for coals treated for longer duration, flowrate in BCBM reservoirs is expected to improve with longer treatment periods.

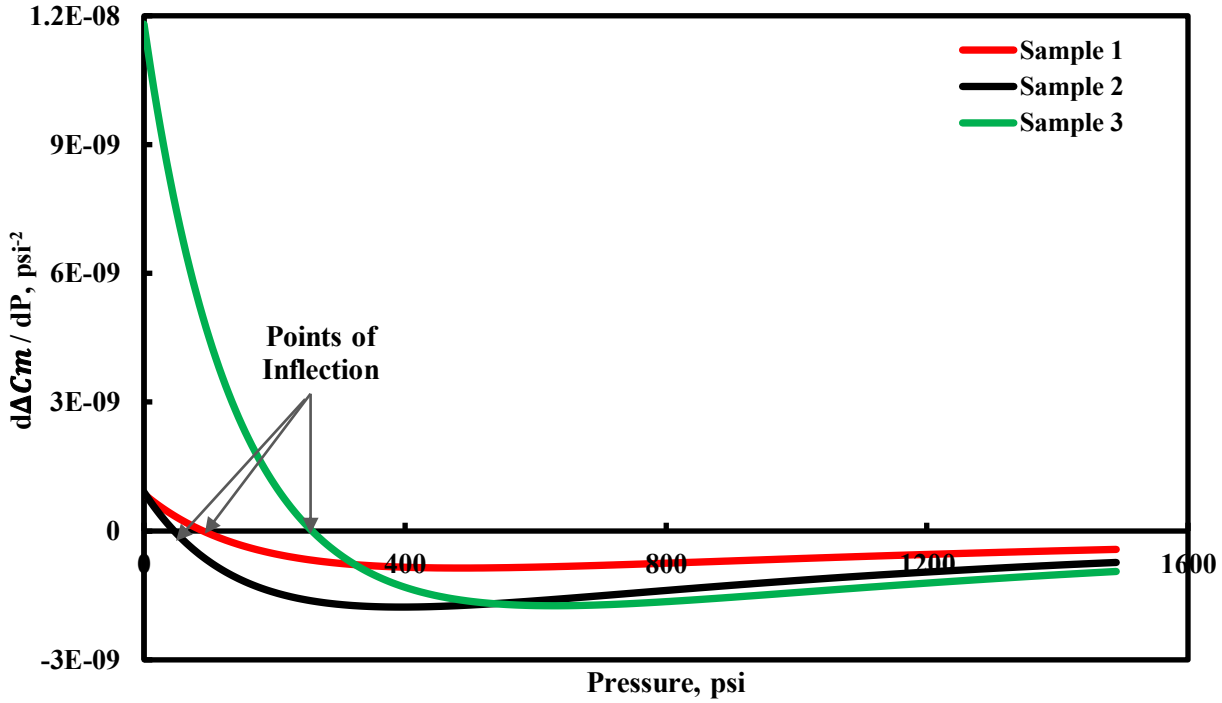

Figure 44: Variation in $\frac{d\Delta C_m}{dP}$ vs pore pressure (p) in the three coal samples.

3.2 Stress Behavior

3.2.1 Effective Stress

Permeability evolution in a CBM reservoir is the result of the combined effect of changes in effective stress and desorption-induced shrinkage behavior. To better understand this inter-relationship, Shi and Durucan (J. Q. Shi and Durucan 2004) looked into the properties of

effective horizontal stress as a function of pore pressure and defined reduction in effective horizontal stress during depletion as $f(\boldsymbol{p}) = \boldsymbol{\sigma_0} - \boldsymbol{\sigma}$, where $\boldsymbol{\sigma_0}$ is the initial effective horizontal stress and $\boldsymbol{\sigma}$ is the effective horizontal stress of the reservoir with continued depletion. The function $f(p)$ was then represented as:

$$\boldsymbol{f(p)} = \frac{\boldsymbol{\nu}}{\boldsymbol{1-\nu}}(\boldsymbol{p} - \boldsymbol{p_0})\left[\boldsymbol{1} - \frac{\boldsymbol{E}}{\boldsymbol{3\nu}}\frac{\boldsymbol{\epsilon_l P_\epsilon}}{(\boldsymbol{p+P_\epsilon})(\boldsymbol{p_0+P_\epsilon})}\right] \quad \textbf{(9)}$$

where **E** is the Young's modulus and $\boldsymbol{\nu}$ is the Poisson's ratio. The stress expression is then used to predict permeability behavior of the reservoir as follows:

$$\frac{\boldsymbol{k}}{\boldsymbol{k_0}} = \boldsymbol{e^{3c_f f(p)}} \quad \textbf{(10)}$$

where $\boldsymbol{k}$ is the cleat permeability, $\boldsymbol{k_0}$ is the initial cleat permeability, $\boldsymbol{c_f}$ is the cleat compressibility. Hence, evaluating reservoir performance from a stress and permeability perspective requires values of Young's modulus, Poisson's ratio and cleat compressibility of the coal type. In this study, these constants were not explicitly measured for the coals tested before and after bioconversion. However, for coals prior to treatment, these parameters are available from past work (Mitra 2010a), presented in table 10. To highlight the effect that sorptive strain parameters have on the reservoir performance due to bioconversion, it was initially assumed that the bioconversion does not change the values of these three parameters. However, in section 4.3, a sensitivity analysis for the variation in the three parameters provides an overall perspective of the expected changes in reservoir behavior due to bioconversion.

Table 10: Values of geomechanical parameters for Illinois #6 coal (Mitra 2010b)

Parameter	**Young's Modulus**	**Poisson's Ratio**	**Cleat Compressibility**
Value	307,000 psi	0.4	0.003 psi^{-1}

From a flow perspective, reduction in effective horizontal stress results in reduced resistance to flow, thereby increasing Darcian flow in the reservoir. Figure 45 plots the function $\boldsymbol{f(p)}$ against pore pressure. For pre-treated coal, decreasing pore pressure lowers the effective stress, thus increasing the change in horizontal stress, $\boldsymbol{f(p)}$. However, bioconversion of coal suppressed the behavior of $\boldsymbol{f(p)}$, where decrease was the least for sample 1 and maximum for sample 3. The change was estimated by calculating the area (units of psi^2) bound by the plots between pre-and post-treated coals: 31,772 psi^2, 56,035 psi^2 and 63,960 psi^2 for the three samples. Hence, longer treatment periods, resulting in increased amount of biogenic methane production, would impede the reduction in effective horizontal stresses with continued depletion, thus lowering the Darcian flow rates.

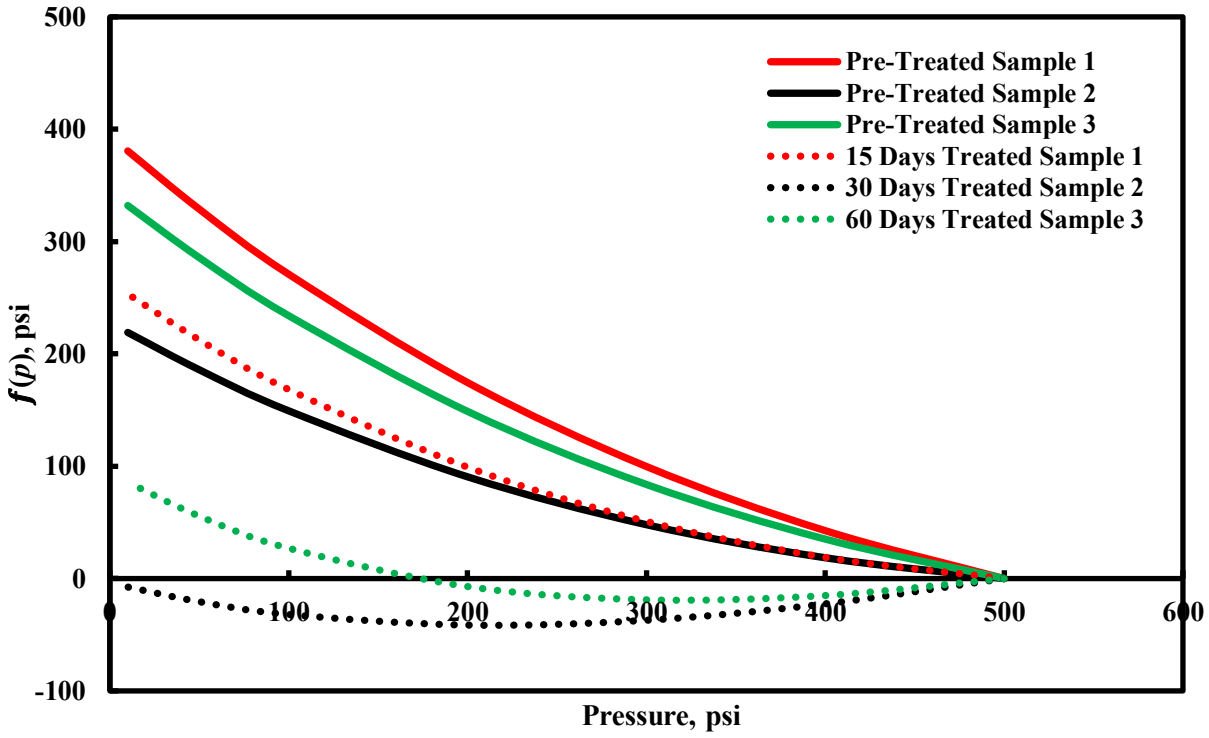

Figure 45: Modeled variation in reduction of effective horizontal stress, $\boldsymbol{f(p)}$, with pore pressure pre- and post-treatment.

3.2.2 Rebound and Recovery Pressures

The behavior of $\boldsymbol{f(p)}$ for samples 2 and 3 presents an interesting aspect of reservoir behavior, understood by the concepts of recovery ($\mathbf{P_{rc}}$) and rebound ($\mathbf{P_{rb}}$) pressures. Post-treatment, sample 2 (figure 4) had negative values of $\boldsymbol{f(p)}$ for the entire depletion period. Sample 3, on the other hand, had a part of the $\boldsymbol{f(p)}$ vs **p** plot in the negative Y-axis and the remaining part in positive axis. The pore pressure at which the function $\boldsymbol{f(p)}$ assumes a minimum value, that is, the value of **p** when $\boldsymbol{f'(p) = 0}$, is the rebound pressure (note: $\boldsymbol{f''(p) > 0}$ and the first derivative equated to zero will give the minimum value). $\mathbf{P_{rb}}$ is expressed as (J. Q. Shi and Durucan 2004):

$$\boldsymbol{P_{rb} = \sqrt{\frac{EP_\epsilon \epsilon_l}{3\nu}} - P_\epsilon} \qquad \textbf{(11)}$$

The rebound pressure marks the point where the positive effect of desorption-induced shrinkage on the effective horizontal stress exceeds the negative effect of cleat compression. Any reduction in pore pressure beyond the rebound pressure increases the effect of desorption-induced shrinkage, thus increasing the value of $\boldsymbol{f(p)}$. From production perspective, the rebound pressure of a coal-type should be as high as possible. Table 11 lists the values of rebound pressures of the three samples, pre- and post-treatment. For all tests, bioconversion resulted in reduction of the rebound pressures, longer treatment duration resulting in larger reduction. Since bioconversion suppresses the sorptive strain response of coal, it takes longer for coal to overcome the negative effect of cleat compression, explaining the decrease in the values of $\mathbf{P_{rb}}$ post bioconversion. Hence, bioconversion increases the sensitivity of coal to changes in effective stress.

The recovery pressure is the pore pressure at which the initial value of effective stress of the reservoir is attained. This is calculated by arriving at the non-trivial solution for $\boldsymbol{f(p) = 0}$, for $\boldsymbol{p \neq p_o}$. The recovery pressure is expressed as (J. Q. Shi and Durucan 2004):

$$P_{rc} = \frac{E}{3\nu}\frac{P_\epsilon\,\epsilon_l}{(p_0+P_\epsilon)} - P_\epsilon \quad \textbf{(12)}$$

Table 11 includes the calculated values of P_{rc} for the three coals tested, pre- and post-treatment. Similar to its effect on rebound pressure, bioconversion of coal resulted in reduction of the recovery pressure for coal, the decrease being least for sample 1 and maximum for sample 3. Hence, it would take longer for the reservoir to attain its initial state of effective stress in bioconverted coals with continued depletion. For sample 2, the recovery pressure attains a negative value, implying that the reservoir would never attain its initial state of effective stress, graphically evident from the plot of $f(p)$ for sample 2 in figure 4.

Table 11: Rebound and recovery pressures pre- and post-treatment.

	Sample 1: 15 Days			**Sample 2: 30 Days**			**Sample 3: 60 Days**		
	Pre-	**Post-**	**Change**	**Pre-**	**Post-**	**Change**	**Pre-**	**Post-**	**Change**
P_{rb} (psi)	915	643	272	672	214	458	841	321	520
P_{rc} (psi)	1432	800	632	862	-8	871	1250	171	1079

Shi and Durucan (J. Q. Shi and Durucan 2004), extending the understanding of reservoir rebound and recovery pressures, put forward five cases of reservoir conditions, based on the values of rebound, recovery and initial pore pressure. Type-A reservoir is one where both rebound and recovery pressures assume a negative value, and the rebound pressure is greater than the recovery pressure, that is $p_0 > 0 > P_{rb} > P_{rc}$. Type-B reservoirs are similar to type-A reservoirs, with the difference that the rebound pressure is positive. The state of the reservoir can be described by $p_0 > P_{rb} > 0 > P_{rc}$. In type-C reservoirs, both rebound and recovery

pressures assume positive values, $\boldsymbol{p_0 > P_{rb} > P_{rc}}$. Type-D reservoir is one where the initial pore pressure is lower than the recovery or rebound pressures, $\boldsymbol{P_{rc} > P_{rb} > p_0}$. In a type-D reservoir, any depletion of methane results in a continually increase in the value of $\boldsymbol{f(p)}$, thus increasing the permeability with continued depletion.

Table 12 lists the reservoir conditions of the coal-types before and after bioconversion. Since coal bioconversion results in reduction in the values of $\mathbf{P_{rc}}$ and $\mathbf{P_{rb}}$, its state transitions from a type-D to type-A reservoir. However, the extent of this transition is a function of the degree of biogenic gasification that the reservoir is subjected to and the initial stress state of the reservoir. A closer look at the expressions for $\mathbf{P_{rc}}$ and $\mathbf{P_{rb}}$ reveals that a coal reservoir with numerically larger Langmuir strain constant $\boldsymbol{(\epsilon_l)}$ would have larger values of rebound and recovery pressures, and $\boldsymbol{f(p)}$ would tend to be positive for a larger range of pore pressures compared to a coal type with lower values of $\boldsymbol{\epsilon_l}$. This would vary the initial state of the reservoir, which is evident in the samples tested, since sample 2, which presented itself with the lowest values of $\boldsymbol{\epsilon_l}$ prior to treatment, transitioned itself to a type-B reservoir. On the other hand, sample 3, which had numerically larger values of $\boldsymbol{\epsilon_l}$, even with larger reduction in the values of $\mathbf{P_{rc}}$ and $\mathbf{P_{rb}}$, transitioned only to a type-C reservoir. If the initial values of $\boldsymbol{\epsilon_l}$ were the same for samples 2 and 3, sample 3 would have transitioned further down the scale in comparison to sample 2. Sample 1, which was treated for the shortest duration exhibited the least reduction in $\mathbf{P_{rc}}$ and $\mathbf{P_{rb}}$ and the bioconverted reservoir remained as a type-D reservoir.

Table 12: Change in reservoir conditions due to bioconversion.

Sample Description		**Reservoir Type: State**
Sample 1	**Before**	$\boldsymbol{D: P_{rc} > P_{rb} > p_0}$
	After	$\boldsymbol{D: P_{rc} > P_{rb} > p_0}$

Sample 2	**Before**	$\boldsymbol{D}: \boldsymbol{P_{rc} > P_{rb} > p_0}$
	After	$\boldsymbol{B}: \boldsymbol{p_0 > P_{rb} > 0 > P_{rc}}$
Sample 3	**Before**	$\boldsymbol{D}: \boldsymbol{P_{rc} > P_{rb} > p_0}$
	After	$\boldsymbol{C}: \boldsymbol{p_0 > P_{rb} > P_{rc}}$

Figure 46 shows the general effect of bioconversion on the stress state of the reservoir where, with increasing degree of bioconversion, a coal reservoir makes the transition down the scale from a type-D to a type-A reservoir. The extent of this transition is a function of the initial stress state and degree of bioconversion. This is indicative of the negative effect of bioconversion on the reservoir response to depleting a BCBM reservoir.

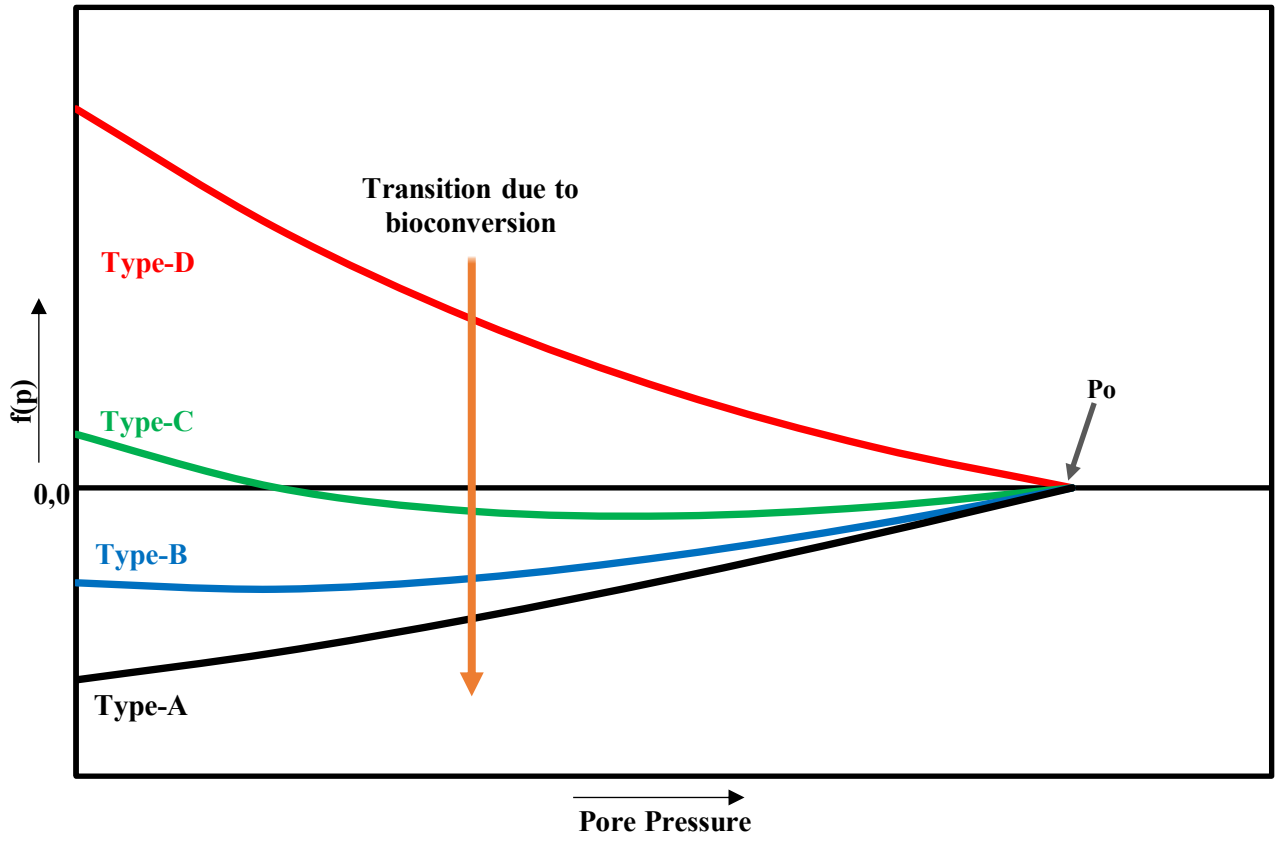

Figure 46: Transition of reservoir state due to bioconversion.

3.3 Reservoir Permeability Behavior

The permeability of a coal reservoir and the nature of its evolution with continued depletion play a vital role in determining the productivity and, in turn, its economic feasibility. The permeability model presented by Shi and Durucan (J. Q. Shi and Durucan 2004) uses the uniaxial strain approach and has seen widespread practical application. Assuming a bundle of matchstick geometry, the permeability behavior of a CBM reservoir is given by equation 10.

Given the inter-relationship between permeability and $\boldsymbol{f(p)}$, any change in $\boldsymbol{f(p)}$ due to bioconversion would subsequently affect the permeability behavior of the reservoir. The modeled pressure-dependent permeability behavior for the three samples, pre- and post-treatment is shown in figure 47. For pre-treated coal, reduction of pore pressure increases the permeability. At the lowest pore pressure, the increase in permeability is ~30, 8, and 20 times the initial permeability for the three coals tested. Sample 2 had lower values of Langmuir strain pre-treatment, possibly due to relatively higher inorganic content in the sample compared to 1 and 3, and resulted in smaller increase of permeability with depletion. Post-bioconversion, the increase in permeability with depletion was severely stunted in all three samples. Permeability of samples 1 and 3 increased by ~10 and 2 times the initial permeability respectively, whereas sample 2, which had lower permeability increase pre-treatment, failed to recover to the initial permeability of the reservoir after bioconversion, with $\boldsymbol{k/k_0}$ at complete depletion estimated at ~0.93. Taking a closer look at the nature of $\boldsymbol{k/k_0}$ vs $\mathbf{p}$ for sample 3, it is apparent that initial depletion, that is, at higher pore pressures, permeability of the reservoir decreased. Around 250 psi, the permeability started increasing and the initial state of permeability during depletion was recovered, that is, $\boldsymbol{(k/k_0)_{250} = 1}$. At complete depletion, the reservoir had a permeability higher than the initial state. This behavior was not seen for sample 2 and can be explained. First,

the value of ϵ_l for sample 3 was higher than sample 2 post-bioconversion although the decrease in the value of ϵ_l was larger for sample 3. Therefore, the modeled k/k_0 values showed relatively improved performance at lower pore pressures. Second, let us look at the behavior of C_m with depletion. It was explained in section 3.1 that the shrinkage/swelling compressibility increases for sample 3 past an inflection point. Since the sorption-induced deformation past the inflection pressure in sample 3 increases, the cleats/fractures open up more, resulting in increased permeability.

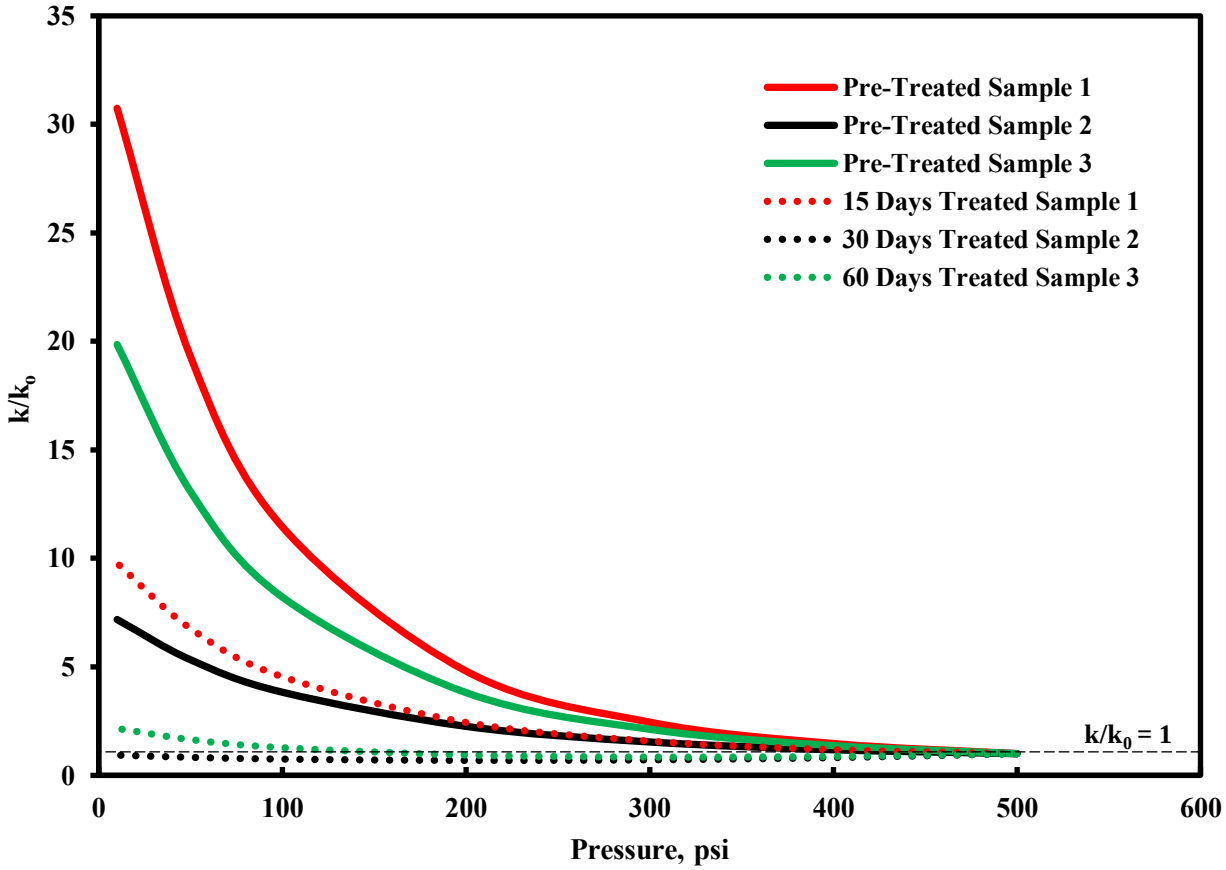

Figure 47: Variation in modeled permeability with depletion pre- and post-treatment using Shi and Durucan model.

3.4.4 Variation in Absolute Permeability

Production from a BCBM reservoir can be divided in three stages. First, there is depletion

of the original CBM reservoir prior to bioconversion. Second, the depleted CBM reservoir is re-charged by injecting nutritionally amended microbial solution engineered to produce methane. This increases the pore pressure of the reservoir. The third and final stage is production from the bioconverted BCBM reservoir until depletion. Experimental results obtained from helium and methane flooding revealed two distinct changes in the structure of coal which would affect the absolute permeability of the reservoir: matrix softening post-bioconversion and excess volumetric shrinkage post-depletion of bioconverted coals.

The absolute permeability of a coal reservoir is a function of the associated coal geometry: cleat aperture (p) and cleat spacing (q). Considering a matchstick model, permeability is given as:

$$\boldsymbol{k = \frac{p^3}{12q}} \qquad \textbf{(13)}$$

During re-charge of a depleted CBM reservoir, softer coal matrix post-bioconversion would result in inelastic matrix compression. This is because *in situ* coal bioconversion would be conducted at elevated pore pressures (~0.43 psi per foot of depth in feet) which, acting on the softer coal matrix will cause it to compress (shrink). This behavior is evident from the inelastic strains measured during initial helium flooding of treated coals. Additionally, at the end of methane injection-depletion cycle, the coal matrix exhibited negative strains. The negative strains indicate excess volumetric shrinkage of coal matrix at the end of the biogenic methane production cycle. The shrunk coal matrix as a result of these effects would result in increased permeability. However, core flooding experiments conducted at University of Alberta (Stephen et al. 2014) revealed continuous decrease in coal permeability due to bioconversion. Such decrease was explained by Pandey and Harpalani (R. Pandey and Harpalani 2018) as the result of 'matrix swelling due to bioconversion', resulting in smaller cleat apertures, thereby reducing the

flow rates.

Figure 48 schematically illustrates the individual effects of bioconversion induced swelling, matrix softening, and excess volumetric shrinkage on coal permeability. The figure is divided into four sections, each section representing the matrix and cleat structure of coal corresponding to a unique effect of bioconversion. Initially, two matrix matchsticks of width 'x' were separated by cleat aperture 'b'. This represents the structure of a depleted CBM reservoir, prior to treatment. The corresponding permeability of the reservoir at that stage is included. As the reservoir is recharged, the effect of coal 'matrix swelling due to bioconversion' is illustrated in the second part of figure 48, where the cleat width reduces by '2c'. This results in a decrease in reservoir permeability, as the aperture size reduces to 'b-2c'. The next effect illustrated is the 'matrix softening' effect of bioconversion. As coal gets softer, increased pore pressure will compress the matrix, increasing the aperture to 'b-2c+2y', slightly improving the permeability of the reservoir. The fourth illustration highlights the effect of 'excess volumetric shrinkage' that will be observed in the BCBM reservoir at the end of depletion. This effect would improve the permeability of the depleted reservoir since the cleat widens to an aperture of 'b-2c+2y+2z'. However, based on the results of this study along with the results reported previously, it was realized that the effect of matrix swelling due to the process of bioconversion was much greater than the cumulative effect of the two other changes, i.e., $c >> y + z$. Additionally, since the effect of bioconversion induced swelling starts affecting the flow right before production of the reservoir, this negative aspect of bioconversion is predominant throughout the producing life of the reservoir, severely undermining any expected positive effects at any stage.

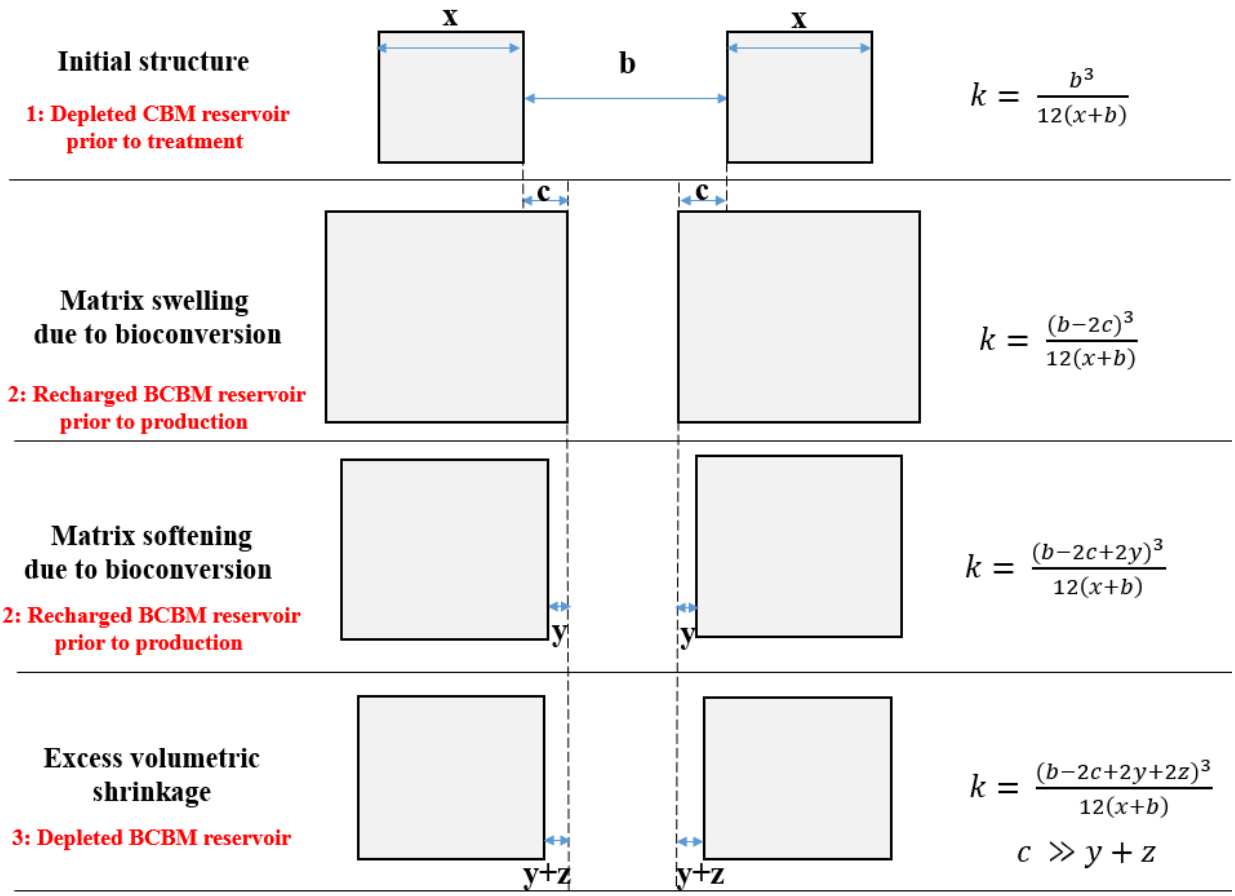

Figure 48: Factors leading to permeability variation of a bioconverted reservoir.

The above discussion is based on the results of experimental investigations, where core imaging results revealed a reservoir permeability of 42 md for the coal type used in this study (Pandey and Harpalani 2018). Considering isotropic strain behavior, the effect of inelastic strains due to matrix softening and excess shrinkage increased the reservoir permeability by ~0.1 mD. The results of the permeability increase over 60 days of treatment is presented in figure 49, where the effect of excess shrinkage was fairly constant over the treatment duration. The permeability increase due to inelastic strain was much more noticeable, and indicates a positive effect with treatment duration. The bounds to this increase are not known at this time and requires further experimental investigations into this behavior. However, the decrease in permeability due to bioconversion induced swelling, as reported by Pandey and Harpalani (R.

Pandey and Harpalani 2018), was ~33 md, rendering the calculated increase in permeability negligible. This is the trend observed for Illinois coals, and has been used to describe the process. However, a general comment about the relative nature of these different types of strains for different types of coals cannot be made at this time given the limited data. Thus, in addition to accounting for the sorption-induced-strain behavior and effective stress response of a CBM reservoir, models for permeability of BCBM reservoirs should include expressions for excess shrinkage, matrix softening, and bioconversion induced swelling of coal, theoretically given as:

$$\frac{k}{k_{0_{Bio}}} = f\left(\begin{matrix}\boldsymbol{effective\ stress}\\ \boldsymbol{sorptive\ strains}\\ \boldsymbol{matrix\ softening\ strains}\\ \boldsymbol{excess\ shrinkage}\\ \boldsymbol{bioconversion\ induced\ swelling}\end{matrix}\right) \qquad \textbf{(14)}$$

where $\frac{k}{k_{0_{Bio}}}$ is the permeability response of a BCBM reservoir.

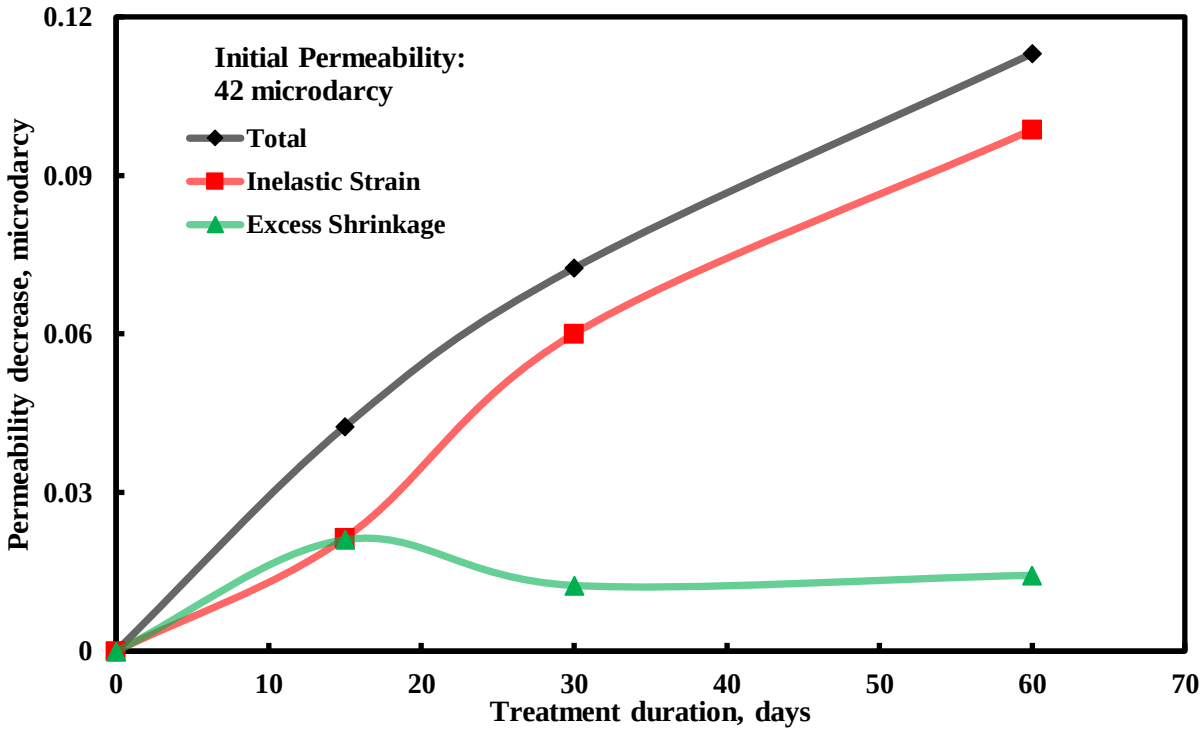

Figure 49: Increase of reservoir permeability due to excess shrinkage and matrix softening effects.

4 Discussion

4.1 Parametric Interrelationship

So far, we have looked at the changes in strain behavior of coals when subjected to bioconversion. The behavior is characterized by the Langmuir constants, solid-matrix and shrinkage/swelling compressibility, rebound and recovery pressures and permeability evolution of the reservoir. The effect of bioconversion on a majority of the parameters is shown to be similar: negative from a reservoir perspective, the effect becoming more pronounced with longer treatment duration, which translated to increasing volumes of methane generated. Figure 9 shows the change (before - after) in the values of $\boldsymbol{\epsilon_l}$, $\boldsymbol{P_\epsilon}$, $\mathbf{P_{rc}}$ and $\mathbf{P_{rb}}$ with the volume of methane produced. The results indicate that increasing volumes of methane resulted in larger changes in the parameters, that is, greater decrease in the values post-bioconversion. This change bears a 'near-linear' relationship with the volumes of gas produced by coal. Given the nature of relationship between treatment duration and gas production, Suman and Harpalani (Suman Saurabh and Harpalani 2018) showed that, for a given microbial consortia, biogenic methane production would reach a maximum over time and methane production would cease to increase beyond that. For Illinois coal, methane production reached the near-maximum at the end of the 60-day treatment period. Hence, there exists an upper-bound, ~700 scft in our case as shown in figure 50, which would restrict further change in the values of the parameters. The implication of such behavior is that, increasing the treatment duration extensively would not result in variation of the Langmuir's constants and recovery and rebound pressures. However, if the BCBM reservoir is subjected to multiple rounds of bioconversion and production, continual decrease in these parameters is expected with each cycle of bioconversion.

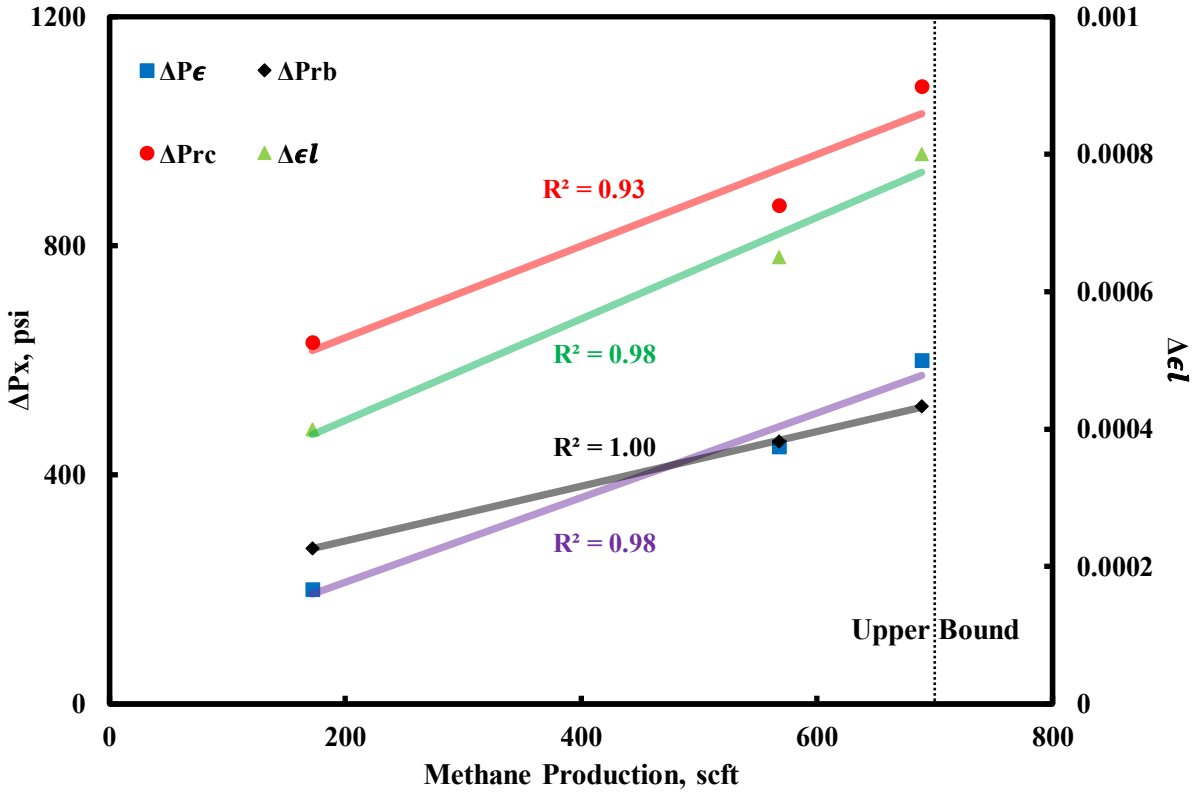

Figure 50: Variation in Langmuir parameters, rebound and recovery pressures with biogenic methane production.

4.2 Nomenclature

The economics of a BCBM reservoir can be divided into two aspects: gas generation and reservoir performance. Economic assessment of a BCBM reservoir from the gas generation perspective was presented by Zhang et al (Ji Zhang et al. 2016) and Park and Liang (Park and Liang 2016). There exist only a few studies that investigate the reservoir scale effect of coal bioconversion (Pandey et al. 2016; Pandey and Harpalani 2018; Pandey 2015b; R. Zhang et al. 2017). Given the understanding of coal as a reservoir and the associated changes observed in this study, it is possible to rate the suitability of a potential BCBM reservoir from an effective stress perspective.

As discussed in section 3.4.2, bioconversion results in transitioning the reservoir from a type-D

to a type-A reservoir, which negatively affects the permeability evolution of the reservoir. The start and end points of the transition are a function of the sorptive strain response of untreated coal and biogenic methane volumes produced respectively.

Considering multiple coalbeds with same initial permeability ($\mathbf{k_o}$) and producing equal volumes of biogenic methane over a treatment duration, the suitability of the BCBM reservoirs can then be evaluated by its initial stress state, and the number of transitions (degree of bioconversion) it makes. It is also assumed that, over the course of bioconversion, the change in the expression $\boldsymbol{f(p)}$ as a function of pore pressure, as given by eq. 9, and calculated by the area bound by the $\boldsymbol{f(p)}$ vs **p** plot before and after bioconversion, are the same. Based on the proposed system, a biogenic reservoir can be identified by a T-Xn nomenclature, where T-X stands for the initial state of the reservoir, as in Type-D, -C, -B or -A and n stands for the degree of bioconversion. The degree of bioconversion can have numeric values from 0 to 3, 0 being when the final state of the reservoir is same as the initial state, and 3 being when the reservoir transitions through the three types of reservoir states due to bioconversion. The values of 1 and 2 imply that the reservoir transitioned through one and two reservoir types respectively. Table 13 presents the different types of coalbed methane reservoirs in decreasing order of suitability for biogenic conversion, solely from a reservoir perspective.

In accordance with the nomenclature, sample 1 representative of a T-D0 biogenic reservoir was most suitable for bioconversion. Sample 3 which represented a T-D1 reservoir, ranked next in suitability. Sample 2, being a T-D2 reservoir, was the least suitable from a reservoir perspective. The impact of sample 1 representing the most suitable and sample 3 representing the least suitable can also be seen in the permeability evolution modeled for the three samples in figure 47. Hence, a more suitable reservoir showed a greater rebound in

permeability of the bioconverted reservoir with depletion. This behavior was suppressed with subsequent decrease in suitability of the samples 3 and 2 respectively.

Table 13: Reservoir suitability for bioconversion.

Suitability	**Type of Biogenic Reservoir**	**Final State**
Most Suitable ↓ **Least**	T-D0	D
	T-D1	C
	T-C0	
	T-D2	B
	T-C1	
	T-B0	
	T-D3	A
	T-C2	
	T-B1	
	T-A0	

It needs to be borne in mind that this ranking/classification system does not consider the biogenic methane productivity or duration of treatment in its design, and is solely a measure of reservoir performance and can, therefore, not be used to assess the feasibility of BCBM as a process in its entirety. Another aspect that is overlooked in the proposed system is the absolute permeability (**k**) of the biogenic reservoir. A reservoir with higher absolute permeability would evidently be more suitable for bioconversion than a coal reservoir with a lower absolute permeability. For example, a reservoir with an initial absolute permeability of 500 md (milidarcy) and a final absolute permeability of 300 md post-bioconversion, would obviously be

a better choice than a reservoir of 20 µd (microdarcy) initial permeability and 200 µd final permeability, irrespective of the type of the reservoir. The proposed system, however, makes it easier to ascertain suitability of bioconversion of similar-type coals in terms of its absolute permeability.

4.3 Sensitivity Analysis

The analysis of the strain response of a reservoir, as presented above, assumed that the Young's modulus, Poisson's ratio and the cleat compressibility did not change due to bioconversion. Such an assumption results in errors in the behavioral estimation of $\boldsymbol{f(p)}$ and $\mathbf{k/k_o}$ vs **p**. Therefore, a sensitivity analysis was carried out to ascertain the reservoir scale effect of bioconversion in its entirety, primarily the impact of the variation of E and $\boldsymbol{\nu}$ on $\boldsymbol{f(p)}$. The baseline case was that of sample 1, with a $\boldsymbol{\epsilon_l}$ of 0.0145, $\boldsymbol{P_\epsilon}$ of 1200 psi, where post 60 days treatment, $\boldsymbol{\epsilon_l}$ reduced by 0.008, and $\boldsymbol{P_\epsilon}$ by 600 psi.

The strain response to helium flooding enabled estimation of bulk modulus, which is inverse of the solid-matrix compressibility ($\mathbf{C_s}$). Hence, changes in Young's modulus can be determined from the ratio of bulk compressibility pre- and post- treatment. For the three samples treated, increase in Young's modulus for bioconverted sample 3 was the highest, 1.65 times the initial value, which set the upper bound for the value of **E**. The sensitivity of $\boldsymbol{f(p)}$ of bioconverted coal to changes in Young's modulus (constant $\boldsymbol{\nu}$) was then established, and the results are graphically illustrated in figure 51. Evidently, bioconversion induced change in Young's modulus results in recovery of stress state (shaded in yellow), undoing the effect of decrease in the reservoir parameters as discussed above. However, it needs to be pointed out that loss of compressibility is also associated with increase in Poisson's ratio. Figure 51 includes the plot of variation of $\boldsymbol{f(p)}$ with increase in Poisson's ratio (constant **E**). The upper bound of the

value of $\boldsymbol{\nu}$ was set to the theoretical maximum of 0.5 to identify the worst-case scenario. Decrease in $\boldsymbol{\nu}$ affects the reservoir stress state negatively, as seen in the green-shaded region of figure 10. Effects of varying both the Young's modulus and Poisson's ratio due to bioconversion would then be represented by the combination of both the green and yellow regions. In comparison to the behavior of $\boldsymbol{f}(\boldsymbol{p})$ for untreated coal, the overall effect of bioconversion on the stress state was negative. However, past the 200 psi mark, for the highest possible values of Young's modulus, the analysis predicts a slightly improved stress state of bioconverted coal, the probability of which was calculated to be 0.095 (area above baseline/area below baseline). Increase in Young's modulus can also be viewed as a stiffer coal. As the coal matrix becomes stiffer, it becomes more susceptible to desorption induced shear failure (Espinoza et al. 2015; S. Saurabh, Harpalani, and Singh 2016). As coal fails during depletion, it is associated with fines and fracture formation. Fines serve to block the flow paths in coal, thereby reducing permeability. Removal of these fines requires well cleanout, after which the permeability of a CBM reservoir increases (Okotie and Moore 2011). Determining the exact mechanics of such fracture formation, or its possibility, requires extensive flow-coupled geomechanical testing, beyond the scope of this work, and has been suggested as an area of future work.

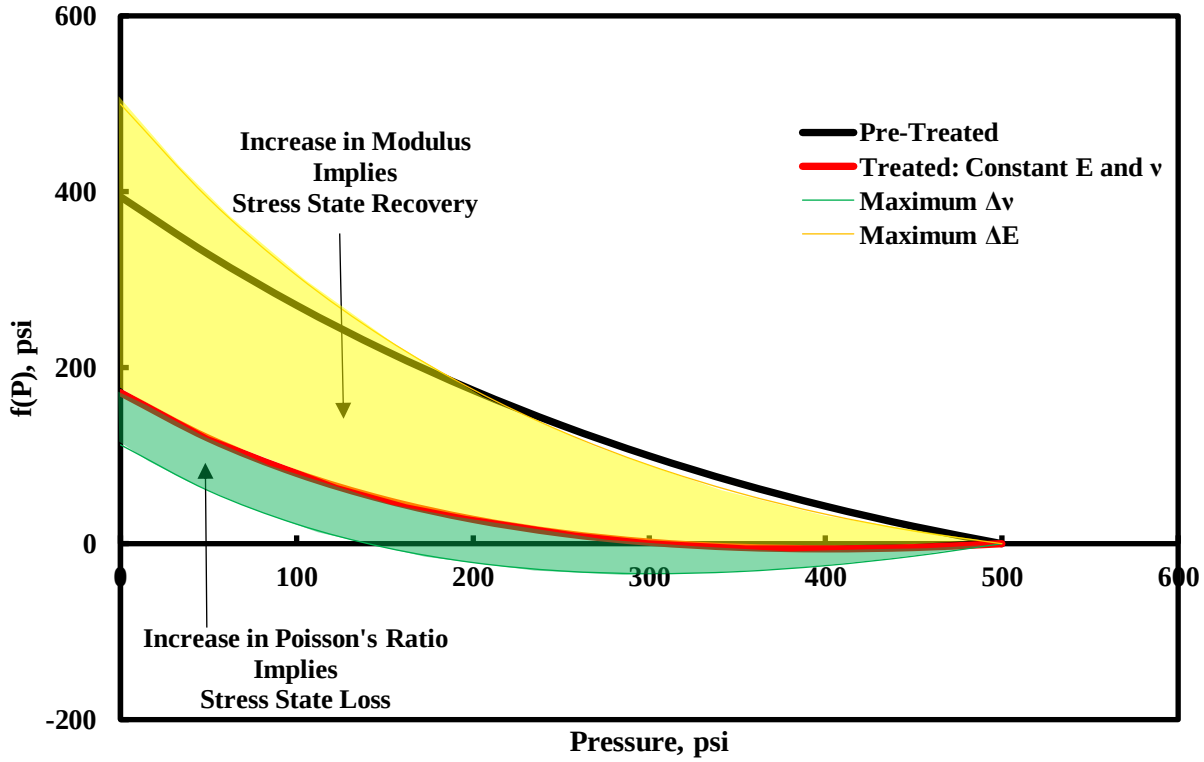

Figure 51: Sensitivity of $f(p)$ to Young's modulus and Poisson's ratio of bioconverted coal.

Trends observed in $f(p)$ vs p (figure 51) can be directly correlated to the behavior of k/k_o vs p trend. However, the value of cleat compressibility governs the permeability of a coal reservoir, and a further understanding of the behavior of c_f with bioconversion is required. Cleat compressibility is defined as the change in cleat volume due to changes in pore pressure. Given the well-accepted matchstick model of coal, the nature of cleat compressibility would depend on both the solid matrix and shrinkage/swelling compressibility. This is because change in pore pressure varies the stresses acting on the coal matrix. Deformation of the matrix as a result of the pore pressure variation is a function of how compressible the coal matrix is. More compressible the matrix, larger would be the deformation, and higher the cleat compressibility. A stiffer matrix would result in smaller deformation of the coal matrix which, in turn, would result in a smaller change in cleat volume. Experimental results suggest an increase in solid-matrix compressibility

with bioconversion, implying a decrease in cleat compressibility. Additionally, bioconversion decreased C_m, thereby reducing the volumetric shrinkage due to depletion. Quantitative determination of the decrease in cleat compressibility would require measuring flow behavior of coal cores under triaxially stressed condition, an aspect beyond the scope of the current study. The sensitivity of the pressure-dependent permeability to the reduction in cleat compressibility is presented in figure 52. As seen in the figure, decrease of cleat compressibility due to bioconversion would further serve to suppress the reservoir permeability.

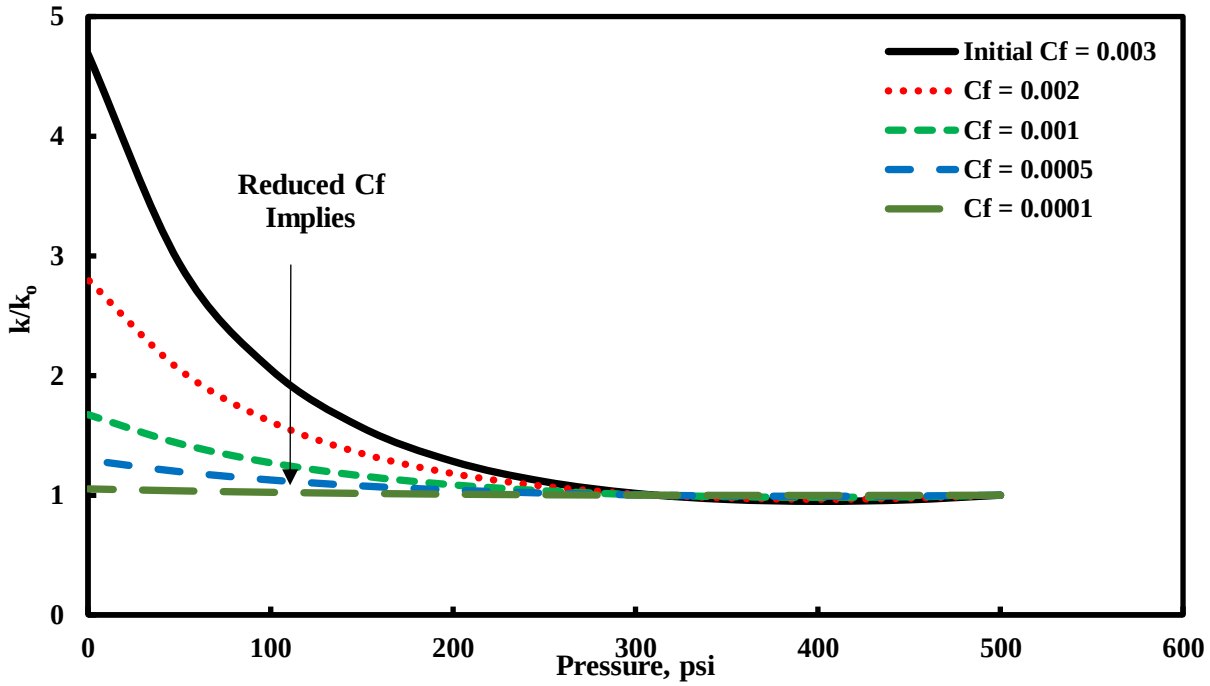

Figure 52: Sensitivity of k/k_0 to cleat compressibility.

5. Conclusions

Experimental data revealing suppression of sorption-induced-strain response of a CBM reservoir due to bioconversion, along with initial matrix softening followed by a stiffer coal matrix post-bioconversion, was interpreted from a reservoir perspective. Based on the work presented, the following conclusions are made:

a) Methane flooding revealed decrease in the Langmuir-type parameters of maximum strain

and pressure post-bioconversion. This decrease bore a near-linear relationship with the volume of gas produced by coal, and is bounded by the maximum volume of gas produced.

b) Reduced strain response of a bioconverted reservoir results in suppression of the pressure-dependent-permeability behavior of the reservoir, which is detrimental from a production perspective, especially for low permeability coals, like in the Illinois basin.

c) The matrix softening (inelastic strains) and excess volumetric shrinkage effects help increasing the permeability of a biogenic CBM reservoir. However, the slight increase is overshadowed by the negative effect of bioconversion induced swelling of Illinois coals.

d) Analyzing from an effective stress perspective, bioconversion delays the onset of rebound and recovery pressures for a reservoir, negatively affecting the reservoir performance. Greater the volume of gas produced, longer is the delay.

e) The shrinkage/swelling compressibility of the coal reduced post-bioconversion. However, with longer treatment duration, the compressibility rebounded past an inflection pressure (**P_I**), which was defined as a function of the bioconversion induced changes in Langmuir-type parameters. Such behavior predicts slightly improved reservoir performance with longer treatment duration.

f) Bioconversion transitions a reservoir from a Type-D to Type-A reservoirs. However, the extent of transition is a function of the degree of gasification, and the initial stress state of the reservoir. A system was introduced, with a **T-Xn** nomenclature, which rates the suitability of a coalbed methane reservoir to bioconversion from a reservoir perspective.

g) Sensitivity analysis of geo-mechanical parameters indicated a possibility of stress-state recovery, primarily due to increase in Young's modulus of coal. However, the combined

effect of variation in Young's modulus, Poisson's ratio and cleat compressibility indicated suppression of flow rates in a bioconverted CBM reservoir.

6. Future Work

The work presented here establishes the suppression of the strain response of coal due to bioconversion. Given the nature of the outcome, and possible effects of such behavior, there are a number of related aspects that need to be studied further. These are listed below:

a) A rigorous analysis of the changes in flow coupled geo-mechanical behavior of coal due to bioconversion needs to be carried out.

b) Unconstrained strain response due to sorption can only be used to model stress and permeability behavior of a coal reservoir. An accurate representation of the behavior of stress and permeability requires triaxially stressed core flooding experiments, missing in current literature. The experimental approach requires coupling the work and analysis with a permeability model developed for biogenic CBM reservoirs, accounting for strains observed due to bioconversion.

c) Given the organic origin of the generated microbial methane, a detailed analysis of the change in the maceral constituents of coal and related geologic parameters is required.

Acknowledgement

We gratefully acknowledge support from the US Department of Energy, award number DE-FE0026161.

CHAPTER 5

SUMMARY

The primary objective of this dissertation was to investigate the effect of bioconversion on flow-coupled-geomechanical response of a producing MECBM reservoir. The focus of the work was on evaluating the changes in visible micro- and macro- porous structure of coal due to bioconversion. This enabled validating the preliminary results in previously reported work investigating micro-scale flow behavior in bioconverted coal. Additionally, variation in the dynamic strain response of coal due to bioconversion to helium and methane flooding was measured. This provided insights into the flow-coupled geomechanical behavior of MECBM reservoirs, and the effect of bioconversion on parameters governing the behavior.

Scanning electron microscopy of coal, pre- and post-bioconversion, revealed significant changes to the flow-governing macro- and micro- structure of coal. Bioconversion resulted in swelling of the coal matrix, thereby decreasing the cleat width/aperture. This explains the observed decrease in permeability of coal to fluid flow, as reported in recent experimental studies (Pandey and Harpalani 2019; Stephen et al. 2014). Prolonged bioconversion also revealed creation of new pores, microcracks and fractures, which in the short-term do not contribute to fluid flow, but indicated the possibility of improved long-term flow conditions. Increase in visible micro-porosity also validated previously reported increase in sorption and diffusion behavior observed in bioconverted coal (Pandey 2015b). Although decrease in cleat aperture was the widely observed effect of bioconversion, fractures larger than 5 micron in width (<5% of observed fractures) increased in width post-bioconversion, presenting a possibility of using artificially induced fracturing techniques to enhance production and flow in a microbially recharged coalbed methane reservoir.

Variation in the strain response of coal to helium and methane flooding, pre- and post-bioconversion provided valuable insights into the expected behavior of a MECBM reservoir during its recharge and production cycle. Helium flooding revealed that bioconversion softened the coal matrix, which results in unrecoverable matrix compression during the treatment period. This resulted in a slight increase in the modeled reservoir permeability at the end of the treatment period, but was overcome by the significantly larger bioconversion induced swelling, which lowered the reservoir permeability. Methane flooding revealed that bioconversion suppressed the sorptive-strain response of the reservoir. This is detrimental from a production perspective, as the increase in reservoir permeability with methane depletion, which is typically associated with CBM reservoirs due to its desorption-induced shrinkage effect, will be suppressed. The change in all the parameters associated with governing reservoir performance, such as Langmuir's constants, rebound and recovery pressures bore a near-linear relationship with the volume of biogenic gas produced by coal, and was bounded by the maximum volume of gas produced. A theoretical framework was also presented based on the results obtained, which identified the onset of an 'inflection point' with longer treatment duration, beyond which flow-behavior in the reservoir improved. Finally, a **T-Xn** nomenclature was introduced, which can be used to rank the suitability of coal seams to bioconversion from a reservoir perspective.

REFERENCES

Agyarko, L B, and G A Mansoori. 2013. “A Review of Non-Renewable Energy Options in Illinois.” *International Journal of Oil, Gas and Coal Technology* 6(3): 288–347. http://dx.doi.org/10.1504/IJOGCT.2013.052246.

Ahmed, Manzur, and J. W. Smith. 2001. “Biogenic Methane Generation in the Degradation of Eastern Australian Permian Coals.” *Organic Geochemistry* 32(6): 809–16.

Demir, I; Damberger, H H. 2000. “Coalbed and Coal Mine Methane Potential of Illinois Basin.” In *Rocky Mountain Association of Geologists*,.

Espinoza, D. N. et al. 2015. “Desorption-Induced Shear Failure of Coal Bed Seams during Gas Depletion.” *International Journal of Coal Geology*.

Everhart, T. E., and R. F M Thornley. 1960. “Wide-Band Detector for Micro-Microampere Low-Energy Electron Currents.” *Journal of Scientific Instruments* 37(7): 246–48.

Faiz, Mohinudeen, and Phil Hendry. 2006. “Significance of Microbial Activity in Australian Coal Bed Methane Reservoirs - A Review.” *Bulletin of Canadian Petroleum Geology*.

Flores, Romeo M. et al. 2008. “Methanogenic Pathways of Coal-Bed Gas in the Powder River Basin, United States: The Geologic Factor.” *International Journal of Coal Geology* 76(1–2): 52–75.

Gray, I. 1987. “Reservoir Engineering in Coal Seams: Part 1 - The Physical Process of Gas Storage and Movement in Coal Seams.” *SPE Reservoir Evaluation & Engineering* 2(1): 28–34.

Harpalani, Satya, and Guoliang Chen. 1995. “Estimation of Changes in Fracture Porosity of Coal with Gas Emission.” *Fuel* 74(10): 1491–98.

———. 1997. “Influence of Gas Production Induced Volumetric Strain on Permeability of Coal.” *Geotechnical & Geological Engineering* 15(4): 303–25. http://dx.doi.org/10.1007/BF00880711%5Cnhttp://link.springer.com/article/10.1007%2FBF00880711.

Harpalani, Satya, and Richard A. Schraufnagel. 1990. “Shrinkage of Coal Matrix with Release of Gas and Its Impact on Permeability of Coal.” *Fuel* 69(5): 551–56.

Jabłoński, Sławomir, Paweł Rodowicz, and Marcin Łukaszewicz. 2015. “Methanogenic Archaea Database Containing Physiological and Biochemical Characteristics.” *International Journal of Systematic and Evolutionary Microbiology* 65: 1360–68.

Jones, Elizabeth J P, Mary A. Voytek, Margo D. Corum, and William H. Orem. 2010. “Stimulation of Methane Generation from Nonproductive Coal by Addition of Nutrients or a Microbial Consortium.” *Applied and Environmental Microbiology* 76(21): 7013–22.

Levine, Jeffrey R. 1996a. “Model Study of the Influence of Matrix Shrinkage on Absolute Permeability of Coal Bed Reservoirs.” *Geological Society, London, Special Publications* 109(1): 197–212. http://sp.lyellcollection.org/lookup/doi/10.1144/GSL.SP.1996.109.01.14.

———. 1996b. “Model Study of the Influence of Matrix Shrinkage on Absolute Permeability of Coal Bed Reservoirs.” *Geological Society, London, Special Publications* 109(1): 197–212.

Liu, Chun, Bin Shi, Jian Zhou, and Chaosheng Tang. 2011. “Quantification and Characterization of Microporosity by Image Processing, Geometric Measurement and Statistical Methods: Application on SEM Images of Clay Materials.” *Applied Clay Science* 54(1): 97–106.

Liu, Shimin, and Satya Harpalani. 2013. “A New Theoretical Approach to Model Sorption-Induced Coal Shrinkage or Swelling.” *AAPG Bulletin* 97(7): 1033–49.

———. 2014a. “Compressibility of Sorptive Porous Media: Part 1. Background and Theory.”

AAPG Bulletin.

———. 2014b. “Compressibility of Sorptive Porous Media: Part 2. Experimental Study on Coal.” *AAPG Bulletin*.

Liu, Shimin, Yi Wang, and Satya Harpalani. 2016. “Anisotropy Characteristics of Coal Shrinkage/Swelling and Its Impact on Coal Permeability Evolution with CO2 Injection.” *Greenhouse Gases: Science and Technology* 6(5): 615–32.

Liu, Xianfeng, and Baisheng Nie. 2016. “Fractal Characteristics of Coal Samples Utilizing Image Analysis and Gas Adsorption.” *Fuel* 182: 314–22.

Mandelbrot, B. 1990. “Fractals - a Geometry of Nature.” *New Scientist* 15 Sept. 1: 38–43.

Midgley, David J. et al. 2010. “Characterisation of a Microbial Community Associated with a Deep, Coal Seam Methane Reservoir in the Gippsland Basin, Australia.” *International Journal of Coal Geology* 82(3–4): 232–39.

Mitra, Abhijit. 2010a. PhD Southern Illinois University “Laboratory Investigation of Coal Permeability Under Replicated in Situ Stress Regime.” Southern Illinois University, Carbondale.

———. 2010b. “LABORATORY INVESTIGATION OF COAL PERMEABILITY UNDER REPLICATED IN SITU STRESS REGIME.” Southern Illinois University, Carbondale.

Moffat, D. H., and K. E. Weale. 1954. “Sorption by Coal of Methane at High Pressure.” *Fuel* 34: 449–62.

Moore, Tim a. 2012a. “Coalbed Methane: A Review.” *Int. J. Coal Geol.* 101: 36–81. http://linkinghub.elsevier.com/retrieve/pii/S0166516212001760.

———. 2012b. “Coalbed Methane: A Review.” *Int. J. Coal Geol.* 101: 36–81.

Okotie, V U, and R L Moore. 2011. “Well-Production Challenges and Solutions in a Mature,

Very-Low-Pressure Coalbed-Methane Reservoir.” *SPE Production and Operations*.

Opara, A. et al. 2012. “Microbial Production of Methane and Carbon Dioxide from Lignite, Bituminous Coal, and Coal Waste Materials.” *International Journal of Coal Geology* 96–97: 1–8.

Palmer, Ian, and John Mansoori. 1998. “How Permeability Depends on Stress and Pore Pressure in Coalbeds: A New Model.” *SPE Reservoir Evaluation & Engineering* 1(6): 539–44.

Pandey, R. et al. 2016. “Changes in Gas Storage and Transport Properties of Coal as a Result of Enhanced Microbial Methane Generation.” *Fuel* 179.

Pandey, R., and S. Harpalani. 2018. “An Imaging and Fractal Approach towards Understanding Reservoir Scale Changes in Coal Due to Bioconversion.” *Fuel* 230.

Pandey, Rohit. 2015a. “Changes in Properties of Coal as a Result of Continued Bioconversion.” Southern Illinois University Carbondale.

———. 2015b. “Changes in Properties of Coal as a Result of Continued Bioconversion.” Southern Illinois University Carbondale. https://core.ac.uk/download/pdf/60579166.pdf.

Pandey, Rohit, and Satya Harpalani. 2018. “An Imaging and Fractal Approach towards Understanding Reservoir Scale Changes in Coal Due to Bioconversion.” *Fuel* 230: 282–97.

———. 2019. “Evaluation of Dynamic Flow and Production Behavior of Biogenic Methane Reservoirs.” In *ARMA*, New York, 145.

Park, Stephen Y., and Yanna Liang. 2016. “Biogenic Methane Production from Coal: A Review on Recent Research and Development on Microbially Enhanced Coalbed Methane (MECBM).” *Fuel*.

Penner, Tara J., Julia M. Foght, and Karen Budwill. 2010. “Microbial Diversity of Western Canadian Subsurface Coal Beds and Methanogenic Coal Enrichment Cultures.”

International Journal of Coal Geology 82(1–2): 81–93.

Perrotti, Vittoria et al. 2011. "Fractal Analysis: A Novel Method to Assess Roughness Organization of Implant Surface Topography." *International Journal of Periodontics and Restorative Dentistry* 31(6): 663–639.

Rasband, W. S. 1997. "ImageJ." *National Institutes of Health, Bethesda, Maryland, USA.*: http://imagej.nih.gov/ij/. http://imagej.nih.gov/ij/.

RICE, DUDLEY D., U. S. Geological S. 2002. "Composition and Origins of Coalbed Gas." *AAPG Bulletin*.

Saurabh, S., S. Harpalani, and V. K. Singh. 2016. "Implications of Stress Re-Distribution and Rock Failure with Continued Gas Depletion in Coalbed Methane Reservoirs." *International Journal of Coal Geology*.

Saurabh, Suman, and Satya Harpalani. 2018. "Modeling of Microbial Methane Generation from Coal and Assessment of Its Impact on Flow Behavior." *Fuel* 216: 274–83.

Sawyer, W.K., G.W. Paul, and R.A. Schraufnagel. 1990. "Development And Application Of A 3-D Coalbed Simulator." *Annual Technical Meeting*. http://www.onepetro.org/doi/10.2118/90-119.

Scott, AR. 1999a. "Improving Coal Gas Recovery with Microbially Enhanced Coalbed Methane." *Coalbed Methane: Scientific, Environmental and …*: 89–110.

———. 1999b. "Improving Coal Gas Recovery with Microbially Enhanced Coalbed Methane." *Coalbed Methane: Scientific, Environmental and …*: 89–110. http://link.springer.com/chapter/10.1007/978-94-017-1062-6_7%5Cnhttp://link.springer.com/10.1007/978-94-017-1062-6_7.

Seidle, John R., and L.G. Huitt. 1995. "Experimental Measurement of Coal Matrix Shrinkage

Due to Gas Desorption and Implications for Cleat Permeability Increases." *International Meeting on Petroleum Engineering*. http://www.onepetro.org/doi/10.2118/30010-MS.

Shi, J. Q., and S. Durucan. 2004. "Drawdown Induced Changes in Permeability of Coalbeds: A New Interpretation of the Reservoir Response to Primary Recovery." *Transport in Porous Media* 56(1): 1–16.

Shi, Ji-Quan, and Sevket Durucan. 2005. "A Model for Changes in Coalbed Permeability during Primary and Enhanced Methane Recovery." *SPE Reservoir Evaluation & Engineering* 8(4): 291–99. http://www.onepetro.org/mslib/app/Preview.do?paperNumber=SPE-87230-PA&societyCode=SPE%5Cnhttp://www.onepetro.org/mslib/servlet/onepetropreview?id=SPE-87230-PA.

Song, Hu et al. 2004. "Fractal Characteristic of Three Chinese Coals." *Fuel* 83(10): 1307–13.

Stephen, Anil et al. 2014. "Bioconversion of Coal: New Insights from a Core Flooding Study." *RSC Advances* 4(43): 22779. http://xlink.rsc.org/?DOI=c4ra01628a.

Strąpoć, Dariusz et al. 2008. "Methane-Producing Microbial Community in a Coal Bed of the Illinois Basin." *Applied and Environmental Microbiology* 74(8): 2424–32.

Strapoć, Dariusz, Maria Mastalerz, Cortland Eble, and Arndt Schimmelmann. 2007. "Characterization of the Origin of Coalbed Gases in Southeastern Illinois Basin by Compound-Specific Carbon and Hydrogen Stable Isotope Ratios." *Organic Geochemistry* 38(2): 267–87.

Suman, Saurabh, and Satya Harpalani. 2018. "Modeling of Microbial Methane Generation from Coal and Assessment of Its Impact on Flow Behavior." *Fuel* 216: 274–83. https://doi.org/10.1016/j.fuel.2017.12.015.

Sun, Wenjing, Yanyan Feng, Chengfa Jiang, and Wei Chu. 2015. "Fractal Characterization and

Methane Adsorption Features of Coal Particles Taken from Shallow and Deep Coalmine Layers." *Fuel* 155: 7–13.

Tollefson, Jeff. 2012. "Air Sampling Reveals High Emissions from Gas Field." *Nature* 482(7384): 139–40.

Xie, Ke Chang. 2015. "Physical Characteristics of Coal." In *Structure and Reactivity of Coal: A Survey of Selected Chinese Coals*, , 29–65.

Yang, Feng, Zhengfu Ning, and Huiqing Liu. 2014. "Fractal Characteristics of Shales from a Shale Gas Reservoir in the Sichuan Basin, China." *Fuel* 115: 378–84.

Zhang, J., Y. Liang, P.M. Yau, et al. 2015. "A Metaproteomic Approach for Identifying Proteins in Anaerobic Bioreactors Converting Coal to Methane." *International Journal of Coal Geology* 146.

Zhang, J., Y. Liang, R. Pandey, and S. Harpalani. 2015. "Characterizing Microbial Communities Dedicated for Conversion of Coal to Methane in Situ and Ex Situ." *International Journal of Coal Geology* 146.

Zhang, Ji, Kaitlyn Anderson, David Britt, and Yanna Liang. 2018. "Sustaining Biogenic Methane Release from Illinois Coal in a Fermentor for One Year." *Fuel*.

Zhang, Ji, Zheting Bi, and Yanna Liang. 2018. "Development of a Nutrient Recipe for Enhancing Methane Release from Coal in the Illinois Basin." *International Journal of Coal Geology* 187: 11–19.

Zhang, Ji, and Yanna Liang. 2017. "Evaluating Approaches for Sustaining Methane Production from Coal through Biogasification." *Fuel* 202: 233–40.

Zhang, Ji, Yanna Liang, and Satya Harpalani. 2016. "Optimization of Methane Production from Bituminous Coal through Biogasification." *Applied Energy* 183: 31–42.

Zhang, Ji, Stephen Y. Park, Yanna Liang, and Satya Harpalani. 2016. “Finding Cost-Effective Nutrient Solutions and Evaluating Environmental Conditions for Biogasifying Bituminous Coal to Methane Ex Situ.” *Applied Energy*.

Zhang, Rui et al. 2017. “Changes in Pore Structure of Coal Caused by Coal-to-Gas Bioconversion.” *Scientific Reports* 7(1).

Zimmerman, R. W. 1991. *Compressibility of Sandstones*. Elsevier Science.

APPENDICES

APPENDIX A

APPENDIX B

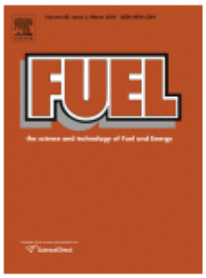

Title: Impact of bioconversion on matrix strain response of coal reservoirs: Part 1-Experimental insights

Author: Rohit Pandey,Satya Harpalani

Publication: Fuel

Publisher: Elsevier

Date: 1 March 2019

LOGIN

If you're a copyright.com user, you can login to RightsLink using your copyright.com credentials.

Already **a RightsLink user** or want to learn more?

Please note that, as the author of this Elsevier article, you retain the right to include it in a thesis or dissertation, provided it is not published commercially. Permission is not required, but please ensure that you reference the journal as the original source. For more information on this and on your other retained rights, please visit: https://www.elsevier.com/about/our-business/policies/copyright#Author-rights

BACK CLOSE WINDOW

APPENDIX C

Title: An imaging and fractal approach towards understanding reservoir scale changes in coal due to bioconversion
Author: Rohit Pandey,Satya Harpalani
Publication: Fuel
Publisher: Elsevier
Date: 15 October 2018

LOGIN

If you're a copyright.com user, you can login to RightsLink using your copyright.com credentials.

Already **a RightsLink user** or want to learn more?

Please note that, as the author of this Elsevier article, you retain the right to include it in a thesis or dissertation, provided it is not published commercially. Permission is not required, but please ensure that you reference the journal as the original source. For more information on this and on your other retained rights, please visit: https://www.elsevier.com/about/our-business/policies/copyright#Author-rights

BACK CLOSE WINDOW

VITA

Graduate School
Southern Illinois University

Rohit Pandey

rohit.mining1990@gmail.com

Education:
Bengal Engineering and Science University, Shibpur
Bachelor of Engineering, Mining Engineering, January 2013

Southern Illinois University Carbondale
Master of Science in Mining Engineering, July 2015

Special Honors and Awards:
Dissertation Research Award, 2018-2019

Dissertation Paper Title:
Reservoir Scale Implication of Microbial Coal-to-Methane Conversion.

Major Professor: Satya Harpalani

Publications:

1. **Pandey R**, Harpalani S; Impact of bioconversion on the strain response of coal reservoirs, Part 1: Experimental insights, Fuel, Vol 239, 2019.
2. **Pandey R**, Harpalani S; Impact of bioconversion on the strain response of coal reservoirs, Part 2: Reservoir insights, Fuel, Vol 239, 2019.
3. **Pandey R**, Harpalani S; Imaging and fractal-based approach to understand reservoir-scale changes in bioconverted coal, Fuel, Vol 230, 2018.
4. Feng R, **Pandey R**; Investigation of various pressure transient techniques on permeability measurement of unconventional gas reservoirs, Transport in Porous Media, Vol 120, 2017.
5. Feng R, Harpalani S, **Pandey R**; Evaluation of various pulse-decay laboratory permeability measurement technique for highly stressed coals, Rock Mechanics & Rock Engineering, 2016.
6. **Pandey R**, Harpalani S, Feng R, Zhang J, Liang Y; Changes in gas storage and transport properties of coal as a result of enhanced microbial methane generation, Fuel, Vol 179, 2016.
7. Feng R, Harpalani S, **Pandey R**; Laboratory measurement of stress dependent coal permeability using pulse-decay technique and flow modeling with gas depletion, Fuel, Vol 177, 2016.
8. Zhang J, Liang Y, **Pandey R**, Harpalani S; Characterizing microbial communities dedicated for converting coal to methane in situ and ex situ, International Journal of Coal Geology, Vol 146, 2015.

9. Zhang J, Liang Y, Yau P, **Pandey R**, Harpalani S; A metaproteomic approach for identifying proteins in anaerobic bioreactors converting coal to methane, International Journal of Coal Geology, Vol 146, 2015.
10. **Pandey R**, Harpalani S; Evaluation of dynamic flow and production behavior of biogenic methane reservoirs, ARMA 2019.
11. **Pandey R**, Harpalani S; Modeling fluid flow in biogenic gas reservoirs using imaging approaches, ARMA 2019.
12. Saurabh S, **Pandey R**, Harpalani S; Geomechanical and flow characterization of deep coal with continued generation of biogenic gas, ISRM 2019
13. **Pandey R**, Harpalani S; Modeling fluid flow behavior in microbially recharged coalbed methane reservoirs, presented at 2019 SME Annual Conference, Denver.
14. **Pandey R**, Harpalani S; Feasibility of *in situ* coal bio-conversion: a reality check, presented at 2018 SME Annual Conference, Minnesota.
15. **Pandey R**, Harpalani S; Poromechanical changes in coal properties due to bioconversion: shrinkage/swelling characteristics and associated compressibility, poster presented at 6th Biot Conference on Poromechanics, Paris 2017.
16. **Pandey R**, Harpalani S; Changes in gas storage, transport and mechanical properties of coal with continued bioconversion, presented at 2017 SME Annual Conference, Denver.
17. **Pandey R**, Harpalani S, Zhang J, Liang Y; Changes in gas storage and transport properties with continued bioconversion of coal, presented at AAPG Annual Convention, Calgary, 2016.
18. Park S, Zhang J, Liang Y, **Pandey R**, Harpalani S; Optimization and techno-economic analysis of the microbial conversion of coal to methane, presented at 40th Clean Coal and Fuel Systems Conference, Clearwater, Florida, 2015.
19. Zhang J, Liang Y, **Pandey R**, Harpalani S; Bioconversion of coal waste to methane-study of microbial community, conversion pathway and residual property of coal, presented at 40th Clean Coal and Fuel Systems Conference, Clearwater, Florida, 2015.
20. **Pandey R**; Optimization of loads of dumpers in an open cast mine subjected to different hauling conditions, presented at 23rd National Convention of Mining Engineers, India, 2012.